Calculation of Time Correlation Functions and Rate Constants in Liquid Solutions

by

Francisco Xavier Vázquez

A dissertation submitted in partial fulfillment
of the requirements for the degree of
Doctor of Philosophy
(Chemistry)
in The University of Michigan
2010

Doctoral Committee:

Professor Eitan Geva, Chair
Professor Robert Krasny
Professor Roseanne J. Sension
Assistant Professor Barry Dunietz

"Physical chemistry is power, it is exactness, it is life."
-From Lewis Sinclair's *Arrowsmith*

To my wife, Anne.

ACKNOWLEDGEMENTS

First I would like to thank my wife Anne. She has always been there for me and I love her for it. I would also like to thank my family for always supporting me throughout this process. Very importantly, I would like to thank my advisor Eitan Geva. Under his training, I have learned to always appreciate and seek out the deep truths underlying all of chemistry. I would like to thank my committee members. Robert Krasny, for our conversations involving vibrational energy relaxation. Barry Dunietz, for always being willing to answer my questions about electronic structure. Roseanne Sension, for giving me an exciting project to work on. I would also like to thank all of the past and present members of the group who have helped me along the way. Specifically, I would like to thank Irina Narotskaya, for helping me when I first joined and letting me take over the work she had started, and Surma Talapatra, for taking over the work that I have started.

TABLE OF CONTENTS

LIST OF FIGURES

LIST OF TABLES

CHAPTER I

Introduction

1.1 Background

The calculation of time dependent observables in liquids can be a very difficult and computationally intensive process; however, many time dependent properties are of central importance to understanding chemical phenomena. Vibrational energy relaxation, diffusion, and reaction kinetics are a few examples of important chemical phenomena that are time dependent and also can be computationally expensive to simulate. This becomes especially true if the system must be described quantum mechanically. As opposed to equilibrium observables, which can be calculated from complete knowledge of the partition function of the system, nonequilibrium observables require a different time correlation function (TCF) which can then be related to the time dependent observable of interest. Computer simulations can then be used to calculate the TCF; however, this may not be a trivial task. If the system requires a quantum mechanical description, some sort of semiclassical (SC) approach is needed, as the exact quantum simulation of TCFs is beyond the reach of modern computer resources. Even with a SC procedure, the calculation can still be extremely computationally expensive; however, an accurate description of time dependent phenomena in liquids can provide important microscopic insight into time dependent

phenomena that may not be able to be shown by experiment.

1.2 Equilibrium and Nonequilibrium Statistical Mechanics

Statistical mechanics provides the way to calculate macroscopic observables, which are functions of pressure, volume, internal energy, etc., in terms of microscopic properties, specifically, molecular and atomic positions. Given complete knowledge of the system's equilibrium partition function, any macroscopic equilibrium observable, $\langle A \rangle_0$, can be calculated from given microscopic properties. If the system can be described classically, the equilibrium partition function is defined as [83, 12]

$$Z = \int d\mathbf{Q} \int d\mathbf{P} e^{-\beta H(\mathbf{Q},\mathbf{P})} \tag{1.1}$$

where $\beta = \frac{1}{k_B T}$, k_B is the Boltzmann constant, T, is the temperature, $\mathbf{Q}$ and $\mathbf{P}$ are the phase space atomic positions and momenta, respectively, and $H(\mathbf{Q}, \mathbf{P})$ is classical Hamiltonian for the system. Using the partition function, any classical macroscopic equilibrium observable, $\langle A \rangle_0^{Cl}$, can be written as

$$\langle A \rangle_0^{Cl} = \frac{\int d\mathbf{Q} \int d\mathbf{P} \ A(\mathbf{Q},\mathbf{P}) \ e^{-\beta H(\mathbf{Q},\mathbf{P})}}{Z} \tag{1.2}$$

where the equilibrium phase space probability density is given by $\rho = \frac{e^{-\beta H(\mathbf{Q},\mathbf{P})}}{Z}$. For example, the total internal energy of a classical system can be written as

$$\langle H \rangle_0^{Cl} = \frac{\int d\mathbf{Q} \int d\mathbf{P} \ H(\mathbf{Q},\mathbf{P}) \ e^{-\beta H(\mathbf{Q},\mathbf{P})}}{Z} \tag{1.3}$$

If quantum mechanical effects play a significant role, then the equilibrium quantum mechanical partition function of the system must be used, which is defined as

$$Z = Tr \left[e^{-\beta \widehat{H}} \right] \tag{1.4}$$

where $\hat{H}$, is the quantum mechanical Hamiltonian operator. Any quantum mechanical equilibrium macroscopic observable can then be written as

$$\left\langle \widehat{A} \right\rangle_0^{QM} = \frac{Tr\left[\widehat{A}e^{-\beta\widehat{H}}\right]}{Z} \tag{1.5}$$

where the quantum mechanical equilibrium phase space density operator is given by $\hat{\rho} = \frac{e^{-\beta\widehat{H}}}{Z}$. Analogous to the previous example, the quantum mechanical internal energy of the system can be written as

$$\left\langle \widehat{H} \right\rangle_0^{QM} = \frac{Tr\left[\widehat{H}e^{-\beta\widehat{H}}\right]}{Z}. \tag{1.6}$$

The calculation of time dependent phenomena requires the use of nonequilibrium statistical mechanics. Within this formalism, many time dependent observables can be related to different TCFs. As opposed to equilibrium statistical mechanics, where a single partition function corresponding to the system at a particular equilibrium state is used to calculate all equilibrium observables for the system, a different TCF must be used for each observable of interest. The general formula for a classical time correlation function is

$$C(t) = \langle A(t_0)B(t + t_0)\rangle = \lim_{\tau\to\infty} \frac{1}{\tau} \int_0^\tau dt A(t_0)B(t_0 + t) \tag{1.7}$$

where $A(t) = A\left[\mathbf{Q}(t), \mathbf{P}(t)\right]$, $B(t) = B\left[\mathbf{Q}(t), \mathbf{P}(t)\right]$. and $\{\mathbf{Q}(t), \mathbf{P}(t)\}$ evolve according to Newton's equations of motion. If the system is ergodic, then, given a long enough amount of time, a single trajectory will be able sample all available state points in phase space. If this is the case, then the general time average Eq. (1.7) can be replaced by the following classical ensemble average expression

$$C(t) = \frac{1}{Z} \int d\mathbf{Q} \int d\mathbf{P} \; e^{-\beta H(\mathbf{Q},\mathbf{P})} \; A(\mathbf{Q},\mathbf{P}) \; B\left[\mathbf{Q}(t), \mathbf{P}(t)\right] \tag{1.8}$$

The quantum mechanical expression for a general TCF analogous to equation 1.8 is given by

$$C(t) = \frac{1}{Z} Tr \left[e^{-\beta \hat{H}} \hat{A} \ \hat{B}(t) \right] \tag{1.9}$$

where $\hat{B}(t) = e^{i \hat{H} t / \hbar} \hat{B} \ e^{-i \hat{H} t / \hbar}$ is the operator $\hat{B}$ in the Heisenberg representation.

1.3   Linear Response Theory

Using a first order perturbation approach, linear response theory (LRT) can be used to understand time-dependent phenomena using a time correlation function formalism[68, 12]. Here and in what follows the system will be assumed to be classical, although this formalism can easily be generalized to a quantum system. Assume a system in thermal equilibrium with the Hamiltonian H_0. A perturbation, A, is applied to the system to push it slightly away from equilibrium and the system is then allowed to equilibrate with respect to the perturbation. The Hamiltonian describing this situation is $H_{tot} = H_0 + fA$, where f is a parameter detailing the strength of the perturbation. At time $t = 0$, the perturbation is turned off and the system is allowed to relax. The phase space probability density describing the perturbed system at time $t \leq 0$ is
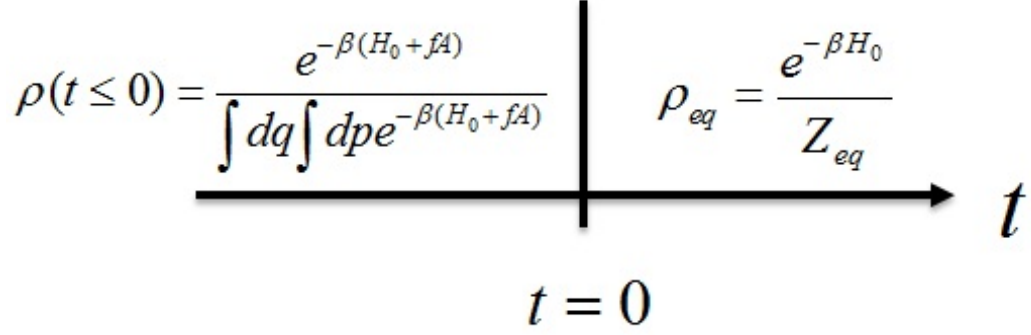
$$\rho = \frac{e^{-\beta(H_0 + fA)}}{\int d\mathbf{Q} \int d\mathbf{P} e^{-\beta(H_0 + fA)}}, \tag{1.10}$$

and the probability density at time $t \gg 0$ is given by

$$\rho_{eq} = \frac{e^{-\beta H_0}}{Z_{eq}} \tag{1.11}$$

where $Z_{eq} = \int d\mathbf{Q} \int d\mathbf{P} e^{-\beta H_0}$ is the equilibrium partition function. This is shown schematically in Fig. 1.1.

To understand the phase space probability density of the system at $t = 0$, Eq. (1.10) is written in terms of Eq. (1.11). Because the perturbation was assumed to

$$\rho(t \le 0) = \frac{e^{-\beta(H_0 + fA)}}{\int dq \int dp \, e^{-\beta(H_0 + fA)}} \qquad \rho_{eq} = \frac{e^{-\beta H_0}}{Z_{eq}}$$

$$t \xrightarrow{\qquad} t$$

$$t = 0$$

Figure 1.1: Schematic represenation of a system slightly pertubed from equilbrium at $t < 0$.

be small such that $H_0 \gg fA$, Eq. (1.11) can be expanded linearly in terms of A:

$$
\begin{aligned}
\rho &= \frac{e^{-\beta(H_0 + fA)}}{\int d\mathbf{Q} \int d\mathbf{P} e^{-\beta(H_0 + fA)}} \approx \frac{e^{-\beta H_0}}{\int d\mathbf{Q} \int d\mathbf{P} e^{-\beta H_0} \left[1 - \beta fA\right]} \left[1 - \beta fA\right] \quad (1.12) \\
&= \frac{e^{-\beta H_0}}{Z_{eq} - Z_{eq}\beta \langle A \rangle_0} \left[1 - \beta fA\right] \\
&= \frac{e^{-\beta H_0}}{Z_{eq}} \left[1 - \beta fA\right]\left[1 + \beta f \langle A \rangle_0\right] \\
&= \rho_{eq} \left[1 - \beta f \left(A - \langle A \rangle_0\right)\right] = \rho_{eq} \left[1 - \beta f \, \delta A\right]
\end{aligned}
$$

where $\delta A \equiv A - \langle A \rangle_0$. Because the unperturbed Hamiltonian is time invariant and because of the time-reversal symmetry arising from Hamilton's equations of motion for propagating the positions and momenta, $\mathbf{Q}$ and $\mathbf{P}$ respectively, in time, the time propagation of the probability density $\rho(t)$, can be written as

$$\rho(t) = \rho_{eq} \left[1 - \beta f \, \delta A(-t)\right] \qquad (1.13)$$

The time dependent probability density in Eq. (1.13) can now be used to calculate the macroscopic time dependent average value of some observable, $\bar{B}(t)$:

$$
\begin{aligned}
\bar{B}(t) &= \int d\mathbf{Q} \int d\mathbf{P} \rho(\mathbf{Q}, \mathbf{P}, t) B(\mathbf{Q}, \mathbf{P}) \qquad (1.14) \\
&= \int d\mathbf{Q} \int d\mathbf{P} \rho_{eq} \left[1 - \beta f \, \delta A(\mathbf{Q}_{-t}, \mathbf{P}_{-t})\right] B(\mathbf{Q}, \mathbf{P}) \\
&= \langle B \rangle_0 - \beta f \, \langle \delta A(-t) B \rangle
\end{aligned}
$$

Using the property of classical time correlation functions such that $\langle \delta A(-t)B(0) \rangle = \langle \delta A(0) \delta B(t) \rangle_0$, the final result of Eq. (1.14) can be rewritten as

$$\langle B \rangle_0 - \beta f \ \langle \delta A(-t)B(0) \rangle = \langle B \rangle_0 - \beta f \ \langle \delta A(0) \delta B(t) \rangle_0 \qquad (1.15)$$

This leads to the final result

$$\delta \bar{B}(t) = -\beta f \ \langle \delta A(0) \delta B(t) \rangle_0 \qquad (1.16)$$

which is a TCF. The importance of this formalism and its resulting expression is that it is able to take a macroscopic nonequilibrium time dependent average and relate it back to an equilibrium time correlation function. The expression in Eq. (1.16) is a measure of microscopic fluctuations around some equilibrium value, and the correlation of those fluctuations can be used to simulate time dependent phenomena. This result is equivalent to the Onsager Hypothesis, which states that the relaxation of nonequilibrium disturbances is governed by the same laws as the fluctuations in a microscopic equilibrium system. This is also known as the Fluctuation Dissipation Theorem.

1.4   Chemical Kinetics

The calculation of first order chemical reaction rate constants can be treated within the linear response formalism[12, 11]. Here and in what follows, the system will be assumed to be classical, although this formalism can be generalized to a quantum system. Assume a first order chemical reaction with a one dimensional collective reaction coordinate, q, that takes the system from the reactant state to the product state. The phase space corresponding to this system will include a bottleneck region corresponding to the area of the reaction barrier that is assumed

to be centered at q^*. When the reaction coordinate crosses the barrier the reaction will proceed from reactants to products or vice versa. Phenomenologically, the rate constant can be written as

$$\frac{x_p(t)}{x_p(0)} = e^{-kt} \tag{1.17}$$

where $x_p(t)$ is the mole fraction of the products at time t and k is the chemical reaction rate constant. In this case, the observable is the mole fraction, which can be written microscopically as a ensemble average of the Heaviside function of the reaction coordinate

$$x_p = \langle h(q - q^*) \rangle_0 \tag{1.18}$$

where

$$h(q - q^*) = \begin{cases} 1 \,, & q > q^* \\ 0 \,, & q < q^* \end{cases} \tag{1.19}$$

The choice of perturbation in this case will also be a Heaviside function however, other perturbations can be used provided they perturb the chemical equilibrium. The phenomenological rate constant can now be written in terms of the Heaviside function such that

$$\frac{x_p(t)}{x_p(0)} = \frac{\bar{h}\left[q - q^*\right](t)}{\bar{h}\left[q - q^*\right](0)} = e^{-kt} \tag{1.20}$$

In the long time limit such that $t \gg 1/k$, the time derivative is applied to both sides of Eq (1.20), resulting in the following expression:

$$\frac{\partial}{\partial t} \frac{\langle h(q - q^*) \rangle\,(t)}{\langle h(q - q^*) \rangle\,(0)} = -k \tag{1.21}$$

The Heaviside averages can then be rewritten using the linear response formalism:

$$\frac{\partial}{\partial t} \frac{\langle \delta h\left[q(0) - q^*\right] \delta h\left[q(t) - q^*\right] \rangle_0}{\langle \delta h\left[q(0) - q^*\right] \delta h\left[q(0) - q^*\right] \rangle_0} = -k \tag{1.22}$$

Applying the time derivative gives

$$\frac{\left\langle \delta h\left[q(0) - q^*\right] \delta \dot{h}\left[q(t) - q^*\right] \right\rangle_0}{\langle \delta h\left[q(0) - q^*\right] \delta h\left[q(0) - q^*\right] \rangle_0} \tag{1.23}$$

The time derivative of the Heaviside function can then be written as

$$
\begin{aligned}
\delta \dot{h}(q(t) - q^*) &= \dot{h}\left[q(t) - q^*\right] \\
&= \frac{\partial}{\partial q} h\left[q - q^*\right] \dot{q}(t) \\
&= \dot{q}(t)\delta(q - q^*)
\end{aligned}
\tag{1.24}
$$

where $\delta(q - q^*)$ is the Dirac delta function and $\dot{q}(t)\delta(q - q^*)$ is the so called flux. This leads to the final result, known as the reactive-flux (RF) TCF.

$$
k = \frac{\langle \dot{q}(0)\delta(q - q^*)h\left[q(t) - q^*\right]\rangle_0}{\langle h\left[q - q^*\right]\rangle \langle 1 - h\left[q - q^*\right]\rangle_0}
\tag{1.25}
$$

The RF-TCF is able to calculate reaction rate constant in simulations by measuring the amount of recrossing of the reaction coordinate over the free energy barrier and correlating this to the so-called flux of the reaction coordinate over the barrier. The RF-TCF formalism allows the simulation to take into account any recrossing that may be induced by the solvent. If an approximation is made such that the direction of the reaction coordinate velocity, $\dot{q}$, at the top of the free energy barrier determines the final state and thus there can be no recrossing, then Eq. (1.25) leads to the transition state theory (TST) approximation for reaction rate constants, k^{TST}:

$$
k^{TST} = \frac{\langle \dot{q}\delta(q - q^*)h\left[\dot{q}\right]\rangle_0}{\langle h\left[q - q^*\right]\rangle \langle 1 - h\left[q - q^*\right]\rangle_0}
\tag{1.26}
$$

It is important to note that the TST approximation includes no information about the reaction dynamics is entirely dependent on the equilibrium conditions of the system.

1.5 Diffusion

In addition to the LRT formalism, other theoretical methods can be used to relate TCFs to time dependent observables. Diffusion is an important chemical process

that can be described using a time correlation function formalism[68, 83, 163]. The calculation of diffusion coefficients by computer simulation is an important problem because of the wide availability of experimental data. Diffusion can serve as an important benchmark for new intermolecular force fields. Diffusion coefficients are also a common benchmark in testing quantum dynamics methodologies[55, 84, 96, 113, 119, 116, 118, 117, 121, 123].

Here and in what follows the system will be assumed to be classical. To relate the diffusion coefficient to a time correlation function, the diffusion coefficient can be defined in terms of the well known Einstein diffusion equation.

$$\langle x^2 \rangle = 2Dt \tag{1.27}$$

where x is the displacement in one direction around an origin $x = 0$, and D is the diffusion coefficient. From the classical equations of motion, $x(t) = \int_0^t ds \, v_x(s)$, where v is velocity in one direction of the diffusing particle, and the average displacement can be written as

$$\langle x^2 \rangle_0 = \left\langle \int_0^t ds_1 v_x(s_1) \int_0^t ds_1 v_x(s_1) \right\rangle_0 \tag{1.28}$$

This expression can then be substituted into Eq. (1.27) to yield

$$\left\langle \int_0^t ds_1 v_x(s_1) \int_0^t ds_1 v_x(s_1) \right\rangle_0 = 2Dt \tag{1.29}$$

Taking the time derivative of both sides of the equation leads to

$$\int_0^t ds \, \langle v_x(t)v_x(s) \rangle_0 = 2D \tag{1.30}$$

Because the expression in Eq. (1.30) relates equilibrium fluctuations of the velocity to diffusion, the choice of time origin is arbitrary. The left hand side of Eq. (1.30)

can be rewritten as

$$\int_0^t ds \, \langle v_x(t)v_x(s) \rangle_0 \; = \; \int_0^t ds \, \langle v_x(t-s)v_x(0) \rangle_0 \qquad (1.31)$$

$$= \; \int_0^t du \, \langle v_x(u)v_x(0) \rangle_0$$

The diffusion equation can only be assumed to be valid a long times, leading to the resulting expression relating the diffusion coefficient to the velocity-velocity correlation function (VVCF):

$$D = \int_0^\infty du \, \langle v_x(u)v_x(0) \rangle_0 \qquad (1.32)$$

Eq. (1.32) can be generalized to three dimensions:

$$D = \frac{1}{3} \int_0^\infty du \, \langle v(u)v(0) \rangle_0 \qquad (1.33)$$

where $v^2 = v_x^2 + v_y^2 + v_z^2$. Importantly, Eq. (1.32) and Eq. (1.33) can be thought of as memory functions, giving a measure of how much the velocity at later times is affected by the initial velocity. If the diffusing molecule or atom experiences many collisions that change the velocity, then the VVCF will decay faster, and the resulting diffusion coefficient will be smaller. If collisions with the solvent have very little effect on the velocity of the diffusing object, then the VVCF will decay slower and the resulting diffusion coefficient will be larger.

1.6 Vibrational Energy Relaxation

Vibrational energy relaxation (VER) is the process by which a molecular mode is vibrationally excited and gives its energy to the bath. This process has a rate constant associated with it that can be related to a bath correlation function. Because vibrational relaxation often requires treating the dynamics within a quantum mechanical framework, the following derivation will take a quantum mechanical

approach[93]. Consider a harmonic vibrational mode coupled to a the other degrees of freedom in the system. The overall Hamiltonian is given by

$$\hat{H} = \frac{\hat{p}^2}{2} + \frac{1}{2}\omega^2\hat{q}^2 + \sum_{j-1}^{N} \frac{\hat{P}_j}{2} + V(\hat{\mathbf{Q}}, \hat{q}) \tag{1.34}$$

where ω is the vibrational frequency of the relaxing mode, $\hat{q}$ and $\hat{p}$ are the mass weighted vibrational displacement coordinate and conjugate momentum operators, respectively, N is the number of degrees of freedom (DOF) coupled to the vibrational mode, $\hat{\mathbf{Q}} = (\hat{Q}_1, \ldots, \hat{Q}_N)$ and $\hat{\mathbf{P}} = (\hat{P}_1, \ldots, \hat{P}_N)$ are the mass weighted coordinate and momentum operators of the degrees of freedom coupled to the vibrational mode, respectively, and $V(\hat{\mathbf{Q}}, \hat{q})$ is any potential energy other than the vibrational potential energy $\frac{1}{2}\omega^2\hat{q}^2$. If it is assumed there is weak coupling between the system (the relaxing vibrational mode) and the bath (all other degrees of freedom coupled to the mode), then the non-harmonic potential, $V(\hat{\mathbf{Q}}, \hat{q})$, can be expanded to first order in q around $q = 0$:

$$V(\hat{\mathbf{Q}}, \hat{q}) = V(\hat{\mathbf{Q}})\Big|_{q=0} + \frac{\partial V}{\partial q}\Big|_{q=0} \hat{q} \equiv \hat{V}_B(\mathbf{Q}) + F(\hat{Q}) \otimes \hat{q} \tag{1.35}$$

where $F(\hat{Q}) = \frac{\partial V}{\partial q}\Big|_{q=0}$ is the force of the bath on the relaxing mode when the mode is frozen at its equilibrium bond length. This is a reasonable approximation to make because the displacement of the mode due to vibration will generally be small and will cause very little perturbation to the surrounding environment. If this is not the case, this approximation is not valid.

The Hamiltonian in Eq. (1.34) can now be separated into system, bath, and system-bath coupling terms:

$$\hat{H} = \hat{H}_S + \hat{H}_B + \hat{H}_{BS} \tag{1.36}$$

where $\hat{H}_S = \frac{\hat{p}^2}{2} + \frac{1}{2}\omega^2\hat{q}^2$, $\hat{H}_B = \sum_{j-1}^{N} \frac{\hat{P}_j}{2} + \hat{V}_B(\mathbf{Q})$, and $\hat{H}_{BS} = F(\hat{Q}) \otimes \hat{q}$. The system Hamiltonian $\hat{H}_S$, is a one dimensional harmonic oscillator and its stationary states

and energy levels are well known:

$$\hat{H}_S \ket{n} = E_n \ket{n} \tag{1.37}$$

where $E_n = (n + 1/2)\hbar\omega$ for $n = 0, 1, 2, 3, \ldots$. The system-bath coupling term, $\hat{H}_{BS}$, can also be written in terms of the system stationary states:

$$\hat{H}_{BS} = \sum_{n,n'} \hat{\Lambda}_{n,n'} \otimes \ket{n}\bra{n'} \tag{1.38}$$

where $\hat{\Lambda}_{n,n'} \equiv \bra{n'} F(\hat{Q})\hat{q} \ket{n}$ is a bath operator. From Redfield theory, the population relaxation rate constant from some state n to another state n' is given by

$$k_{n' \leftarrow n} = \frac{1}{\hbar^2} \int_{-\infty}^{\infty} d\tau e^{i(n-n')} C_{nn',n'n}(\tau) \tag{1.39}$$

where

$$
\begin{aligned}
C_{nn',n'n}(\tau) &= Tr_B \left[\hat{\rho}_B^{eq} \hat{\Lambda}_{n,n'} \hat{\Lambda}_{n',n} \right] \\
&= |\bra{n} \hat{q} \ket{n'}|^2 Tr_B \left[\hat{\rho}_B^{eq} \hat{F}(\tau) \hat{F} \right] \\
&= |\bra{n} \hat{q} \ket{n'}|^2 C_F(\tau)
\end{aligned}
\tag{1.40}
$$

and $C_F(\tau)$ is the quantum mechanical force-force correlation function (FFCF)

$$C_F(\tau) = Tr_B \left[\hat{\rho}_B^{eq} \hat{F} e^{i\hat{H}\tau/\hbar} \hat{F} e^{-i\hat{H}\tau/\hbar} \right] \tag{1.41}$$

. Using harmonic oscillator raising and lowering operators, the matrix element $\bra{n} \hat{q} \ket{n'}$ can be calculated:

$$
\begin{aligned}
\bra{n} \hat{q} \ket{n'} &= \sqrt{\frac{\hbar}{2\omega}} \bra{n} \hat{a} + \hat{a}^\dagger \ket{n'} \\
&= \sqrt{\frac{\hbar}{2\omega}} \left[\sqrt{n'} \braket{n | n'-1} + \sqrt{n'+1} \braket{n | n'-1} \right] \\
&= \sqrt{\frac{\hbar}{2\omega}} \left[\sqrt{n'} \, \delta(n, n'-1) + \sqrt{n'+1} \, \delta(n, n'-1) \right]
\end{aligned}
\tag{1.42}
$$

As a result, only vibrational transitions between subsequent states are allowed. The rate constants for the allowed transitions are given by

$$
\begin{aligned}
k_{n \leftarrow n+1} &= \frac{(n+1)}{2\hbar\omega} \int_{-\infty}^{\infty} d\tau\, e^{i\omega\tau} C_{FF}(\tau) \qquad (1.43) \\
&\equiv \frac{(n+1)}{2\hbar\omega} \tilde{C}_{FF}(\omega)
\end{aligned}
$$

where $\tilde{C}_{FF}(\omega) = \int_{-\infty}^{\infty} d\tau\, e^{i\omega\tau} C_{FF}(\tau)$ is the Fourier transform (FT) of the FFCF.

At a low enough temperature such that $\beta\hbar\omega \gg 1$, which is true for many molecular vibrations, only states 1 and 2 will be significantly populated. As a result only the $k_{0\leftarrow 1}$ rate constant will be be significant. The resulting expression for the $k_{0\leftarrow 1}$ rate constant is given by the Landau-Teller formula

$$
k_{0\leftarrow 1} = \frac{1 - e^{-\beta\hbar\omega}}{2\hbar\omega} \tilde{C}_{FF}(\omega) \qquad (1.44)
$$

The Landau-Teller formula in Eq. (1.44) has a clear classical limit in the case where $\beta\hbar\omega \ll 1$:

$$
k_{0\leftarrow 1}^{Cl} = \frac{\beta}{2} \tilde{C}_{FF}^{Cl}(\omega) \qquad (1.45)
$$

where $\tilde{C}_{FF}^{Cl}(\omega)$ is the FT of the classical FFCF, which is defined as

$$
C_{FF}^{Cl}(t) = \frac{1}{Z_B} \int d\mathbf{Q} \int d\mathbf{P}\ e^{-\beta H_B(\mathbf{Q},\mathbf{P})} F(t)F(0) \qquad (1.46)
$$

where Z_B is the partition function of the bath. Although the classical FFCF is computationally simpler to calculate, it can lead to very poor approximations to the VER rate constant unless the transition frequency is much smaller than kT, which is rarely the case.

1.7 Linearized Semiclassical approximation

The calculation of an exact quantum mechanical TCF is not computationally feasible for complex systems such as liquids using currently available computational

resources. This is because the computational effort scales exponentially with the number of DOF when simulating quantum dynamics directly. A way to avoid this problem is to use some sort of semiclassical approximation[155, 143, 156, 145, 146, 154, 144]. The linearized semiclassical (LSC) is a particularly attractive method because it can be derived directly from the real time path integral representation of the TCF[133] and the resulting dynamics of the coordinates and momenta will be classical.

Consider a general quantum mechanical TCF:

$$C(t) = \frac{1}{Z} Tr \left[e^{-\beta \widehat{H}} \hat{A} e^{i\widehat{H}/\hbar} \hat{B} e^{-i\widehat{H}/\hbar} \right] \tag{1.47}$$

The TCF, $C(t)$ can also be equivalently expressed as a real time path integral

$$
\begin{aligned}
C(t) &= \int dx_0^+ \int dx_0^- \int x_N^+ \int dx_N^- \left\langle x_0^+ \right| e^{-\beta \widehat{H}} \hat{A} \left| x_0^- \right\rangle \left\langle x_0^- \right| e^{i\widehat{H}/\hbar} \left| x_N^- \right\rangle \quad (1.48) \\
&\quad \times \left\langle x_N^- \right| \hat{B} \left| x_N^+ \right\rangle \left\langle x_N^+ \right| e^{-i\widehat{H}/\hbar} \left| x_0^+ \right\rangle \\
&= \left(\frac{m}{2\pi\hbar\varepsilon} \right)^N \int dx_0^+ \cdots \int x_N^+ \int dx_0^- \cdots \int dx_N^- \quad (1.49) \\
&\quad \times \left\langle x_0^+ \right| e^{-\beta \widehat{H}} \hat{A} \left| x_0^- \right\rangle \left\langle x_N^- \right| \hat{B} \left| x_N^+ \right\rangle e^{i\left(S_N^+ - S_N^-\right)/\hbar} \quad (1.50)
\end{aligned}
$$

where the time is written in discrete terms $\{0, \varepsilon, 2\varepsilon, \ldots, N\varepsilon = t\}$ and the $N \to \infty$ limit will be taken at a later stage. The forward and backward actions, $S_N^{\pm}$, are given by

$$S_N^{\pm} = \varepsilon \sum_{j=0}^{N-1} \left[\frac{1}{2} m \left(\frac{x_{j+1}^{\pm} - x_{\pm j}}{\varepsilon} \right)^2 - V(x_j^{\pm}) \right] \tag{1.51}$$

where $\varepsilon = t/N$. The integration variables can then be changed from $x_0^+, \ldots, x_N^+$, $x_0^-, \ldots x_N^-$ to $y_0, \ldots, y_N$, $z_0, \ldots, z_N$, such that

$$y_j = \frac{1}{2} \left(x_j^+ + x_j^- \right), \, z_j = x_j^+ + x_j^- \tag{1.52}$$

The path integral expression in Eq. (1.48) can then be linearized by expanding the difference between the forward and backward actions, $S_N^+ - S_N^-$, linearly with

respect to the difference between the forward and backward paths, $z_0, \ldots, z_N$, such that

$$
\begin{aligned}
S_N^+ - S_N^- &\approx \varepsilon \sum_{j=0}^{N-1} \left[\frac{m}{\varepsilon^2} (y_{j+1} - y_j)(z_{j+1} - z_j) - V'(y_j) z_j \right] \tag{1.53} \\
&= \varepsilon \sum_{j=0}^{N-1} z_j \left[\frac{m}{\varepsilon^2} (2y_j - y_{j-1} - y_{j+1}) - V'(y_j) \right] \\
&\quad + \varepsilon \, z_0 \left[\frac{m}{\varepsilon^2} (y_1 - y_0) - V'(y_0) \right] \\
&\quad + \varepsilon \, z_N \, \frac{m}{\varepsilon^2} (y_N - y_{N-1})
\end{aligned}
$$

The integration over $z_1, \ldots, z_{N-1}$ can then be preformed analytically using the identity

$$
\begin{aligned}
&\int dz_j e^{-i/\hbar \varepsilon \left[m/\varepsilon^2 (y_{j+1} - 2y_j + y_{j-1}) + V'(y_j) \right] z_j} \tag{1.54} \\
&= \frac{2\pi\hbar}{\varepsilon} \delta \left[\frac{m}{\varepsilon^2} (y_{j+1} - 2y_j + y_{j-1}) + V'(y_j) \right]
\end{aligned}
$$

In the limit of $N \to \infty$ ($\varepsilon \to 0$),

$$
\varepsilon \, z_0 \left[\frac{m}{\varepsilon^2} (y_1 - y_0) - V'(y_0) \right] \to z_0 p_0 \tag{1.55}
$$

and

$$
\varepsilon \, z_N \, \frac{m}{\varepsilon^2} (y_N - y_{N-1}) \to z_N p_N \tag{1.56}
$$

where $p_0/m = \lim_{\varepsilon \to 0} (y_1 - y_0)/\varepsilon$ and $p_N/m = \lim_{\varepsilon \to 0} (y_N - y_{N-1})/\varepsilon$. Changing the integration variables from $y_1, \ldots, y_{N-1}$ to $f_1, \ldots, f_{N-1}$, where

$$
f_j = \frac{m}{\varepsilon^2} (y_{j+1} - 2y_j + y_{j-1}) + V'(y_j), \tag{1.57}
$$

and integrating over the $f_1, \ldots, f_{N-1}$ leads to the following approximation

$$
\begin{aligned}
C(t) &= \frac{1}{2\pi\hbar} \int dy_0 \int dy_t \int dz_0 \int dz_t \left| \frac{\partial p_0}{\partial y_t} \right| \tag{1.58} \\
&\quad \times \langle y_0 + z_0/2 | \, e^{-\beta \widehat{H}} \hat{A} \, | y_0 - z_0/2 \rangle \tag{1.59} \\
&\quad \times \langle y_t - z_t/2 | \, \hat{B} \, | y_t + z_t/2 \rangle \, e^{-i p_0 z_0 / \hbar} e^{i p_t z_t / \hbar} \tag{1.60}
\end{aligned}
$$

Here, the limit $N \to \infty$ has been explicitly been included such that $y_N \to y_t$ and $z_N \to z_t$. It should also be noted that $y_t = y_t(y_0, p_0)$ follows a classical trajectory. This due to the following

$$f_j = \frac{m}{\varepsilon^2}\left(y_{j+1} - 2y_j + y_{j-1}\right) + V'(y_j) = 0 \tag{1.61}$$

$$\stackrel{N \to \infty}{\to} m\frac{d^2}{dt^2}y(t) = -V'(y_t) \tag{1.62}$$

Lastly, changing the integration variable y_t into p_0 and using the definition of the Wigner transform

$$A_w(x, p) = \int d\Delta e^{-ip\Delta/\hbar} \langle x + \Delta/2|\, \hat{A}\, |x - \Delta/2\rangle \tag{1.63}$$

yield the LSC approximation to a quantum mechanical TCF:

$$C(t) \approx \frac{1}{2\pi\hbar} \int dy_0 \int p_0 \left[e^{-\beta\hat{H}}\hat{A}\right]_W (y_0, p_0) B_W(y_t^{Cl}, p_t^{Cl}) \tag{1.64}$$

where y_t^{Cl} and p_t^{Cl} are propagated classically from initial state $\{y_0, p_0\}$. The LSC approximation can provide a computationally feasible way to calculate quantum mechanical time correlation functions because all of the dynamics are propagated classically. Given some initial quantum mechanical distribution of positions and momenta, determined by the Wigner transform $\left[e^{-\beta\hat{H}}\hat{A}\right]_W$, the positions and momenta can be propagated classically, which is quite computationally feasible for liquids simulations. The Wigner transform, $\left[e^{-\beta\hat{H}}\hat{A}\right]_W$, cannot be calculated using standard integral solving methods due the sign problem resulting from the highly oscillatory exponential term, $e^{-ip\Delta/\hbar}$. This means that an alternate method must be used to solve the sign problem if using the LSC approximation to solve a quantum mechanical TCF.

1.8 Semiclassical Force-Force Correlation Function

Calculating the FFCF using a LSC approach will require some sort of strategy to avoid the sign problem resulting from the Wigner transform in Eq. (1.64). One way to solve this problem is to approximate the Wigner transform with the goal of solving it analytically. This is the approach taken by Shi and Geva in their development of a LSC expression to the FFCF[134].

The LSC approximation to the FFCF is given by

$$C(t) \approx \frac{1}{Z_b} \frac{1}{(2\pi\hbar)^N} \int d\mathbf{Q_0} \int d\mathbf{P_0} \left[\delta\hat{F} e^{-\beta\hat{H}_b} \right]_W (\mathbf{Q_0}, \mathbf{P_0}) \delta F_W(\mathbf{Q}_t^{(Cl)}, \mathbf{P}_t^{(Cl)}) , \quad (1.65)$$

where,

$$\delta F_W(\mathbf{Q}_t^{(Cl)}, \mathbf{P}_t^{(Cl)}) = F(\mathbf{Q}_t^{(Cl)}) - \langle F(\mathbf{Q_0}) \rangle_0 , \quad (1.66)$$

and

$$\left[\delta\hat{F} e^{-\beta\hat{H}_b} \right]_W (\mathbf{Q_0}, \mathbf{P_0}) = \int d\mathbf{\Delta} e^{-i\mathbf{P_0}\mathbf{\Delta}/\hbar} \langle \mathbf{Q_0} + \mathbf{\Delta}/2 | e^{-\beta\hat{H}_b} | \mathbf{Q_0} - \mathbf{\Delta}/2 \rangle \delta F(\mathbf{Q_0} + \mathbf{\Delta}/2)$$
$$(1.67)$$

To solve the Wigner transform in Eq. (1.67), it is useful to preform a quadratic expansion of the potential energy of the bath, $V(\mathbf{Q})$, around an arbitrary point $\mathbf{Q} = \mathbf{Q_0}$:

$$\begin{aligned}
V(\mathbf{Q}) &\approx V(\mathbf{Q_0}) + \sum_{k=1}^{N} \left. \frac{\partial V}{\partial Q^{(k)}} \right|_{\mathbf{Q}=\mathbf{Q_0}} \left[Q^{(k)} - Q_0^{(k)} \right] \\
&+ \frac{1}{2} \sum_{k=1}^{N} \sum_{l=1}^{N} \left. \frac{\partial^2 V}{\partial Q^{(k)} \partial Q^{(l)}} \right|_{\mathbf{Q}=\mathbf{Q_0}} \left[Q^{(k)} - Q_0^{(k)} \right] \left[Q^{(l)} - Q_0^{(l)} \right] \quad (1.68)
\end{aligned}$$

The quadratic term in Eq. (1.68) is then rewritten in terms of mass-weighted coordinates, $\left\{ \sqrt{M^{(k)}} \left[Q^{(k)} - Q_0^{(k)} \right] \right\}$, and Hessian matrix elements,

$$\mathcal{H}_{k,l} = \frac{1}{\sqrt{M^{(k)} M^{(l)}}} \left. \frac{\partial^2 V}{\partial Q^{(k)} \partial Q^{(l)}} \right|_{\mathbf{Q}=\mathbf{Q_0}} , \quad (1.69)$$

followed by a normal mode transformation:

$$\frac{1}{2}\sum_{k=1}^{N}\sum_{l=1}^{N}\frac{\partial^2 V}{\partial Q^{(k)}\partial Q^{(l)}}\bigg|_{\mathbf{Q}=\mathbf{Q_0}}\left[Q^{(k)}-Q_0^{(k)}\right]\left[Q^{(l)}-Q_0^{(l)}\right]$$

$$=\frac{1}{2}\sum_{k=1}^{N}\sum_{l=1}^{N}\mathcal{H}_{k,l}\left(\sqrt{M^{(k)}}\left[Q^{(k)}-Q_0^{(k)}\right]\right)\left(\sqrt{M^{(l)}}\left[Q^{(l)}-Q_0^{(l)}\right]\right)$$

$$=\frac{1}{2}\sum_{k=1}^{N}(\Omega^{(k)})^2\left[Q_n^{(k)}\right]^2\ . \tag{1.70}$$

In Eq. (1.70),

$$Q_n^{(k)}=\sum_{l=1}^{N}T_{l,k}\sqrt{M^{(l)}}\left[Q^{(l)}-Q_0^{(l)}\right] \tag{1.71}$$

are the mass-weighted normal mode coordinates, and $\{(\Omega^{(k)})^2\}$ are the eigenvalues of the Hessian matrix, $\{\mathcal{H}_{k,l}\}$. Rewriting the linear term in Eq. (1.68) and the kinetic energy of the bath in terms of the normal mode coordinates and momenta leads to the local harmonic approximation (LHA) of the quantum-mechanical bath Hamiltonian around $\mathbf{Q}=\mathbf{Q_0}$:

$$\hat{H}_b\approx\sum_{k=1}^{N}\frac{1}{2}\left(\hat{P}_n^{(k)}\right)^2+V(\mathbf{Q_0})+\sum_{k=1}^{N}G_n^{(k)}\hat{Q}_n^{(k)}+\frac{1}{2}\sum_{k=1}^{N}(\Omega^{(k)})^2\left[\hat{Q}_n^{(k)}\right]^2\ , \tag{1.72}$$

where

$$\hat{P}_n^{(k)}(\mathbf{Q_0})=\sum_{l=1}^{N}T_{l,k}(M^{(l)})^{-1/2}\hat{P}^{(l)} \tag{1.73}$$

and

$$G_n^{(k)}(\mathbf{Q_0})=\sum_{l=1}^{N}T_{l,k}(M^{(l)})^{-1/2}\frac{\partial V}{\partial Q^{(l)}}\bigg|_{\mathbf{Q}=\mathbf{Q_0}}\ . \tag{1.74}$$

In order to proceed, Eq. (1.67) is rewritten in the following way:

$$\begin{aligned}\left[\delta\hat{F}e^{-\beta\hat{H}_b}\right]_W(\mathbf{Q_0},\mathbf{P_0})&=\langle\mathbf{Q_0}|e^{-\beta\hat{H}_b}|\mathbf{Q_0}\rangle\\&\times\int\mathbf{d\Delta}e^{-i\mathbf{P_0\Delta}/\hbar}\frac{\langle\mathbf{Q_0}+\mathbf{\Delta}/2|e^{-\beta\hat{H}_b}|\mathbf{Q_0}-\mathbf{\Delta}/2\rangle}{\langle\mathbf{Q_0}|e^{-\beta\hat{H}_b}|\mathbf{Q_0}\rangle}\\&\times\delta F(\mathbf{Q_0}+\mathbf{\Delta}/2)\ .\end{aligned} \tag{1.75}$$

The LHA will not be applied to the $\langle \mathbf{Q_0}|e^{-\beta \hat{H}_b}|\mathbf{Q_0}\rangle$ factor preceding the integral (this is essential if the resulting approximation is to yield the correct classical limit and coincide with the exact result at $t = 0$ - see below). Instead the LHA is applied to the ratio, $\langle \mathbf{Q_0} + \mathbf{\Delta}/2|e^{-\beta \hat{H}_b}|\mathbf{Q_0} - \mathbf{\Delta}/2\rangle / \langle \mathbf{Q_0}|e^{-\beta \hat{H}_b}|\mathbf{Q_0}\rangle$ using the following identity (C is a proportionality constant that does not depend on Q_1 and Q_2),

$$\langle Q_1|e^{-\beta[\hat{P}^2/2+\Omega^2\hat{Q}^2/2]}|Q_2\rangle = C \exp \left\{ \begin{array}{c} -\frac{\Omega}{2\hbar}\frac{1}{\sinh(\beta\hbar\Omega)} \\ \times [\cosh(\beta\hbar\Omega)(Q_1^2 + Q_2^2) - 2Q_1Q_2] \end{array} \right\} , \quad (1.76)$$

leading to the following approximation:

$$\frac{\langle \mathbf{Q_0} + \mathbf{\Delta}/2|e^{-\beta \hat{H}_b}|\mathbf{Q_0} - \mathbf{\Delta}/2\rangle}{\langle \mathbf{Q_0}|e^{-\beta \hat{H}_b}|\mathbf{Q_0}\rangle} \approx \exp\left[-\sum_{j=1}^{N} \alpha^{(j)}(\Delta_n^{(j)}/2)^2 \right] , \quad (1.77)$$

where,

$$\Delta_n^{(j)} = \sum_{k=1}^{N} T_{k,j}\sqrt{M^{(k)}}\Delta^{(k)} \quad (1.78)$$

and

$$\alpha^{(j)} = \frac{\Omega^{(j)}}{\hbar} \coth\left[\beta\hbar\Omega^{(j)}/2\right] . \quad (1.79)$$

$\alpha^{(j)}$ in Eq. (1.79) is real and positive when $[\Omega^{(j)}]^2 > 0$. Some of the normal mode frequencies can be imaginary ($[\Omega^{(j)}]^2 < 0$), in which case, $\Omega^{(j)}$ in Eq. (1.79) can be replaced by $i\Omega^{(j)}$, where $\Omega^{(j)}$ is real and positive. In this case, $\hbar\alpha^{(j)} \rightarrow \Omega^{(j)} \cot\left[\beta\hbar\Omega^{(j)}/2\right]$ is still real and positive as long as $\beta\hbar\Omega^{(j)} > \pi$. In actual applications, unusable values of $\alpha^{(j)}$ are very rare (typically showing up less than once per 1000 randomly sampled configurations).

In order to solve Eq. (1.67) analytically, the $\mathbf{\Delta}$ dependence of the force, $\delta F(\mathbf{Q_0} + \mathbf{\Delta}/2)$ needs to be understood. To this end, it is assume that $\delta F(\mathbf{Q_0} + \mathbf{\Delta}/2)$ can also

be approximated by its quadratic expansion, in terms of $\mathbf{\Delta}/2$ around $\mathbf{Q} = \mathbf{Q_0}$:

$$
\begin{aligned}
\delta F(\mathbf{Q_0} + \mathbf{\Delta}/2) &\approx \delta F(\mathbf{Q_0}) + \sum_{k=1}^{N} F'_k \frac{\Delta^{(k)}}{2} + \frac{1}{2} \sum_{k=1}^{N} \sum_{l=1}^{N} F''_{k,l} \frac{\Delta^{(k)}}{2} \frac{\Delta^{(l)}}{2} \\
&= \delta F(\mathbf{Q_0}) + \sum_{k=1}^{N} \tilde{F}'_k \frac{\Delta_n^{(k)}}{2} + \frac{1}{2} \sum_{k=1}^{N} \sum_{l=1}^{N} \tilde{F}''_{k,l} \frac{\Delta_n^{(k)}}{2} \frac{\Delta_n^{(l)}}{2} \ , \quad (1.80)
\end{aligned}
$$

where,

$$
F'_k = \left. \frac{\partial F}{\partial Q^{(k)}} \right|_{\mathbf{Q}=\mathbf{Q_0}} \ ; \ F''_{k,l} = \left. \frac{\partial^2 F}{\partial Q^{(k)} \partial Q^{(l)}} \right|_{\mathbf{Q}=\mathbf{Q_0}} \tag{1.81}
$$

and

$$
\tilde{F}'_k = \sum_{l=1}^{N} (M^{(l)})^{-1/2} T_{l,k} F'_l \ ; \ \tilde{F}''_{k,l} = \sum_{i=1}^{N} \sum_{j=1}^{N} (M^{(i)} M^{(j)})^{-1/2} T_{i,l} T_{j,k} F''_{i,j} \ . \tag{1.82}
$$

Substituting the approximations in Eq. (1.77) and Eq. (1.80) into Eq. (1.75), changing the integration variables from $\{\Delta^{(k)}\}$ to $\{\Delta_n^{(k)}\}$, and performing the Gaussian integral over $\{\Delta_n^{(k)}\}$ analytically, yields the following result:

$$
\left[\delta \hat{F} e^{-\beta \hat{H}_b} \right]_W = \langle \mathbf{Q_0} | e^{-\beta \hat{H}_b} | \mathbf{Q_0} \rangle \prod_{j=1}^{N} \left(\frac{4\pi}{M^{(j)} \alpha^{(j)}} \right)^{1/2} \tag{1.83}
$$

$$
\times \exp\left[-\frac{(P_{n,0}^{(j)})^2}{\hbar^2 \alpha^{(j)}} \right] \left[\delta F(\mathbf{Q_0}) + D(\mathbf{Q_0}, \mathbf{P_{n,0}}) \right] \ , \tag{1.84}
$$

where,

$$
D(\mathbf{Q_0}, \mathbf{P_{n,0}}) = -i \sum_{k=1}^{N} \frac{\tilde{F}'_k P_{n,0}^{(k)}}{\hbar \alpha^{(k)}} + \sum_{k=1}^{N} \frac{\tilde{F}''_{k,k}}{4\alpha^{(k)}} - \sum_{k,l=1}^{N} \frac{\tilde{F}''_{k,l} P_{n,0}^{(k)} P_{n,0}^{(l)}}{2\hbar^2 \alpha^{(k)} \alpha^{(l)}} \ . \tag{1.85}
$$

Substituting Eq. (1.83) back into Eq. (1.65), and changing the integration variables from $\{P_0^{(k)}\}$ to $\{P_{n,0}^{(k)}\}$ then leads to the LSC-LHA to the quantum mechanical FFCF:

$$
\begin{aligned}
C(t) &\approx \int d\mathbf{Q_0} \frac{\langle \mathbf{Q_0} | e^{-\beta \hat{H}_b} | \mathbf{Q_0} \rangle}{Z_b} \int d\mathbf{P_{n,0}} \prod_{j=1}^{N} \left(\frac{1}{\alpha^{(j)} \pi \hbar^2} \right)^{1/2} \exp\left[-\frac{(P_{n,0}^{(j)})^2}{\hbar^2 \alpha^{(j)}} \right] \\
&\quad \left[\delta F(\mathbf{Q_0}) + D(\mathbf{Q_0}, \mathbf{P_{n,0}}) \right] \delta F(\mathbf{Q}_t^{(Cl)})
\end{aligned} \tag{1.86}
$$

The classical limit of Eq. (1.86) coincides with the exact classical result. In order to see this note that in the classical limit:

$$\langle \mathbf{Q_0}|e^{-\beta \hat{H}_b}|\mathbf{Q_0}\rangle/Z_b \to e^{-V(\mathbf{Q_0})}/\int d\mathbf{Q_0}e^{-V(\mathbf{Q_0})}; (2)\alpha^{(j)} \to 2/\beta\hbar^2, \qquad (1.87)$$

since $\beta\hbar\Omega^{(j)} \ll 1$,

$$\sum_{j=1}^{N}(P_{n,0}^{(j)})^2/\hbar^2\alpha^{(j)} \to \beta\sum_{j=1}^{N}(P_{n,0}^{(j)})^2/2 \to \beta\sum_{j=1}^{N}(P_0^{(j)})^2/2M^{(j)}, \qquad (1.88)$$

and $D(\mathbf{Q_0}, \mathbf{P_{n,0}})$, Eq. (1.85), vanishes as $\hbar \to 0$. One is left averaging over the time correlation of the classical forces, $\delta F(\mathbf{Q_0})\delta F(\mathbf{Q}_t^{(Cl)})$.

Quantum effects enter the LSC-LHA-FFCF in several ways. The initial positions are sampled based on the exact quantum probability density,

$$\Pr(\mathbf{Q_0}) = \frac{\langle \mathbf{Q_0}|e^{-\beta \hat{H}_b}|\mathbf{Q_0}\rangle}{Z_b} = \frac{\langle \mathbf{Q_0}|e^{-\beta \hat{H}_b}|\mathbf{Q_0}\rangle}{\int d\mathbf{Q_0}\langle \mathbf{Q_0}|e^{-\beta \hat{H}_b}|\mathbf{Q_0}\rangle} , \qquad (1.89)$$

The initial (normal-mode) momenta are sampled based on a non-classical probability density,

$$\Pr(\mathbf{P_{n,0}}) = \prod_{j=1}^{N}\left(\frac{1}{\alpha^{(j)}\pi\hbar^2}\right)^{1/2} \exp\left[-\frac{(P_{n,0}^{(j)})^2}{\hbar^2\alpha^{(j)}}\right] . \qquad (1.90)$$

It should be noted that $\{\alpha^{(j)}\}$, and therefore $\Pr(\mathbf{P_{n,0}})$, depend parametrically on $\mathbf{Q_0}$. The term $D(\mathbf{Q_0}, \mathbf{P_{n,0}})$, which is referred to as the *delocalized force term*, Eq. (1.85), vanishes at the classical limit and has no classical analogue. It represents a purely quantum-mechanical effect that originates from the fact that $\hat{F}$ does not commute with $\hat{H}_b$, such that $\left(\hat{F}e^{-\beta\hat{H}_b}\right)_W \neq \left(\hat{F}\right)_W\left(e^{-\beta\hat{H}_b}\right)_W$. One may therefore view this purely quantum-mechanical term as representing the delocalized nature of the force at $t = 0$.

Eq. (1.86) provides a computationally feasible way to rigorously include quantum effects when calculating a FFCF and gives rise to the following algorithm for calculating the (approximate) quantum-mechanical FFCF:

1. Sample $\mathbf{Q_0}$, with the probability density of Eq. (1.89), via an imaginary-time path integral molecular-dynamics or Monte-Carlo simulation (PIMD and PIMC respectively), and calculate $F(\mathbf{Q_0})$.

2. Perform a LHA around each value of $\mathbf{Q_0}$, find the normal mode frequencies, $\{\Omega^{(k)}\}$, and transformation matrix, $\{T_{k,l}\}$, and evaluate $\{\alpha^{(k)}\}$, $\{\tilde{F}'_k(\mathbf{Q_0})\}$ and $\{\tilde{F}''_{k,l}(\mathbf{Q_0})\}$.

3. MC Sample the initial (normal-mode) momenta, $\{P_{n,0}^{(k)}\}$, based on the Gaussian probability density in Eq. (1.90).

4. Calculate $\mathbf{Q}_t^{(Cl)}$ via a classical MD simulation, for each set of initial positions and momenta, $\mathbf{Q_0}$ and $\mathbf{P_{n,0}}$, and time correlate $\delta F(\mathbf{Q}_t^{(Cl)})$ with $\delta F(\mathbf{Q_0})$ and $D(\mathbf{Q_0}, \mathbf{P_{n,0}})$.

1.9   Conclusion

The calculation of equilibrium observables in liquids can be done microscopically with knowledge of the systems partition function . The calculation of time dependent phenomena is a more difficult problem because there is no single quantity that can be used to calculate different observables. Instead each observable of interest must be related to a different TCF. The approaches to deriving TCF relationships to observable are numerous. One can use a linear response approach, where the system is assumed to be perturbed somehow and is then allowed to relax back to an unperturbed equilibrium. Among other quantities, this approach can be used to relate chemical reaction rate constants to the RF-TCF, providing a way to calculate chemical reaction rate constants on a time scale much smaller than the actual reaction

lifetimes. An empirical approach can also be taken, where one begins with a macroscopic expression and rewrites the equations in terms of microscopic properties, as is the case in the derivation of the VVCF for calculating diffusion constants. A quantum mechanical approach can also be taken. Beginning with assumptions about the system and the surrounding bath, vibrational relaxation can be treated using perturbation theory in order to relate the relaxation rate constant to the quantum mechanical FFCF.

Because quantum mechanical TCFs cannot be calculated exactly using currently available computational resources, the LSC approach provides a computationally feasible way to calculate the quantum mechanical FFCF. Here, the initial conditions are sampled quantum mechanically and the dynamics is then propagated classically. This leads to a situation where the major computational bottlenecks are in the initial sampling and not in the calculation of dynamics. Specifically, the calculation of the LSC-LHA FFCF involves preforming a normal mode analysis of the entire system (including the system and the solvent), at each set of sampled coordinates. This can be a very expensive calculation, but is not prohibitively expensive and thus still allows us to include quantum mechanical effects in our FFCF in a rigorous fashion.

CHAPTER II

Vibrational Energy Relaxation in Nonpolar Liquids

2.1 Introduction

Vibrational energy relaxation (VER) is the process by which an excited vibrational mode releases its excess energy into other intramolecular and/or intermolecular degrees of freedom (DOF). VER is prevalent in many systems of fundamental, technological and biological importance, and plays a central role in determining chemical reactivity.[7, 14, 20, 21, 35, 34, 106, 107, 108, 15, 16, 45, 86, 142, 105, 30, 8, 73, 127, 50, 48, 49, 44, 110, 103, 92, 65, 161, 115, 109, 129, 150, 149, 151, 104, 71, 160, 95, 94, 128, 42, 27, 31, 32, 74, 23, 22, 136, 77] Recent theoretical and computational studies of VER have been mostly based on the Landau-Teller formula,[105, 162, 72] which gives the VER rate constant in terms of the Fourier transform (FT), at the vibrational transition frequency, of the *quantum-mechanical* TCF of the fluctuating force exerted on the relaxing mode by the other DOF. Importantly, replacing the quantum-mechanical force-force correlation function (FFCF) (Eq. 1.41) by its classical counterpart (Eq. 1.46) can only be justified in cases where the vibrational transition frequency is significantly smaller than $k_B T/\hbar$. Indeed, discrepancies by many orders of magnitude have been reported between experimentally measured

VER rates and those calculated based on purely classical molecular dynamics (MD) simulations when this condition is not met.[106, 5, 3, 26, 29, 140, 125, 126, 33, 4, 36, 139, 1, 28, 131, 25, 67] However, the exact calculation of real-time quantum-mechanical correlation functions for general anharmonic many-body systems remains far beyond the reach of currently available computer resources.[79] A popular approach for dealing with this difficulty in the case of VER calls for multiplying the classical VER rate constant by a frequency-dependent *quantum correction factor (QCF)*.[106, 5, 3, 26, 29, 140, 125, 126, 33, 4, 36, 139, 1, 28, 131, 25, 67] A variety of different approximate QCFs have been proposed in the literature. However, the choice of QCF is somewhat arbitrary and estimates obtained from different QCFs can differ by orders of magnitude. Thus, the development of more rigorous methods for computing VER rate constants is highly desirable.

In a series of recent papers, [134, 135, 61, 60, 97], a linearized semiclassical (LSC) approach has been proposed as a rigorous method for calculating the quantum mechanical FFCF. The LSC method is based on linearizing the forward-backward action in the path-integral expression for the quantum-mechanical FFCF with respect to the difference between the forward and backward paths.[133] The resulting LSC approximation for a real-time quantum-mechanical correlation function of the form:

$$C_{AB}(t) = Tr\left(\hat{A}e^{i\hat{H}t/\hbar}\hat{B}e^{-i\hat{H}t/\hbar}\right) \tag{2.1}$$

is given by Eq. 1.64, here rewritten as

$$C_{AB}^{LSC}(t) = \frac{1}{(2\pi\hbar)^N}\int d\mathbf{Q_0}\int d\mathbf{P_0}A_W\left(\mathbf{Q_0},\mathbf{P_0}\right)B_W\left(\mathbf{Q}_t^{(Cl)},\mathbf{P}_t^{(Cl)}\right)\,, \tag{2.2}$$

where, N is the number of DOF, $\mathbf{Q_0} = (Q_0^{(1)},\ldots,Q_0^{(N)})$ and $\mathbf{P_0} = (P_0^{(1)},\ldots,P_0^{(N)})$ are the corresponding coordinates and momenta, and is the Wigner transform of the

operator $\hat{A}$,[54] and, $\mathbf{Q}_t^{(Cl)} = \mathbf{Q}_t^{(Cl)}(\mathbf{Q_0}, \mathbf{P_0})$ and $\mathbf{P}_t^{(Cl)} = \mathbf{P}_t^{(Cl)}(\mathbf{Q_0}, \mathbf{P_0})$ are propagated *classically* with the initial conditions $\mathbf{Q_0}$ and $\mathbf{P_0}$.

The LSC approximation is known to be *exact* at $t = 0$, at the classical limit, and for harmonic systems. It also provides a convenient starting point for introducing computationally feasible schemes to calculate quantum-mechanical time correlation functions. The main disadvantage of the LSC approximation is that it can only capture quantum effects at short times.[145] However, it should be noted that in complex systems such as liquids, and in the case of high-frequency VER in particular, the quantities of interest are often dominated by the behavior of short-lived correlation functions at relatively short times.

In practice, applying the LSC approximation, Eq. (2.2), requires the calculation of the complex phase-space integrals underlying the Wigner transforms, Eq. (1.63). The numerical calculation of the integral in Eq. (1.63) can be extremely difficult in practice because of the oscillatory phase factor, $e^{-i\mathbf{P}\mathbf{\Delta}/\hbar}$, in the integrand. In the case of the standard FFCF, $\hat{A}$ and $\hat{B}$ in Eq. (2.2) correspond to $\delta\hat{F}e^{-\beta\hat{H}}/Z$ and $\delta\hat{F}$, respectively, where $\delta\hat{F} = \hat{F} - Tr\left[e^{-\beta\hat{H}}\hat{F}\right]/Z$, $\hat{F}$ corresponds to the force exerted on the relaxing mode by the bath, which consists of all the other DOF except for the relaxing mode, $\hat{H}$ is the free bath Hamiltonian and $Z = Tr\left[e^{-\beta\hat{H}}\right]$ is the free bath quantum partition function.

Neglecting centrifugal forces, which are often found to be of only minimal importance, $\hat{F}$ is a function of only the bath coordinates, one finds that $[F(\hat{\mathbf{Q}})]_W(\mathbf{Q}_t^{(Cl)})$ reduces into its classical counterpart, $F(\mathbf{Q}_t^{(Cl)})$. Hence, the only remaining computational challenge has to do with calculating the following Wigner transform:

$$[\delta F(\hat{\mathbf{Q}})e^{-\beta\hat{H}}]_W(\mathbf{Q_0}, \mathbf{P_0}) = \int \mathbf{d\Delta} e^{-i\mathbf{P_0}\cdot\mathbf{\Delta}/\hbar}\langle\mathbf{Q_0} + \frac{\mathbf{\Delta}}{2}|e^{-\beta\hat{H}}|\mathbf{Q_0} - \frac{\mathbf{\Delta}}{2}\rangle\delta F\left(\mathbf{Q_0} + \frac{\mathbf{\Delta}}{2}\right) .$$

$$(2.3)$$

Within the original LSC local harmonic approximation (LHA) method,[134] one proceeds by introducing the following two additional approximations:

1. Evaluating $\langle \mathbf{Q_0} + \frac{\boldsymbol{\Delta}}{2}|e^{-\beta\hat{H}}|\mathbf{Q_0} - \frac{\boldsymbol{\Delta}}{2}\rangle / \langle \mathbf{Q_0}|e^{-\beta\hat{H}}|\mathbf{Q_0}\rangle$ within the framework of the LHA, which amounts to expanding the Hamiltonian to second order around $\mathbf{Q_0}$.

2. Expanding $F\left(\mathbf{Q_0} + \boldsymbol{\Delta}/2\right)$ to second order in terms of $\boldsymbol{\Delta}$ around $\mathbf{Q_0}$.

The resulting Gaussian integral over $\boldsymbol{\Delta}$ can then be solved analytically to yield the LSC-LHA approximation for the FFCF:

$$C^{LHA-LSC}(t) = \int d\mathbf{Q_0} \frac{\langle \mathbf{Q_0}|e^{-\beta\hat{H}}|\mathbf{Q_0}\rangle}{Z} \int d\mathbf{P_{n,0}} \prod_{j=1}^{N} \left(\frac{1}{\alpha^{(j)}\pi\hbar^2}\right)^{1/2} \exp\left[-\frac{(P_{n,0}^{(j)})^2}{\hbar^2\alpha^{(j)}}\right]$$

$$[\delta F(\mathbf{Q_0}) + D(\mathbf{Q_0}, \mathbf{P_{n,0}})] \, \delta F(\mathbf{Q}_t^{(Cl)}) \,. \tag{2.4}$$

Here,

$$\mathbf{P}_n = \mathbf{P}_n(\mathbf{Q_0}) = \left(P_n^{(1)}(\mathbf{Q_0}), ..., P_n^{(N)}(\mathbf{Q_0})\right), \tag{2.5}$$

where $\left\{P_n^{(k)}(\mathbf{Q_0}) = \sum_{l=1}^{N} T_{l,k}(M^{(l)})^{-1/2}P^{(l)}\right\}$ are the normal mode momenta that emerge from diagonalizing the Hessian matrix underlying the quadratic expansion of the bath potential energy around $\mathbf{Q} = \mathbf{Q_0}$ and

$$\alpha^{(j)} = \alpha^{(j)}(\mathbf{Q_0}) = \frac{\Omega^{(j)}(\mathbf{Q_0})}{\hbar} \coth\left[\frac{\beta\hbar\Omega^{(j)}(\mathbf{Q_0})}{2}\right], \tag{2.6}$$

where $\{(\Omega^{(k)})^2(\mathbf{Q_0})\}$ are the eigenvalues of the Hessian matrix. The term $D(\mathbf{Q_0}, \mathbf{P_{n,0}})$ is given by [134]:

$$D(\mathbf{Q_0}, \mathbf{P_{n,0}}) = -i \sum_{k=1}^{N} \frac{\tilde{F}'_k P_{n,0}^{(k)}}{\hbar\alpha^{(k)}} + \sum_{k=1}^{N} \frac{\tilde{F}''_{k,k}}{4\alpha^{(k)}} - \sum_{k,l=1}^{N} \frac{\tilde{F}''_{k,l}P_{n,0}^{(k)}P_{n,0}^{(l)}}{2\hbar^2\alpha^{(k)}\alpha^{(l)}} \tag{2.7}$$

and its calculation requires as input the first and second derivatives of the force with respect to the bath coordinates, that is

$$\tilde{F}'_k = \sum_{l=1}^{N}(M^{(l)})^{-1/2}T_{l,k}F'_l \;;\; \tilde{F}''_{k,l} = \sum_{i=1}^{N}\sum_{j=1}^{N}(M^{(i)}M^{(j)})^{-1/2}T_{i,l}T_{j,k}F''_{i,j} \,. \tag{2.8}$$

where

$$F'_k = \left. \frac{\partial F}{\partial Q^{(k)}} \right|_{\mathbf{Q}=\mathbf{Q_0}} \quad ; \quad F''_{k,l} = \left. \frac{\partial^2 F}{\partial Q^{(k)} \partial Q^{(l)}} \right|_{\mathbf{Q}=\mathbf{Q_0}} \quad . \tag{2.9}$$

Quantum effects enter the expression for $C^{LHA-LSC}(t)$, Eq. (2.4), in two ways:

1. Nonclassical initial sampling of the bath coordinates and momenta.

2. The nonclassical term $D(\mathbf{Q_0}, \mathbf{P_{n,0}})$ which can be shown to vanish in the classical limit.

Both effects were found to be important for the applications considered in Refs. [134, 135, 61, 60, 97]. Importantly, the nonclassical term $D(\mathbf{Q_0}, \mathbf{P_{n,0}})$, which can be traced back to the first and second order terms in the above mentioned expansion of $F(\mathbf{Q_0} + \mathbf{\Delta}/2)$ in powers of $\mathbf{\Delta}$, was found to play an important role in enhancing the VER rate. Although the calculation of the first and second derivatives of the bath-induced force with respect to the bath coordinates, which is required as input for calculating $D(\mathbf{Q_0}, \mathbf{P_{n,0}})$, is in principle straightforward, in practice it can become increasingly cumbersome with the increasing complexity of the force fields. Furthermore, unlike the second derivatives required for calculating the Hessian matrix underlying the LHA, the above mentioned force derivatives are usually not part of the output of standard packages for performing MD simulations. In this chapter we develop an alternative scheme for calculating VER rate constants which, while still based on LSC and LHA, avoids the above mentioned expansion of the bath-induced force in terms of $\mathbf{\Delta}$ and as a result is more accurate and does not require force derivatives as input.

2.2 Theory

Consider the following general quantum-mechanical Hamiltonian of a vibrational mode linearly coupled to a bath:

$$\hat{H}_{tot} = \frac{\hat{p}^2}{2\mu} + v\left(\hat{q}\right) + \sum_{j=1}^{N} \frac{(\hat{P}^{(j)})^2}{2M^{(j)}} + V\left(\hat{\mathbf{Q}}\right) - \hat{q}F\left(\hat{\mathbf{Q}}\right) \ . \tag{2.10}$$

Here, $\hat{q}$, $\hat{p}$, μ and $v\left(\hat{q}\right)$ are the relaxing mode coordinate, momentum, reduced mass and bath-free vibrational potential; $\hat{\mathbf{Q}}$, $\hat{\mathbf{P}}$, $\left\{M^{(1)}, ..., M^{(N)}\right\}$ and $V\left(\hat{\mathbf{Q}}\right)$ are the coordinates, momenta, masses and potential energy of the bath DOF and $F\left(\hat{\mathbf{Q}}\right)$ is the potential force exerted by the bath on the relaxing mode.

The standard expression of the population relaxation rate constant between the first-excited and ground vibrational states is usually given in terms of the FT, at the transition frequency, of the standard FFCF [105, 162, 72]:

$$k_{1\leftarrow 0} = \frac{1}{2\mu\hbar\omega_{10}}\tilde{C}(\omega_{10}) \ . \tag{2.11}$$

Here, ω_{10} is the transition frequency and

$$\tilde{C}(\omega) = \int_{-\infty}^{\infty} dt e^{i\omega t} C(t) \tag{2.12}$$

is the FT of the FFCF, given by

$$C(t) = \frac{1}{Z}Tr\left[\delta\hat{F}e^{-\beta\hat{H}}e^{i\hat{H}t/\hbar}\delta\hat{F}e^{-i\hat{H}t/\hbar}\right] \ , \tag{2.13}$$

where $\hat{H} = \sum_{j=1}^{N}\frac{(\hat{P}^{(j)})^2}{2M^{(j)}} + V\left(\mathbf{Q}\right)$ is the free bath Hamiltonian.

The population relaxation rate constant k_{10} can also be cast in terms of a variety of alternative expressions which are completely equivalent to Eq. (2.11). One such expression, which will be particularly useful for our purpose, can be based on the symmetrized FFCF given by:

$$C_s(t) = \frac{1}{Z}Tr\left[e^{-\beta\hat{H}/2}\delta\hat{F}e^{-\beta\hat{H}/2}e^{i\hat{H}t/\hbar}\delta\hat{F}e^{-i\hat{H}t/\hbar}\right] \ . \tag{2.14}$$

The fact that the FTs of $C_s(t)$ and $C(t)$ are related in a simple manner, namely

$$\tilde{C}(\omega) = e^{\beta\hbar\omega/2}\tilde{C}_s(\omega) \ , \tag{2.15}$$

then allows us to obtain the following alternative expression for the population relaxation rate constant:

$$k_{1\leftarrow 0} = \frac{1}{2\mu\hbar\omega_{10}}e^{\beta\hbar\omega_{10}/2}\tilde{C}_s(\omega_{10}) \ . \tag{2.16}$$

In the next step, we attempt to evaluate $C_s(t)$ within the framework of the LSC and LHA approximations. We first note that within the LSC approximation [see Eq. (2.2)]:

$$C_s^{LSC}(t) = \frac{1}{(2\pi\hbar)^N}\int d\mathbf{Q_0}\int d\mathbf{P_0}\left[e^{-\beta\hat{H}/2}\delta\hat{F}e^{-\beta\hat{H}/2}\right]_W(\mathbf{Q_0},\mathbf{P_0})\,\delta F\left(\mathbf{Q}_t^{(Cl)}\right) \ . \tag{2.17}$$

Clearly, the main challenge in calculating $C_s^{LSC}(t)$ lies in evaluating the following Wigner transform:

$$\left[e^{-\beta\hat{H}/2}\delta\hat{F}e^{-\beta\hat{H}/2}\right]_W(\mathbf{Q_0},\mathbf{P_0})$$
$$= \int d\mathbf{\Delta}\,e^{-i\mathbf{P_0}\mathbf{\Delta}/\hbar}\left\langle\mathbf{Q_0}+\frac{\mathbf{\Delta}}{2}\right|e^{-\beta\hat{H}/2}\delta\hat{F}e^{-\beta\hat{H}/2}\left|\mathbf{Q_0}-\frac{\mathbf{\Delta}}{2}\right\rangle . \tag{2.18}$$

Using the closure relation $\int d\mathbf{Q'}|\mathbf{Q'}\rangle\langle\mathbf{Q'}| = \hat{1}$ we can rewrite the matrix element in the integrand in the following from:

$$\left\langle\mathbf{Q_0}+\frac{\mathbf{\Delta}}{2}\right|e^{-\beta\hat{H}/2}\delta\hat{F}e^{-\beta\hat{H}/2}\left|\mathbf{Q_0}-\frac{\mathbf{\Delta}}{2}\right\rangle$$
$$= \int d\mathbf{Q'}\delta F(\mathbf{Q'})\left\langle\mathbf{Q_0}+\frac{\mathbf{\Delta}}{2}\right|e^{-\beta\hat{H}/2}\left|\mathbf{Q'}\right\rangle\left\langle\mathbf{Q'}\right|e^{-\beta\hat{H}/2}\left|\mathbf{Q_0}-\frac{\mathbf{\Delta}}{2}\right\rangle$$
$$= \int d\mathbf{Q'}\delta F(\mathbf{Q'})\left\langle\mathbf{Q_0}\right|e^{-\beta\hat{H}/2}\left|\mathbf{Q'}\right\rangle\left\langle\mathbf{Q'}\right|e^{-\beta\hat{H}/2}\left|\mathbf{Q_0}\right\rangle$$
$$\frac{\left\langle\mathbf{Q_0}+\frac{\mathbf{\Delta}}{2}\right|e^{-\beta\hat{H}/2}\left|\mathbf{Q'}\right\rangle\left\langle\mathbf{Q'}\right|e^{-\beta\hat{H}/2}\left|\mathbf{Q_0}-\frac{\mathbf{\Delta}}{2}\right\rangle}{\left\langle\mathbf{Q_0}\right|e^{-\beta\hat{H}/2}\left|\mathbf{Q'}\right\rangle\left\langle\mathbf{Q'}\right|e^{-\beta\hat{H}/2}\left|\mathbf{Q_0}\right\rangle} \tag{2.19}$$

The ratio in the integrand,

$$\frac{\langle \mathbf{Q}_0 + \frac{\boldsymbol{\Delta}}{2} | e^{-\beta\hat{H}/2} | \mathbf{Q}' \rangle \langle \mathbf{Q}' | e^{-\beta\hat{H}/2} | \mathbf{Q}_0 - \frac{\boldsymbol{\Delta}}{2} \rangle}{\langle \mathbf{Q}_0 | e^{-\beta\hat{H}/2} | \mathbf{Q}' \rangle \langle \mathbf{Q}' | e^{-\beta\hat{H}/2} | \mathbf{Q}_0 \rangle} \ , \tag{2.20}$$

can then be evaluated within the LHA. To this end, we expand the bath potential energy to second order around the yet to be specified point $\mathbf{Q} = \mathbf{Q}_*$, and then analytically solve the resulting Gaussian integral over $\boldsymbol{\Delta}$, to obtain the LSC-LHA approximation of $C_s(t)$:

$$\begin{aligned} C_s^{LHA-LSC}(t) &= \int d\mathbf{Q_0} \int d\mathbf{Q}' \frac{\langle \mathbf{Q}_0 | e^{-\beta\hat{H}/2} | \mathbf{Q}' \rangle \langle \mathbf{Q}' | e^{-\beta\hat{H}/2} | \mathbf{Q}_0 \rangle}{Z} \\ &\quad \int d\mathbf{P_n} \prod_{j=1}^{N} \left(\frac{1}{\alpha^{(j)}\pi\hbar^2} \right)^{1/2} \exp\left[-\frac{(P_n^{(j)})^2}{\hbar^2\alpha^{(j)}} \right] \times \\ &\quad \delta F(\mathbf{Q}') \delta F(\mathbf{Q}_t^{(Cl)}[\mathbf{Q_0},\mathbf{P_0}]) \end{aligned} \tag{2.21}$$

Here, $\mathbf{P}_n = \mathbf{P}_n(\mathbf{Q}_*) = \left(P_n^{(1)}(\mathbf{Q}_*), ..., P_n^{(N)}(\mathbf{Q}_*) \right)$ are the normal mode momenta that emerge from diagonalizing the Hessian matrix underlying the quadratic expansion of the bath potential energy around $\mathbf{Q} = \mathbf{Q}^*$ and $\{\alpha^{(j)}\}$ are the same as in Eq. (2.6), where $\{(\Omega^{(k)})^2\}$ are the eigenvalues of the Hessian matrix.

Eq. (2.21) represents the main theoretical result of this work. Similarly to Eq. (2.4), it reduces to the classical FFCF in the classical limit. However, it should be noted that the high-frequency FT of the standard and symmetrized FFCFs is expected to exhibit nonclassical behavior, and therefore differs quite significantly. It should also be noted that in deriving Eq. (2.21) we did not resort to expanding $\delta F(\mathbf{Q}')$ to second order around $\mathbf{Q}_0$ (or any other point). In this respect, Eq. (2.21) is in fact less approximate than Eq. (2.4). At the same time calculating Eq. (2.21) does not require force derivatives as input! One consequence of this is that the $D(\mathbf{Q_0}, \mathbf{P_{n,0}})$ term, Eq. (2.7), which played such an important role in accounting for the nonclassical behavior of the standard FFCF, is no longer present. Instead, the

nonclassical behavior of the symmetrized FFCF is accounted for by the following attributes:

1. Nonclassical sampling of bath coordinates and momenta (similar to that in Eq. (2.4)).

2. The initial force is not calculated at the initial position used to generate the classical trajectory leading to the force at a later time t.

3. The factor $e^{\beta\hbar\omega_{10}/2}$ (see Eq. (2.16)) which actually coincides with the so-called Schofield QCF.[131]

It should also be noted that up to this point, we have not specified the point $\mathbf{Q}_*$ around which the LHA is performed. This choice will obviously affect the actual frequencies of the instantaneous normal modes and thereby the values of $\alpha^{(j)}$, which will in turn affect the values of the initial momenta that are sampled and the resulting $C_s^{LHA-LSC}(t)$. Below, we will consider three possible and rather natural choices for $\mathbf{Q}_*$, namely:

- $\mathbf{Q}_* = \mathbf{Q}_0$, which corresponds to the initial configuration for the classical trajectory that generates the force at time t, $\delta F(\mathbf{Q}_t^{(Cl)})$.

- $\mathbf{Q}_* = \mathbf{Q}'$, which corresponds to the configuration used for calculating the initial force, $\delta F(\mathbf{Q}')$.

- $\mathbf{Q}_* = \mathbf{Q}_c$, which correspond to the centroid configuration of the cyclic imaginary time path integral.

It should be noted that the distinction between the first two choices is absent from Eq. (2.4) since in this equation the initial force is calculated at the initial

configuration which is used as an initial condition for the classical trajectory. As will be shown below, at least for the applications that we have considered, performing the LHA around $\mathbf{Q}'$ appear to yield results that are similar to these obtained via Eq. (2.4) and also compare well with experiment.

The calculations of $C_s^{LHA-LSC}(t)$ reported below were based on Eq. (2.21) and carried out following the algorithm:

1. Perform an imaginary-time path integral molecular-dynamics or Monte-Carlo simulation (PIMD and PIMC respectively), [6, 10] and use it to sample the initial configuration, $\mathbf{Q_0}$, and the configuration at which the initial force is calculated, $\mathbf{Q}'$. To this end, it should be noted that within the context of a PIMD/PIMC simulation, each DOF is represented by a ring polymer of P beads labeled $0, 1, 2, ..., P-1$. Assuming that P is even, $\mathbf{Q_0}$ is identified with the configuration of the beads labeled 0, while $\mathbf{Q}'$ is identified with the configuration of the beads labeled $P/2$.

2. Perform a LHA around either $\mathbf{Q}'$ or $\mathbf{Q}_0$ or $\mathbf{Q}_c$, find the normal mode frequencies, $\{\Omega^{(k)}\}$, and corresponding transformation matrix, $\{T_{l,k}\}$, and use it to calculate $\{\alpha^{(k)}\}$ and sample the initial (normal-mode) momenta, $\{P_n^{(k)}\}$.

3. Calculate $\mathbf{Q}_t^{(Cl)}$ via a classical MD simulation for each sampled initial configuration $\mathbf{Q_0}$ and normal mode momenta $\mathbf{P_{n,0}}$, and time correlate $\delta F(\mathbf{Q}_t^{(Cl)})$ with $\delta F(\mathbf{Q}')$.

4. Repeat steps 1-3 until reaching the desired convergence.

2.3   Applications

2.3.1   Exponential Coupling to a Harmonic Bath

The first model that we will consider involves a bath consisting of uncoupled harmonic oscillators of different frequencies,

$$\hat{H} = \sum_{j=1}^{N} \left(\frac{(\hat{P}^{(j)})^2}{2M^{(j)}} + \frac{1}{2}M^{(j)}(\omega^{(j)})^2(\hat{Q}^{(j)})^2 \right) , \tag{2.22}$$

and a force which is exponential in the bath coordinates,

$$\hat{F}(\hat{\mathbf{Q}}) = \exp\left[\sum_{j=1}^{N} c^{(j)} \sqrt{\frac{2M^{(j)}\omega^{(j)}}{\hbar}} \hat{Q}^{(j)} . \right] . \tag{2.23}$$

The exact quantum-mechanical FFCF can be obtained analytically for this model and is given by [99, 120, 28]:

$$C(t) = e^{B(0)}(e^{B(t)} - 1) , \tag{2.24}$$

where

$$B(t) = \int_0^\infty d\omega \Gamma(\omega)\{[n(\omega) + 1]e^{-i\omega t} + n(\omega)e^{i\omega t}\} , \tag{2.25}$$

$$\Gamma(\omega) = \sum_{k=1}^{N} \left(c^{(k)}\right)^2 \delta(\omega - \omega^{(k)}) \tag{2.26}$$

and $n(\omega) = [\exp(\beta\hbar\omega) - 1]^{-1}$.

It should be noted that the LSC approximation is exact when the system is harmonic. Thus, for this model, Eq. (2.21) actually coincides with the exact symmetrized FFCF. To this end, we note that for the bath harmonic Hamiltonian in Eq. (2.22) one can show that:

$$\frac{1}{Z} \langle \mathbf{Q}_0 | e^{-\beta\hat{H}/2} | \mathbf{Q}' \rangle \langle \mathbf{Q}' | e^{-\beta\hat{H}/2} | \mathbf{Q}_0 \rangle =$$

$$\prod_{j=1}^{N} \left(\frac{M^{(j)}\omega^{(j)}}{\pi\hbar} \right) \exp\left[-\alpha^{(j)} \left(Q_0^{(j)}\right)^2 + (Q'^{(j)})^2 \right] \tag{2.27}$$

$$\times \exp\left[-\frac{M^{(j)}(\omega^{(j)})}{\hbar} \frac{2}{\sinh\left(\beta\hbar\omega^{(j)}/2\right)} Q_0^{(j)} Q'^{(j)} \right] . \tag{2.28}$$

Substituting this result into Eq. (2.21) then yields:

$$C_s^{LHA-LSC}(t) = \exp\left[\sum_{j=1}^{N} \left(c^{(j)}\right)^2 \left\{\coth\left(\frac{\beta\hbar\omega^{(j)}}{2}\right) + \frac{\cos\left(\omega^{(j)}t\right)}{\sinh\left(\beta\hbar\omega^{(j)}/2\right)}\right\} - 1\right].$$
(2.29)

The exact standard FFCF, Eq. (2.24), can then be obtained from Eq. (2.29) by using the identity $C(t) = C_s(t + \frac{i\beta\hbar}{2})$. Details of this derivation are shown in the Appendix. This should be contrasted with Eq. (2.4) which involves the additional expansion of the force $\delta F(\mathbf{Q_0} + \mathbf{\Delta}/2)$ around $\mathbf{Q_0}$, to second order in terms of $\mathbf{\Delta}$. Indeed, in this case it can be shown that[134]

$$C^{LHA-LSC}(t) = e^{B_R(0)}\left[\left(e^{B_R(t)} - 1\right) + ie^{B_R(t)}B_I(t) - \frac{1}{2}e^{B_R(t)}B_I^2(t)\right],$$
(2.30)

where $B_R(t)$ and $B_I(t)$ are the real and imaginary parts of $B(t)$, respectively, which clearly differs from the exact result, Eq. (2.24).

$\tilde{C}(\omega)$ as obtained via Eqs. (2.24) and (2.30) are compared to the corresponding fully classical result in Fig. 2.1. The calculations were performed with the following spectral density,

$$\Gamma(\omega) = 2\lambda\frac{\omega^\alpha}{\omega_c^{\alpha+1}}\exp\left(-\frac{\omega^2}{\omega_c^2}\right),$$
(2.31)

and for the following values of the parameters: $\lambda = 0.20$, $\alpha = 3$ and $\beta\hbar\omega_c = 4.0$. Fig. 2.1 shows that although Eq. (2.4) is in rather good agreement with the exact results for a wide range of frequencies, discrepancies start appearing with increasing frequency which can be attributed to the additional approximation embodied in the above mentioned expansion of $\delta F(\mathbf{Q_0} + \mathbf{\Delta}/2)$ to second order with respect to $\mathbf{\Delta}$. At the same time, Eq. (2.21) is seen to coincide with the exact result at all frequencies, thereby testifying to its less approximate nature.
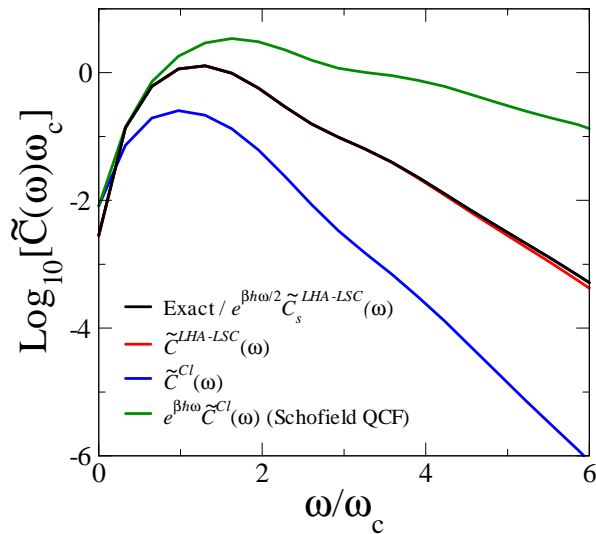
Figure 2.1: The exact $\tilde{C}(\omega)$ in the case of a harmonic bath and a force which is exponential in the bath coordinates. Note that in this case $\tilde{C}(\omega)$ coincides with $\tilde{C}_s^{LHA-LSC}(\omega)e^{\beta\hbar\omega/2}$. Also shown are $\tilde{C}^{LHA-LSC}(\omega)$, $\tilde{C}^{Cl}(\omega)$ and $e^{\beta\hbar\omega/2}\tilde{C}^{Cl}(\omega)$ (Schofield QCF).

2.3.2 The Breathing Sphere Model

The next system studied was VER of a spherically symmetric solute (so called breathing sphere) in a monatomic solvent.[27, 17, 47, 134] Calculations were performed on a two-dimensional liquid and under the assumption that the solvent atoms and the solute have the same mass and interact via identical pair potentials of the Lennard-Jones type (for more details see Ref. [134]). The calculations reported below were performed using a square simulation cell containing 81 atoms at a reduced density and temperature of $\rho^* = 0.70$ and $T^* = 0.68$, respectively. Periodic boundary conditions and a potential cutoff at 3σ have been employed. PIMD simulations were performed with 16 beads per atom. The classical equations of motion were solved via the velocity Verlet algorithm, and the FFCF was obtained by averaging over 30,000 trajectories of length 8.0ps each.

In Fig. 2.2a, we compare $C_s^{LHA-LSC}(t)$ as obtained via Eq. (2.21) with the

real part of $C^{LHA-LSC}(t)$ as obtained via Eq. (2.4), and the corresponding classical FFCF, $C^{Cl}(t)$. The LHA underlying the calculation of $C_s^{LHA-LSC}(t)$ was performed around the above mentioned three different configurations, namely $\mathbf{Q}_0$, $\mathbf{Q}'$ and $\mathbf{Q}_c$. It should be noted that the initial value and rate of decay of $C_s^{LHA-LSC}(t)$ are *smaller* than these of $C^{Cl}(t)$. This is contrast to the initial value and rate of decay of the real part of $C^{LHA-LSC}(t)$ which are *larger* in comparison to their classical counterparts. As a result, $\tilde{C}_s^{LHA-LSC}(\omega) < \tilde{C}^{Cl}(\omega) < \tilde{C}^{LHA-LSC}(\omega)$ throughout the entire range of frequencies. Thus, in the case of $C_s^{LHA-LSC}(t)$ the combined effect of nonclassical initial sampling and the fact that the initial force is calculated at $\mathbf{Q} = \mathbf{Q}'$, rather than at $\mathbf{Q}_0$, is to *diminish* the value of $\tilde{C}_s^{LHA-LSC}(\omega)$ relative to its classical counterpart. In contrast, in the case of $C^{LHA-LSC}(t)$, the combined effect of the very same nonclassical sampling and a nonclassical initial force that includes the $D(\mathbf{Q_0}, \mathbf{P_{n,0}})$ term enhances $\tilde{C}^{LHA-LSC}(\omega)$ relative to its classical counterpart. However, it should be remembered that $\tilde{C}(\omega) = e^{\beta\hbar\omega/2}\tilde{C}_s^{LHA-LSC}(\omega)$ (see Eq. (2.16)). Hence, a more meaningful comparison is between $\tilde{C}^{LHA-LSC}(\omega)$ and $e^{\beta\hbar\omega/2}\tilde{C}_s^{LHA-LSC}(\omega)$. Indeed, as we show in Fig. 2.2b, $e^{\beta\hbar\omega/2}\tilde{C}_s^{LHA-LSC}(\omega)$ is comparable to $\tilde{C}^{LHA-LSC}(\omega)$, regardless of the choice of LHA. It should also be noted that $e^{\beta\hbar\omega/2}\tilde{C}_{Cl}(\omega)$ is significantly larger than both $\tilde{C}^{LHA-LSC}(\omega)$ and $e^{\beta\hbar\omega/2}\tilde{C}_s^{LHA-LSC}(\omega)$. It should also be noted that the Schofield QCF significantly overestimates of the VER rate (see Fig. 2.2b).

An interesting observation is related to the numerical convergence of $\tilde{C}_s^{LHA-LSC}(\omega)$ in comparison to $\tilde{C}^{LHA-LSC}(\omega)$. As is well known, in the absence of resonance with other vibrations, $\tilde{C}(\omega)$ is expected to decay asymptotically with frequency in an exponential manner. As a result, it becomes increasingly more difficult to average out the statistical noise accompanying any real-life simulation, which is needed to calculate the increasingly small value of $\tilde{C}(\omega)$ at high frequencies. In fact, it is a common
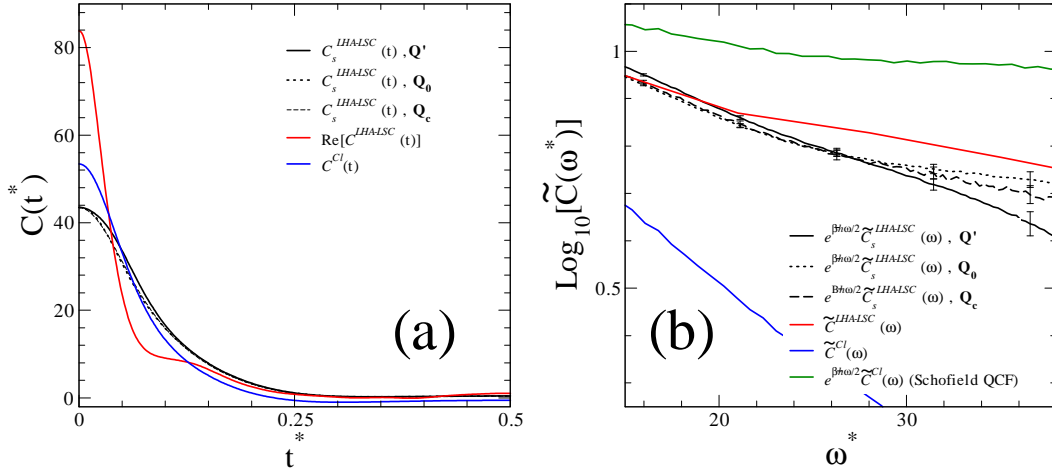
Figure 2.2: (a) A comparison of $C_s^{LHA-LSC}(t)$ (with the LHA performed around either $\mathbf{Q'}$ or $\mathbf{Q_0}$ or $\mathbf{Q_c}$), $Re[C^{LHA-LSC}(t)]$ and $C^{Cl}(t)$ for the breathing sphere model; (b) A semilog plot of $\tilde{C}_s^{LHA-LSC}(\omega)e^{\beta\hbar\omega/2}$ (with the LHA performed around either $\mathbf{Q'}$ or $\mathbf{Q_0}$ or $\mathbf{Q_c}$) $\tilde{C}^{LHA-LSC}(\omega)$, $\tilde{C}^{Cl}(\omega)$ and $e^{\beta\hbar\omega/2}\tilde{C}^{Cl}(\omega)$ (Schofield QCF) for the breathing sphere model.

practice to obtain $\tilde{C}(\omega)$ at high frequencies by extrapolating the exponential gap law, which usually emerges at low frequencies, to much higher frequencies.[98, 99] Now, because $\tilde{C}_s(\omega) = e^{-\beta\hbar\omega/2}\tilde{C}(\omega)$, its high frequency value is significantly smaller than $\tilde{C}(\omega)$, which in turn makes it even more difficult to obtain a converged result. Thus, one expects that obtaining a converged estimate of $\tilde{C}_s(\omega)$ at a given frequency will be computationally more demanding than obtaining a converged estimate of $\tilde{C}(\omega)$ at the same frequency. However, in practice, we found that it is still possible to obtain converged estimates of $\tilde{C}_s(\omega)$ over a wide enough range of frequencies for the exponential gap law to emerge and serve as basis for extrapolation to higher frequencies.

Another interesting observation is the dependence of $\tilde{C}_s(\omega)$ on the LHA. Although the results of different types of LHA are relatively similar, there are discernible differences that become increasingly larger upon extrapolation to the high frequency domain. In practice, we have observed that, at least for the systems considered here,

the best agreement with the estimates obtained via the original LSC-LHA method, as well with experiment when available (see next section), were obtained when the LHA was performed around $\mathbf{Q}'$, that is around the configuration used for calculating the initial force. This can be explained by the fact that performing the LHA around $\mathbf{Q}'$ leads to the most nonclassical sampling of momenta, thereby *maximizing* the quantum effect, which in this case corresponds to *lowering* the value of $\tilde{C}_s(\omega)$.

2.3.3   Neat liquid oxygen and nitrogen

Finally, we consider the VER of the homonuclear diatomic molecules O_2 and N_2 in the corresponding neat liquid. Calculations were performed on a three-dimensional liquid at 77K, with densities of 22.64 nm^{-3} and 17.37 nm^{-3} for O_2 and N_2, respectively, using site-site pair potentials of the Lennard-Jones type (for more details see Refs. [135, 61]). All calculations were preformed with 108 molecules contained in a cubic cell with periodic boundary conditions. PIMD simulations were performed with 16 beads per atom. Each FFCF was averaged over 50,000 trajectories, each of length 40ps. In the case of $C_s^{LHA-LSC}(t)$, the calculations were performed using the above mentioned three types of LHA around $\mathbf{Q}'$, $\mathbf{Q}_0$ and $\mathbf{Q}_c$.

In Figs. 2.3a and 2.4a, we compare $C_s^{LHA-LSC}(t)$ as obtained via Eq. (2.21) with the real part of $C^{LHA-LSC}(t)$ as obtained via Eq. (2.4), and the corresponding classical $C^{Cl}(t)$, in the cases of liquid oxygen and liquid nitrogen, respectively. The LHA underlying the calculation of $C_s^{LHA-LSC}(t)$ was performed around $\mathbf{Q}_0$, $\mathbf{Q}'$ and $\mathbf{Q}_c$. The corresponding frequency domain results are shown in 2.3b and 2.4b. The results are seen to follow trends similar to those observed in the case of the breathing sphere model, namely:

- The initial value and rate of decay of $C_s^{LHA-LSC}(t)$ are *smaller* than these of

Figure 2.3:   (a) A comparison of $C_s^{LHA-LSC}(t)$ (with the LHA performed around $\mathbf{Q'}$), $Re[C^{LHA-LSC}(t)]$ and $C^{Cl}(t)$ for neat liquid oxygen; (b) A semilog plot of $\tilde{C}_s^{LHA-LSC}(\omega)$ (with the LHA performed around $\mathbf{Q'}$), $\tilde{C}^{LHA-LSC}(\omega)$, $\tilde{C}^{Cl}(\omega)$ and $e^{\beta\hbar\omega/2}\tilde{C}^{Cl}(\omega)$ (Schofield QCF) for neat liquid oxygen. Solid lines were obtained from the simulation and dashed lines correspond to extrapolations. The experimental value is indicated by $*$ at the vibrational transition frequency of oxygen (1553cm^{-1}). The insert shows $\tilde{C}_s^{LHA-LSC}(\omega)$ on a narrower range of frequencies.

$C^{Cl}(t)$, which are in turn smaller than these of the real part of $C^{LHA-LSC}(t)$. As a result, $\tilde{C}_s^{LHA-LSC}(\omega) < \tilde{C}^{Cl}(\omega) < \tilde{C}^{LHA-LSC}(\omega)$ throughout the entire range of frequencies.

- The calculation of $\tilde{C}_s^{LHA-LSC}(\omega)$ at high frequencies converges significantly more slowly than that of $\tilde{C}^{LHA-LSC}(\omega)$ due to the fact that $\tilde{C}_s(\omega) = e^{-\beta\hbar\omega/2}\tilde{C}(\omega)$ becomes increasingly smaller than $\tilde{C}(\omega)$ with increasing frequency.

- The best agreement with the predictions of the LSC-LHA method as well as with experiment (see Table 2.1) are obtained when the LHA is performed around $\mathbf{Q'}$.

- The agreement of the prediction obtained via Eq. (2.21) with experiment in the case of oxygen is somewhat inferior to that obtained via Eq. (2.4) in the case
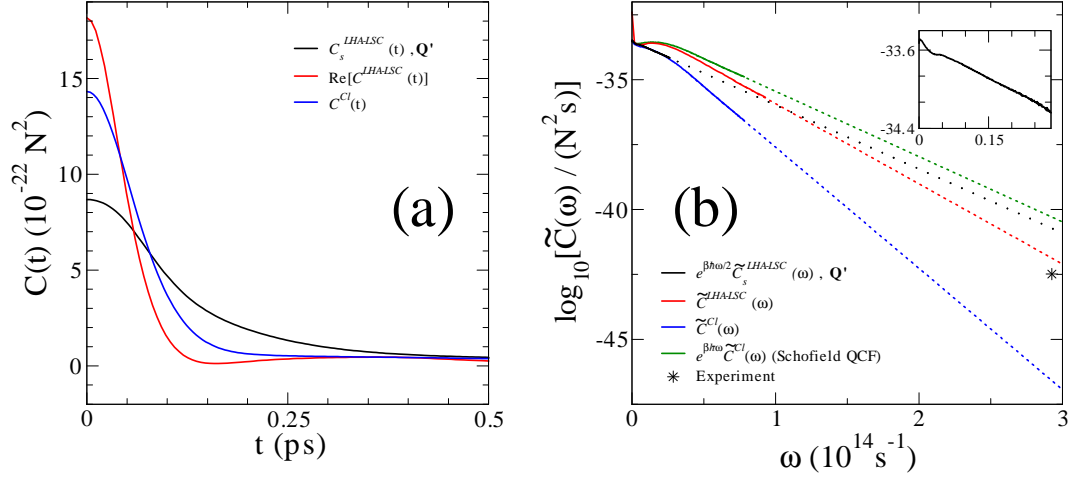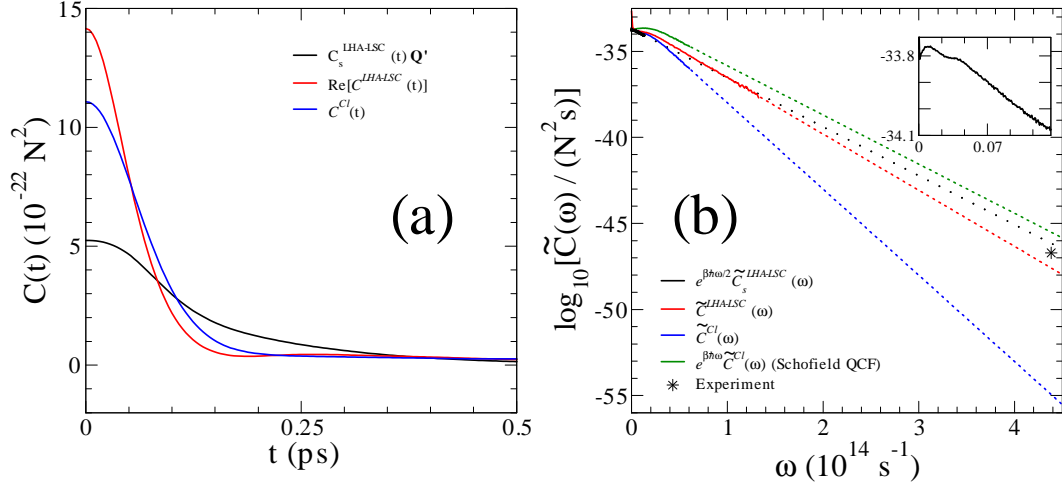
Figure 2.4: (a) A comparison of $C_s^{LHA-LSC}(t)$ (with the LHA performed around $\mathbf{Q}'$), $Re[C^{LHA-LSC}(t)]$ and $C^{Cl}(t)$ for neat liquid nitrogen; (b) A semilog plot of $\tilde{C}_s^{LHA-LSC}(\omega)$ (with the LHA performed around $\mathbf{Q}'$), $\tilde{C}^{LHA-LSC}(\omega)$, $\tilde{C}^{Cl}(\omega)$ and $e^{\beta\hbar\omega/2}\tilde{C}^{Cl}(\omega)$ (Schofield QCF) for neat liquid nitrogen. Solid lines were obtained from the simulation and dashed lines correspond to extrapolations. The experimental value is indicated by $*$ at the vibrational transition frequency of nitrogen (2327cm^{-1}). The insert shows $\tilde{C}_s^{LHA-LSC}(\omega)$ on a narrower range of frequencies.

of oxygen, and vice versa in the case of nitrogen. However, both predictions are far superior to the corresponding classical predictions which underestimate the VER rates by many orders of magnitude.

- The Schofield QCF alone significantly overestimates the VER rate. However, the agreement with experiment can be significantly improved by replacing $\tilde{C}^{Cl}(\omega)$ by $\tilde{C}_s^{LHA-LSC}(\omega)$.

	Oxygen	Nitrogen
Experiment	395 ± 18	$(1.8 \pm 0.5) \times 10^{-2}$
Classical	$(285 \pm 31) \times 10^{-4}$	$(3.1 \pm 0.4) \times 10^{-10}$
Eq. (2.4)	783 ± 62	$(1.9 \pm 0.3) \times 10^{-3}$
Eq. (2.21)	$(2.0 \pm 1.2) \times 10^4$	$(6 \pm 3) \times 10^{-2}$

Table 2.1: k_{10}/s^{-1} for neat liquid oxygen and nitrogen at 77 K. The experimental results for oxygen and nitrogen were adopted from Refs. [147] and [56], respectively.

2.4 Conclusion

This work has presented a new approach for calculating VER rates based on the LSC and LHA approximations. The new approach is based on applying the LSC and LHA approximations to the symmetrized FFCF, rather than to the standard FFCF. The main advantage of the resulting scheme is that it does not involve a power expansion of the initial force in terms of the Wigner transform integration variable Δ and as a result is more accurate and does not require force derivatives as input. The main disadvantages of the new scheme are its slower convergence rate, due to the fact that $\tilde{C}_s(\omega) \ll \tilde{C}(\omega)$ at high frequencies and its ambiguity with respect to the choice of configuration around which the LHA is to be performed. Nevertheless, we were able to demonstrate that the new approach is computationally feasible despite its slow convergence even in the highly challenging case of nonpolar liquids. In this context, it should be noted that one expects much faster VER rates in polar systems, thereby making it easier to overcome the slow convergence rate. We have also observed that performing the LHA around the configuration used for computing the initial force, which corresponds to the most nonclassical momentum sampling, yields the best predictions in comparison to the original LSC-LHA approach as well as experiment.

It should be noted that while quantum effects tend to *enhance* $\tilde{C}(\omega)$ relative to $\tilde{C}^{Cl}(\omega)$, they actually tend to *diminish* $\tilde{C}_s(\omega)$ relative to $\tilde{C}^{Cl}(\omega)$. Thus, the ability of the LSC and LHA approximations to capture this trend reversal in a quantitative manner is a testimony to the robustness and versatility of these approximations. Because of the methods elimination of the need to calculate force-derivatives, it is well suited for use with package software and complicated potentials where the

calculation of the force derivatives would prove cumbersome and computationally expensive.

2.5 Appendix

In this appendix we will prove that the application of Eq. 2.21 to a bath of uncoupled harmonic oscillators

$$\hat{H}_b = \sum_{j=1}^{f} \left(\frac{(\hat{P}^{(j)})^2}{2M^{(j)}} + \frac{1}{2} M^{(j)} (\omega^{(j)})^2 (\hat{Q}^{(j)})^2 \right) \tag{2.32}$$

with a force that is exponential in the force coordinates

$$\hat{F}(\hat{\mathbf{Q}}) = e^{R(\hat{\mathbf{Q}})} \tag{2.33}$$

where

$$R(\hat{\mathbf{Q}}) = \sum_{j=1}^{f} c^{(j)} \sqrt{\frac{2M^{(j)}\omega^{(j)}}{\hbar}} \hat{Q}^{(j)} \ . \tag{2.34}$$

yields the exact quantum mechanical solution.

The exact quantum mechanical result to the FFCF is given analytically by

$$C(t) = e^{B(0)}(e^{B(t)} - 1) \ , \tag{2.35}$$

where $B(t) = \langle \hat{R}_0(t)\hat{R}(0) \rangle_0$ and

$$
\begin{aligned}
B(t) &= \int_0^\infty d\omega \sum_{k}^{f} \left(c^{(k)} \right)^2 \delta(\omega - \omega^{(k)}) \{ [n(\omega) + 1] e^{-i\omega t} + n(\omega) e^{i\omega t} \} \tag{2.36} \\
&= \sum_{k}^{f} \left(c^{(k)} \right)^2 \{ [n(\omega) + 1] e^{-i\omega t} + n(\omega) e^{i\omega t} \}, \tag{2.37}
\end{aligned}
$$

defining the real part of $B(t)$ as

$$B_R = \sum_{j=1}^{f} \left(c^{(j)} \right)^2 \coth \left(\frac{\beta \hbar \omega^{(j)}}{2} \right) \cos \left(\omega^{(j)} t \right) \tag{2.38}$$

and the imaginary part as

$$B_I = -\sum_{j=1}^{f} \left(c^{(j)}\right)^2 \sin\left(\omega^{(j)}t\right).$$ (2.39)

In order to calculate the FFCF, we apply Eq. (2.21) to this system.

The $\delta F(\mathbf{Q}') \times \delta F(\mathbf{Q}_t^{(Cl)}[\mathbf{Q_0},\mathbf{P_0}])$ term in the previous equation can be expressed explicitly as

$$F(\mathbf{Q}')F(\mathbf{Q}_t^{(Cl)}[\mathbf{Q_0},\mathbf{P_0}]) - \langle\hat{F}\rangle F(\mathbf{Q}') - \langle\hat{F}\rangle F(\mathbf{Q}_t^{(Cl)}[\mathbf{Q_0},\mathbf{P_0}]) + \langle\hat{F}\rangle^2$$ (2.40)

To solve Eq. (2.21), we will employ the identity

$$\frac{\langle\mathbf{Q_0}| e^{-\frac{\beta}{2}\sum_{j=1}^{f}\left(\frac{(\hat{P}^{(j)})^2}{2M^{(j)}}+\frac{1}{2}M^{(j)}(\omega^{(j)})^2(\hat{Q}^{(j)})^2\right)} |\mathbf{Q}'\rangle \langle\mathbf{Q}'| e^{-\frac{\beta}{2}\sum_{j=1}^{f}\left(\frac{(\hat{P}^{(j)})^2}{2M^{(j)}}+\frac{1}{2}M^{(j)}(\omega^{(j)})^2(\hat{Q}^{(j)})^2\right)} |\mathbf{Q_0}\rangle}{Z}$$

$$= \prod_{j=1}^{N} \left(\frac{M^{(j)}(\omega^{(j)})}{\pi\hbar}\right) \exp\left\{-\alpha^{(j)}\left(\mathbf{Q}_0^{(j)}\right)^2 + \left(\mathbf{Q}'^{(j)}\right)^2\right\} \times$$ (2.41)

$$\exp\left\{-\frac{M^{(j)}(\omega^{(j)})}{\hbar}\frac{2}{\sinh\left(\beta\hbar\omega^{(j)}/2\right)}\mathbf{Q}_0^{(j)}\mathbf{Q}'^{(j)}\right\}.$$

Solving the four integrals arising from Eq. (2.40) yields the following solutions :

$$\int d\mathbf{Q_0} \int d\mathbf{Q}' \frac{\langle\mathbf{Q_0}| e^{-\frac{\beta}{2}\hat{H}_b} |\mathbf{Q}'\rangle \langle\mathbf{Q}'| e^{-\frac{\beta}{2}\hat{H}_b} |\mathbf{Q_0}\rangle}{Z} \times$$ (2.42)

$$\int d\mathbf{P_0} \prod_{j=1}^{N} \left(\frac{1}{\alpha^{(j)}\pi\hbar^2}\right)^{1/2} \exp\left[-\frac{(P_0^{(j)})^2}{\hbar^2\alpha^{(j)}}\right] \times F(\mathbf{Q}')F(\mathbf{Q}_t^{(Cl)}[\mathbf{Q_0},\mathbf{P_0}])$$

$$= \exp\left[\sum_{j=1}^{f}\left(c^{(j)}\right)^2 \coth\left(\frac{\beta\hbar\omega^{(j)}}{2}\right)\right] \times \exp\left[-\sum_{j=1}^{f}\left(c^{(j)}\right)^2 \left(\frac{\beta\hbar\omega^{(j)}}{2}\right)\right]$$

$$\int d\mathbf{Q_0} \int d\mathbf{Q}' \frac{\langle\mathbf{Q_0}| e^{-\frac{\beta}{2}\hat{H}_b} |\mathbf{Q}'\rangle \langle\mathbf{Q}'| e^{-\frac{\beta}{2}\hat{H}_b} |\mathbf{Q_0}\rangle}{Z} \times$$ (2.43)

$$\int d\mathbf{P_0} \prod_{j=1}^{N} \left(\frac{1}{\alpha^{(j)}\pi\hbar^2}\right)^{1/2} \exp\left[-\frac{(P_0^{(j)})^2}{\hbar^2\alpha^{(j)}}\right] \times \langle\hat{F}\rangle F(\mathbf{Q}')$$

$$= \exp\left[\sum_{j=1}^{f}\left(c^{(j)}\right)^2 \coth\left(\frac{\beta\hbar\omega^{(j)}}{2}\right)\right]$$

$$\int d\mathbf{Q_0} \int d\mathbf{Q'} \frac{\langle \mathbf{Q_0}| e^{-\frac{\beta}{2}\hat{H}_b} |\mathbf{Q'}\rangle \langle \mathbf{Q'}| e^{-\frac{\beta}{2}\hat{H}_b} |\mathbf{Q_0}\rangle}{Z} \times \tag{2.44}$$

$$\int d\mathbf{P_0} \prod_{j=1}^{N} \left(\frac{1}{\alpha^{(j)}\pi\hbar^2}\right)^{1/2} \exp\left[-\frac{(P_0^{(j)})^2}{\hbar^2\alpha^{(j)}}\right] \times \langle \hat{F}\rangle F(\mathbf{Q}_t^{(Cl)}[\mathbf{Q_0},\mathbf{P_0}])$$

$$= \exp\left[\sum_{j=1}^{f} \left(c^{(j)}\right)^2 \coth\left(\frac{\beta\hbar\omega^{(j)}}{2}\right)\right]$$

$$\int d\mathbf{Q_0} \int d\mathbf{Q'} \frac{\langle \mathbf{Q_0}| e^{-\frac{\beta}{2}\hat{H}_b} |\mathbf{Q'}\rangle \langle \mathbf{Q'}| e^{-\frac{\beta}{2}\hat{H}_b} |\mathbf{Q_0}\rangle}{Z} \times \tag{2.45}$$

$$\int d\mathbf{P_0} \prod_{j=1}^{N} \left(\frac{1}{\alpha^{(j)}\pi\hbar^2}\right)^{1/2} \exp\left[-\frac{(P_0^{(j)})^2}{\hbar^2\alpha^{(j)}}\right] \times \langle \hat{F}\rangle^2$$

$$= \exp\left[\sum_{j=1}^{f} \left(c^{(j)}\right)^2 \coth\left(\frac{\beta\hbar\omega^{(j)}}{2}\right)\right]$$

Combining all of these results we find that

$$C^{(s)}(t) = \exp\left[\sum_{j=1}^{f} \left(c^{(j)}\right)^2 \coth\left(\frac{\beta\hbar\omega^{(j)}}{2}\right)\right] \tag{2.46}$$

$$\times \left(\exp\left[\sum_{j=1}^{f} \left(c^{(j)}\right)^2 \cos\left(\omega^{(j)}t\right) \frac{1}{\sinh\left(\frac{\beta\hbar\omega^{(j)}}{2}\right)}\right] - 1\right)$$

In order to find the standard FFCF from the symmetrized result, we use the identity $C(t) = C^{(s)}(t + \frac{i\beta\hbar}{2})$. We find that

$$\exp\left[\sum_{j=1}^{f} \left(c^{(j)}\right)^2 \cos\left(\omega^{(j)}\left[t + \frac{i\beta\hbar\omega^{(j)}}{2}\right]\right) \frac{1}{\sinh\left(\frac{\beta\hbar\omega^{(j)}}{2}\right)}\right] \tag{2.47}$$

$$= \exp\left[\sum_{j=1}^{f} \left(c^{(j)}\right)^2 \left\{\begin{array}{c} \cos\left(\omega^{(j)}t\right)\cos\left(\frac{i\beta\hbar\omega^{(j)}}{2}\right) \\ -\sin\left(\omega^{(j)}t\right)\sin\left(\frac{i\beta\hbar\omega^{(j)}}{2}\right) \end{array}\right\} \frac{1}{\sinh\left(\frac{\beta\hbar\omega^{(j)}}{2}\right)}\right]$$

$$= \exp\left[\sum_{j=1}^{f} \left(c^{(j)}\right)^2 \left\{\begin{array}{c} \cosh\left(\frac{\beta\hbar\omega^{(j)}}{2}\right)\cos\left(\omega^{(j)}t\right) \\ -i\sinh\left(\frac{\beta\hbar\omega^{(j)}}{2}\right)\sin\left(\omega^{(j)}t\right) \end{array}\right\} \frac{1}{\sinh\left(\frac{\beta\hbar\omega^{(j)}}{2}\right)}\right]$$

$$= \exp\left[\sum_{j=1}^{f} \left(c^{(j)}\right)^2 \left\{\coth\left(\frac{\beta\hbar\omega^{(j)}}{2}\right)\cos\left(\omega^{(j)}t\right) - i\sin\left(\omega^{(j)}t\right)\right\}\right]$$

$$= e^{B(t)}$$

Lastly, because $B(0) = \sum_{j=1}^{f} \left(c^{(j)}\right)^2 \coth\left(\frac{\beta\hbar\omega^{(j)}}{2}\right)$, we see that the application of Eq. (2.21) to this system yields the exact quantum mechanical solution,

$$C(t) = e^{B(0)}\left(e^{B(t)} - 1\right). \qquad (2.48)$$

CHAPTER III

Vibrational Energy Relaxation in Polar Liquids

3.1   Introduction

Vibrational energy relaxation (VER), is an important physical phenomena to understand because of the fact that the way energy flows in and out of reactive modes has a major influence on chemical reactivity[7, 14, 20, 21, 35, 34, 106, 107, 108, 15, 16, 45, 86, 142, 105, 30, 8, 73, 127, 50, 48, 49, 44, 110, 103, 92, 65, 161, 115, 109, 129, 150, 149, 151, 104, 71, 160, 95, 94, 128, 42, 27, 31, 32, 74, 23, 22, 136, 77]. Previous work in our group [152] has presented a calculation of VER in nonpolar solvents using the Landau-Teller formula,[105, 162, 72] and a force-derivative-free (FDF) version of the LSC-LHA previously used in our group [134, 135, 61, 60, 97]. This FDF-LSC method is based applying a symmetrized time correlation function (TCF) to the LSC approximation. The original LSC expression derived by linearizing the forward-backward action in the path-integral expression for the quantum-mechanical force-force correlation function (FFCF) with respect to the difference between the forward and backward paths[133],resulting in the following form for a real-time quantum-mechanical correlation:

$$C_{AB}(t) = Tr\left(\hat{A}e^{i\hat{H}t/\hbar}\hat{B}e^{-i\hat{H}t/\hbar}\right) \tag{3.1}$$

47

given by

$$C_{AB}^{LSC}(t) = \frac{1}{(2\pi\hbar)^N} \int \mathbf{dQ_0} \int \mathbf{dP_0} A_W (\mathbf{Q_0}, \mathbf{P_0}) B_W \left(\mathbf{Q}_t^{(Cl)}, \mathbf{P}_t^{(Cl)} \right) , \qquad (3.2)$$

where N is the number of DOF, $\mathbf{Q_0} = (Q_0^{(1)}, \dots, Q_0^{(N)})$ and $\mathbf{P_0} = (P_0^{(1)}, \dots, P_0^{(N)})$ are the corresponding coordinates and momenta, and

$$A_W(\mathbf{Q}, \mathbf{P}) = \int \mathbf{d\Delta} e^{-i\mathbf{P\Delta}/\hbar} \langle \mathbf{Q} + \mathbf{\Delta}/2 | \hat{A} | \mathbf{Q} - \mathbf{\Delta}/2 \rangle \qquad (3.3)$$

is the Wigner transform of the operator $\hat{A}$,[54] and $\mathbf{Q}_t^{(Cl)} = \mathbf{Q}_t^{(Cl)}(\mathbf{Q_0}, \mathbf{P_0})$ and $\mathbf{P}_t^{(Cl)} = \mathbf{P}_t^{(Cl)}(\mathbf{Q_0}, \mathbf{P_0})$ are propagated *classically* with the initial conditions $\mathbf{Q_0}$ and $\mathbf{P_0}$.

Applying a local harmonic approximation and a second order expansion of the force allows the highly oscillatory Wigner transform in Eq. 3.3 to be solved analytically (cf. Chapters 1 and 2) resulting in the LSC-LHA approximation for the FFCF:

$$C^{LHA-LSC}(t) = \int d\mathbf{Q_0} \frac{\langle \mathbf{Q_0} | e^{-\beta \hat{H}} | \mathbf{Q_0} \rangle}{Z} \int d\mathbf{P_{n,0}} \prod_{j=1}^{N} \left(\frac{1}{\alpha^{(j)} \pi \hbar^2} \right)^{1/2} \exp \left[-\frac{(P_{n,0}^{(j)})^2}{\hbar^2 \alpha^{(j)}} \right]$$
$$[\delta F(\mathbf{Q_0}) + D(\mathbf{Q_0}, \mathbf{P_{n,0}})] \, \delta F(\mathbf{Q}_t^{(Cl)}) . \qquad (3.4)$$

Here,

$$\mathbf{P}_n = \mathbf{P}_n(\mathbf{Q_0}) = \left(P_n^{(1)}(\mathbf{Q_0}), ..., P_n^{(N)}(\mathbf{Q_0}) \right) , \qquad (3.5)$$

where $\left\{ P_n^{(k)}(\mathbf{Q_0}) = \sum_{l=1}^{N} T_{l,k} (M^{(l)})^{-1/2} P^{(l)} \right\}$ are the normal mode momenta that emerge from diagonalizing the Hessian matrix underlying the quadratic expansion of the bath potential energy around $\mathbf{Q} = \mathbf{Q}_0$ and

$$\alpha^{(j)} = \alpha^{(j)}(\mathbf{Q_0}) = \frac{\Omega^{(j)}(\mathbf{Q_0})}{\hbar} \coth \left[\frac{\beta \hbar \Omega^{(j)}(\mathbf{Q_0})}{2} \right] , \qquad (3.6)$$

where $\{(\Omega^{(k)})^2(\mathbf{Q_0})\}$ are the eigenvalues of the Hessian matrix. The term $D(\mathbf{Q_0}, \mathbf{P_{n,0}})$ is given by [134]:

$$D(\mathbf{Q_0}, \mathbf{P_{n,0}}) = -i \sum_{k=1}^{N} \frac{\tilde{F}'_k P_{n,0}^{(k)}}{\hbar \alpha^{(k)}} + \sum_{k=1}^{N} \frac{\tilde{F}''_{k,k}}{4\alpha^{(k)}} - \sum_{k,l=1}^{N} \frac{\tilde{F}''_{k,l} P_{n,0}^{(k)} P_{n,0}^{(l)}}{2\hbar^2 \alpha^{(k)} \alpha^{(l)}} \qquad (3.7)$$

and its calculation requires as input the first and second derivatives of the force with respect to the bath coordinates, that is

$$\tilde{F}'_k = \sum_{l=1}^{N}(M^{(l)})^{-1/2}T_{l,k}F'_l \ ; \ \ \tilde{F}''_{k,l} = \sum_{i=1}^{N}\sum_{j=1}^{N}(M^{(i)}M^{(j)})^{-1/2}T_{i,l}T_{j,k}F''_{i,j} \ . \tag{3.8}$$

where $F'_k = \left.\frac{\partial F}{\partial Q^{(k)}}\right|_{\mathbf{Q}=\mathbf{Q_0}} \ ; \ F''_{k,l} = \left.\frac{\partial^2 F}{\partial Q^{(k)}\partial Q^{(l)}}\right|_{\mathbf{Q}=\mathbf{Q_0}} \ .$

The delocalized force term, $D(\mathbf{Q_0}, \mathbf{P_{n,0}})$, is purely quantum mechanical and has been found to contribute significantly to VER in previous studies [134, 135, 61, 60, 97]. Specifically, the nonclassical term $D(\mathbf{Q_0}, \mathbf{P_{n,0}})$, which can be traced back to the first and second order terms in the above mentioned expansion of $F(\mathbf{Q_0} + \mathbf{\Delta}/2)$ in powers of $\mathbf{\Delta}$, was found to play an important role in enhancing the VER rate. Although the calculation of the first and second derivatives of the bath-induced force with respect to the bath coordinates, which is required as input for calculating $D(\mathbf{Q_0}, \mathbf{P_{n,0}})$, is in principle straightforward, in practice it can become increasingly cumbersome for complex force fields, for example, the simulation of polar solvents using Ewald summations to capture long range electrostatic forces. Furthermore, unlike the second derivatives required for calculating the Hessian matrix underlying the LHA, these force derivatives are usually not part of the output of standard packages for performing MD simulations. In previous work, we developed an alternative scheme for calculating VER rate constants which, while still based on LSC and LHA, avoids the above mentioned expansion of the bath-induced force in terms of $\mathbf{\Delta}$ and as a result is more accurate and does not require force derivatives as input. Part of the motivation for this work was to eventually be able to calculate quantum mechanical VER rates in complex systems using package software such as AMBER, specifically for polar liquids.

Experimentally, it is known that VER in a polar solvent occurs much faster than

in a nonpolar solvent. For example, while the relaxation lifetime in liquid oxygen and nitrogen is on the order of milliseconds [147, 56], in liquid HCl it is on the order nanoseconds[15, 16]. When using the Landau-Teller formula to calculate the VER rate constant from the FFCF, the enhancement of the rate can be thought to come about from some extra force in the TCF. In polar liquids, the nonbonded force of the solvent on the vibrating mode will consist of Lennard-Jones contributions and electrostatic contributions

$$F_{tot} = F_{LJ} + F_{el}. \tag{3.9}$$

As a result, the FFCF in a polar liquid can be broken into the following parts:

$$C(t) = \langle F_{LJ}(0)F_{LJ}(t)\rangle_0 + \langle F_{el}(0)F_{el}(t)\rangle_0 + \langle F_{LJ}(0)F_{el}(t)\rangle_0 + \langle F_{el}(0)F_{LJ}(t)\rangle_0 \tag{3.10}$$

The enhancement of this rate can be due to either new contributions from the electrostatic parts of the force, the cross terms, or from from modifications to the Lennard-Jones terms that arise from rearrangement of the solvent around the relaxing molecule due to electrostatic forces. Previous work by Ladanyi and Stratt has shown that the enhancement of the rate is mainly dependent on the Lennard-Jones part of the force and not the electrostatic or cross terms[70]. The mechanism they proposed is that the electrostatic forces in the polar solvent lead to so called electrostriction, where the solvent is positioned close enough to the relaxing molecule to allow the usually inaccessible parts of the Lennard-Jones repulsive wall to be reached. In this case it is the Lennard-Jones forces that contribute to the rate with little contribution from the electrostatic and cross terms. What is not understood is role quantum mechanical effects will play, if any, on VER in polar systems. Previous studies on polar liquids were all done using a classical model to study VER; however, as we have shown before[134, 135, 61, 60, 97, 152], for systems where quantum effects play

an important role, a classical description may lead to an inadequate description of the system. To this end, we have applied our FDF-LSC-LHA methodology to the problem of calculating VER in neat polar liquids to clarify if the electrostriction explanation holds when quantum effects are taken into account. It should also be noted that this work is the first ever application of a LSC method to calculating a quantum mechanical FFCF in polar liquids.

3.2 Theory

Because the electrostatic forces are only position dependent, the theoretical framework developed for VER in nonpolar solvents can be used to calculate the quantum mechanical FFCF. Section 2.2 contains a detailed description of the theory. The FDF-LSC-LHA is applied to the calculation of VER in polar liquids in the same way as was shown previously.

3.3 Applications

3.3.1 Liquid Methyl Chloride

The first system we considered was the VER in neat liquid methyl chloride. The methyl chloride molecules were modeled as rigid dipolar diatomic molecules using site-site Lennard-Jones and Coulomb interactions, where the force-field parameters are taken from the model developed by Hammes-Schiffer and Tully[43]. Calculations were performed using the AMBER molecular dynamics software package[19] on a liquid at 249 K, with a density of 12.0 nm^{-3}. All calculations were preformed with 500 molecules contained in a cubic cell with periodic boundary conditions. PIMD simulations were preformed with 32 beads per atom. Each FFCF was averaged over 15,000 trajectories, each of length 4 ps. In the case of $C_s^{LHA-LSC}(t)$, the calculations

Figure 3.1: A semilog plot of $\tilde{C}_s^{LHA-LSC}(\omega)$ (with the LHA performed around $\mathbf{Q}'$), $\tilde{C}_s(\omega)$, $\tilde{C}^{Cl}(\omega)$ and $e^{\beta\hbar\omega/2}\tilde{C}^{Cl}(\omega)$ (Schofield QCF) for neat methyl chloride at 249 K

were performed using the above mentioned LHA around $\mathbf{Q}'$.

In Fig. 3.1 we compare the Fourier transform of the quantum mechanical FFCF, $e^{\beta\hbar\omega/2}\tilde{C}_s^{LHA-LSC}(\omega)$ and the uncorrected symmetrized FFCF, $\tilde{C}_s^{LHA-LSC}(\omega)$, as obtained via Eq. (2.21) and the corresponding classical $\tilde{C}^{Cl}(\omega)$ and Schofield QCF $e^{\beta\hbar\omega/2}\tilde{C}^{Cl}(\omega)$ results. The LHA underlying the calculation of $C_s^{LHA-LSC}(t)$ was performed around the above mentioned configuration $\mathbf{Q}'$. As can be seen in the figure, the quantum mechanical FFCF calculated from Eq. (2.21) agrees well with the classical result. This is most likely due to the low characteristic frequency of the vibration ($\omega_0 = 709 \text{ cm}^{-1}$). Although the full quantum mechanical FFCF agrees well with the classical result, the uncorrected symmetrized FFCF is actually lower than the classical result. This is a testament to the robustness of Eq. (2.21). In classical systems, the approximation is able to compensate itself to account for the $e^{\beta\hbar\omega/2}$ factor. It is also apparent from the figure that the corresponding Schofield QCF, in which the classical FFCF is multiplied by the same $e^{\beta\hbar\omega/2}$ factor, overestimates the

quantum effects.

3.3.2 Liquid Hydrogen Chloride

The next system we studied was VER in neat liquid hydrogen chloride. The hydrogen chloride molecules were modeled using Lennard-Jones parameters from the general AMBER force field (GAFF)[158], and the partial charges for the Coulombic charges were assigned using a HF/6-31G* restrained electrostatic potential (RESP)[157]. The quantum mechanical calculations were done using Gaussian 03. Calculations were preformed using the AMBER molecular dynamics software package[19] on a liquid at 188 K, with a density of 19.671 nm^{-3}. This state point was chosen because of the experimental VER rate data available[18]. All calculations were preformed with 500 molecules contained in a cubic cell with periodic boundary conditions. PIMD simulations were preformed with 32 beads per atom. Each FFCF was averaged over 180,000 trajectories, each of length 4 ps. In the case of $C_s^{LHA-LSC}(t)$, the calculations were performed using the above mentioned LHA around $\mathbf{Q}'$.
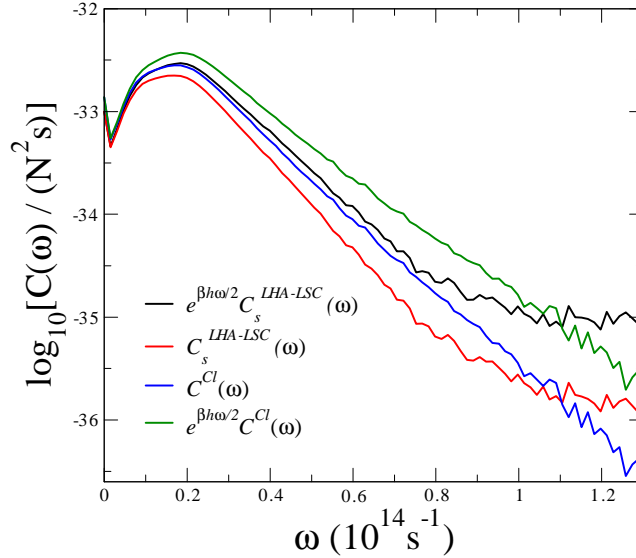
In Fig. 3.2 we compare the Fourier transform (FT) of the quantum mechanical FFCF, $e^{\beta\hbar\omega/2}\tilde{C}_s^{LHA-LSC}(\omega)$ and the uncorrected symmetrized FFCF, $\tilde{C}_s^{LHA-LSC}(\omega)$, as obtained via Eq. (2.21) and the corresponding classical $\tilde{C}^{Cl}(\omega)$ and Schofield QCF $e^{\beta\hbar\omega/2}\tilde{C}^{Cl}(\omega)$ results. As can be seen in the figure, $e^{\beta\hbar\omega/2}\tilde{C}_s^{LHA-LSC}(\omega)$, gives good agreement with the experimental result. Also, because of the relatively high characteristic frequency of the relaxing mode (2783 cm^{-1}), there is definitely a quantum enhancement effect. This quantum effect is manifested in the lowering of the of the uncorrected symmetrized FFCF, $\tilde{C}_s^{LHA-LSC}(\omega)$, which is then multiplied by the $e^{\beta\hbar\omega/2}$. Also, because of the faster rate associated with VER in polar solvents, the quantum mechanical FFCF obtained from Eq. (2.21) can be extrapolated at
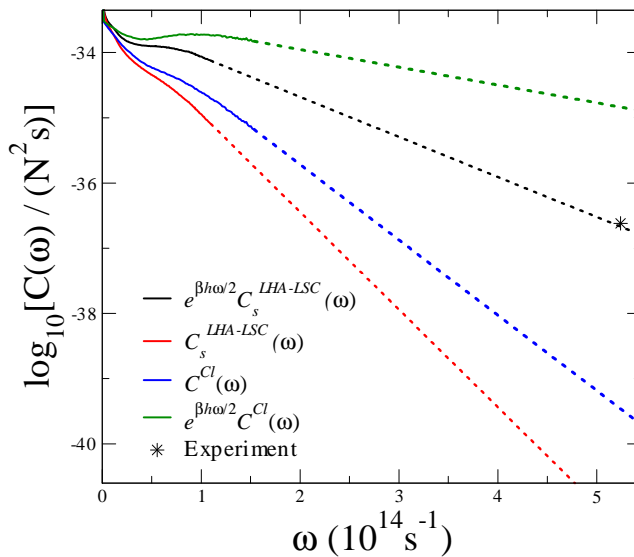
Figure 3.2: A semilog plot of $\tilde{C}_s^{LHA-LSC}(\omega)$ (with the LHA performed around $\mathbf{Q}'$), $\tilde{C}_s(\omega)$, $\tilde{C}^{Cl}(\omega)$ and $e^{\beta\hbar\omega/2}\tilde{C}^{Cl}(\omega)$ (Schofield QCF) for neat liquid hydrogen chloride at 188 K

	Rate (s^{-1})
Experiment	1.3×10^9
Classical	$(0.023 \pm .009) \times 10^9$
Schofield QCF	$(46 \pm 18) \times 10^9$
Eq. (2.21)	$(1.3 \pm 0.9) \times 10^9$

Table 3.1: $k_{1\leftarrow0}/s^{-1}$ for neat liquid hydrigen chloride at 188 K. The experimental result was adopted from Refs. [18].

higher frequencies than in previous work done in nonpolar solvents[152]. The classical FFCF, $\tilde{C}^{Cl}(\omega)$, underestimates the the experimental result and the Schofield QCF, $e^{\beta\hbar\omega/2}\tilde{C}^{Cl}(\omega)$, over estimates the result. Importantly, this result is the first application of a rigorous semiclassical approach to studying VER in polar liquids. A comparison of the calculated VER rate constants for is shown in Table 3.1.

Although the results in Fig. 3.2 provide insight into the quantum effects, they do not show the difference between the classical and quantum mechanical mechanisms of VER. To this end, we decomposed the FFCF into Lennard-Jones, electrostatic, and
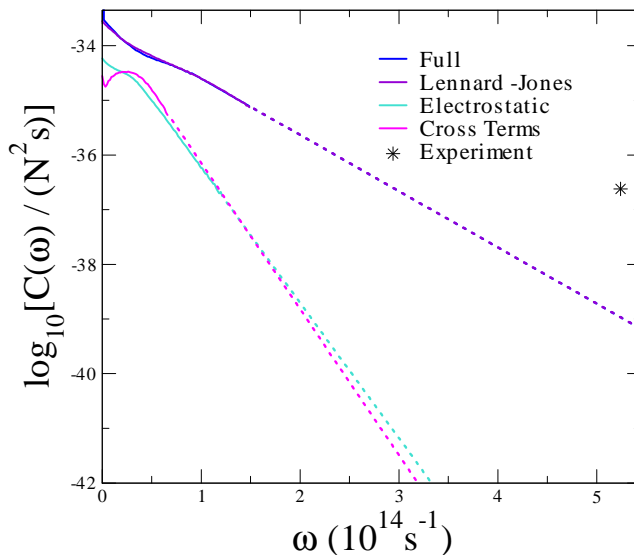
Figure 3.3: A semilog plot of the full, Lennard-Jones, electrostatic, and cross term contributions to $\tilde{C}^{Cl}(\omega)$ for neat hydrogen chloride at 188 K

cross term contributions. In Fig. 3.3 we compare the full, Lennard-Jones, electrostatic, and cross term contributions to the FT of the classical FFCF, $\tilde{C}^{Cl}(\omega)$. As can be seen in the figure, electrostriction seems to explain the enhanced rate constant. The Lennard-Jones contribution to the classical FFCF almost completely dominates the FFCF with almost no contribution to the final result from the electrostatic and cross terms. In the classical FFCF, it is most likely that the electrostatic forces serve to position the solvent close enough to the relaxing molecule to sample regions of the Lennard-Jones repulsive wall that would have been inaccessible in the absence of electrostatic forces.

In Fig. 3.4 we compare the full, Lennard-Jones, electrostatic, and cross term contributions to the FT of the quantum mechanical FFCF, $e^{\beta\hbar\omega/2}\tilde{C}_s^{LSC-LHA}(\omega)$. In contrast to the classical case, the full FFCF is not dominated by the Lennard-Jones term but instead also includes contributions from the electrostatic term. Although
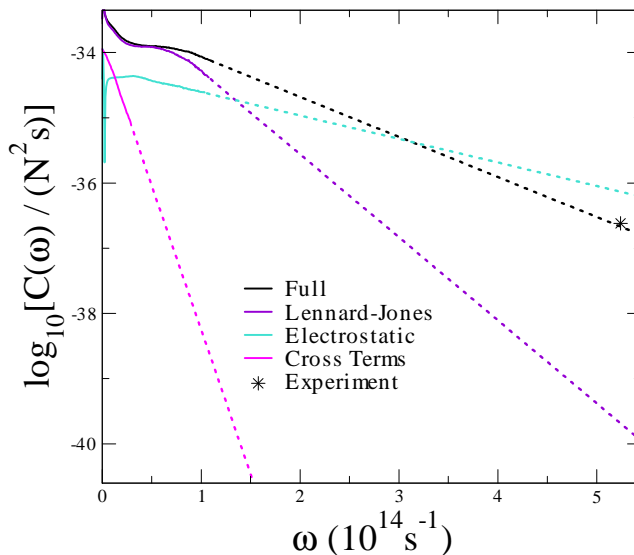
Figure 3.4: A semilog plot of the full, Lennard-Jones, electrostatic, and cross term contributions to $e^{\beta\hbar\omega/2}\tilde{C}_s^{LSC-LHA}(\omega)$ for neat hydrogen chloride at 188 K

electrostriction seems to be the classical mechanism leading to the enhancement of VER rates in polar solvents, quantum mechanically this is not the case. It is possible that the quantum effects instead allow the system to explore classically forbidden regions of both the Lennard-Jones and electrostatic potentials. This may then lead to the enhancement seen in VER rates in polar liquids.

3.4 Conclusion

Building on work previously presented, we have shown that because of its relative ease in implementation, we have used the AMBER molecular dynamics software package to study the quantum mechanical effects of VER in polar solvents using the FDF-LSC-LHA FFCF, which is based on applying the LSC methodology to the symmetrized FFCF. This is the first ever study of VER in a polar solvent using semiclassical methods. We have found that the in the case of methyl chloride, which has a low characteristic vibrational frequency, almost no quantum enhancement was seen.

The classical and quantum FFCFs agreed well with each other. The uncorrected FFCF was still lower than the classical result. This is a testament to the robustness FDF-LSC-LHA method, which is able to take into account the classical character of the system so that the correction term, $e^{\beta\hbar\omega/2}$ does not lead to an overestimated quantum mechanical FFCF. We also found that using the Schofield quantum correction factor, which is analogous to the symmetrized FFCF, leads to an overestimation of quantum effects.

In order to understand whether electrostriction plays a significant role in quantum mechanical VER rates for polar systems, we studied the vibrational relaxation of neat liquid hydrogen chloride. As opposed to the case of VER in methyl chloride, there are indeed significant quantum mechanical effects that enhance the VER rate even further. We also looked at the contributions to the FFCF in the classical and quantum mechanical cases and found that classically, electrostriction seems to be the dominant mechanism for rate enhancement in polar solvents. Classically, the electrostatic forces played no direct role in enhancing FFCF. In the quantum case, the electrostatic forces were found to play a dominant role. This shows that electrostriction is not the dominant mechanism for quantum mechanical enhancement of VER rates in polar solvents. This also shows the importance of including quantum mechanical effects and the danger in assuming that mechanisms that hold in classical systems will also hold in quantum mechanical systems.

CHAPTER IV

Diffusion in Quantum Liquids

4.1 Introduction

The calculation of quantum mechanical time correlation functions (TCF) is of central importance to the study of dynamics processes in liquids where quantum effects play a significant role. For example calculation of quantum mechanical VER rates in liquid oxygen or nitrogen can differ from the classical calculation by many orders of magnitude[61, 56, 135, 147, 152]. Liquid *para*-hydrogen at 25 K is another example of a system where quantum effects cannot be ignored. In this case, if the liquid is simulated using what is generally considered a very accurate force field, the classical state point turns out to lie in the liquid-vapor coexistence regime, whereas experimentally this state point is a liquid[85, 84]. Because of the importance of quantum effects in liquid hydrogen and the availability of experimental data and an accurate force field, the calculation of diffusion coefficients via a quantum mechanical velocity-velocity correlation function (VVCF) has become a benchmark problem for quantum dynamics methods[84, 55, 96, 119, 116, 118, 117, 121, 123].

The exact calculation of quantum mechanical TCFs, however, is beyond the current capability of modern computationally available resources due to the exponential scaling of the computational effort with the number of degrees of freedom (DOF)

involved in quantum calculations. One of the methods proposed to capture quantum dynamics is to use a semiclassical approach, where the initial conditions are sampled quantum mechanically and the dynamics are propagated classically. One such method, the linearized semiclassical (LSC) approximation, has been derived by Miller and coworkers[143, 155, 145, 146, 154, 144, 156] via linearizing the forward-backward action in the semiclassical [79, 143, 155, 156, 153, 39, 40, 41, 78, 111, 76, 75, 82, 112, 88, 87, 53, 51, 62, 100, 101, 81, 90, 132, 148, 69, 102, 91, 80] initial value representation [87, 53, 51, 62, 91, 89, 52, 66, 63, 114, 37, 64, 141] expression for a real-time quantum mechanical correlation function, with respect to the difference between the forward and backward trajectories. Shi and Geva have also shown that the very same approximation can also be derived by linearizing the *exact* real-time path integral expression for the correlation function, without explicitly invoking the semiclassical approximation[133]. The LSC approximation for a general time correlation function is given by

$$C(t) \approx \frac{1}{Z_b} \frac{1}{(2\pi\hbar)^N} \int d\mathbf{Q_0} \int d\mathbf{P_0} \left[\hat{A}e^{-\beta\hat{H}_b}\right]_W (\mathbf{Q_0}, \mathbf{P_0}) B_W(\mathbf{Q}_t^{(Cl)}, \mathbf{P}_t^{(Cl)}) , \qquad (4.1)$$

where the Wigner transforms are

$$[\hat{A}e^{-\beta\hat{H}_b}]_W = \int d\mathbf{\Delta}\, e^{-i\mathbf{P_0}\mathbf{\Delta}/\hbar} \langle \mathbf{Q}_0 + \mathbf{\Delta}/\mathbf{2}|\hat{A}\,e^{-\beta\hat{H}_b}\,|\mathbf{Q}_0 - \mathbf{\Delta}/\mathbf{2}\rangle \qquad (4.2)$$

and

$$B_W = \int d\mathbf{\Delta}\, e^{-i\mathbf{P_0}\mathbf{\Delta}/\hbar} \langle \mathbf{Q}_0 + \mathbf{\Delta}/\mathbf{2}|\hat{B}|\mathbf{Q}_0 - \mathbf{\Delta}/\mathbf{2}\rangle \qquad (4.3)$$

It is important to note that when $\hat{B}$ is a function of only position or momentum, the Wigner transform will be equal to $B^{(Cl)}$. Because of the highly oscillatory nature of the integrals, the Wigner transform cannot be solved directly. One approach to

this problem is to introduce a local harmonic approximation (LHA), where a normal-mode analysis is used to solve the Wigner integral analytically. For the case of solving VER rates via a quantum mechanical force-force correlation function (FFCF) (cf. Chapters 1, 2, and 3), the LHA of the bath Hamiltonian leads to

$$
\hat{H}_b = \sum_{j=1}^{N} \frac{(\hat{P}^{(j)})^2}{2M^{(j)}} + V\left(\hat{\mathbf{Q}}\right) \tag{4.4}
$$

$$
\approx \sum_{k=1}^{f} \frac{1}{2}(\hat{P}_n^{(k)})^2 + V(\mathbf{Q}_0) + \sum_{k=1}^{f} G_n^{(k)} \hat{Q}_n^{(k)} + \frac{1}{2}\sum_{k=1}^{f}(\Omega^{(k)})^2[\hat{Q}_n^{(k)}]^2
$$

where

$$
\hat{Q}_n^{(k)} = \sum_{l=1}^{f} T_{l,k} M^{1/2}[Q^{(l)} - Q_0^{(l)}] \tag{4.5}
$$

$$
\hat{P}_n^{(k)}(Q_0) = \sum_{l=1}^{f} T_{l,k} M^{-1/2} \hat{P}^{(l)} \tag{4.6}
$$

are the mass weighted normal mode coordinates and momenta, respectively, $\{(\Omega^{(k)})^2\}$ are the eigenvalues of the corresponding mass weighted Hessian matrix

$$
\mathcal{H}_{ij} = \frac{1}{(M^{(i)}M^{(j)})^{1/2}} \frac{\partial^2 V}{\partial Q^{(i)} \partial Q^{(j)}} \tag{4.7}
$$

and

$$
G_n^{(k)}(Q_0) = \sum_{l=1}^{f} T_{l,k} M^{-1/2} \left.\frac{\partial V}{\partial Q^{(l)}}\right|_{\mathbf{Q}=\mathbf{Q}_0} \tag{4.8}
$$

Ultimately this approximation will allow us to solve the Wigner integral in Eq. (4.2) analytically with respect to $\boldsymbol{\Delta}$; however, the normal mode calculation leads to a computational bottleneck when diagonalizing the mass weighted Hessian matrix. Each trajectory of the simulation requires a normal mode analysis of the entire simulation. As the the number of degrees of freedom increases, this can become computationally expensive. Because of this we have introduced an normal mode free (NMF) approximation to the LSC-LHA developed by Shi and Geva[134, 135].

The application of this method to calculating the FFCF in a model system showed that although this NMF-LSC method overestimated the quantum effects at the high frequencies required to calculate VER rate constants, the real time part of the FFCF agreed well with the exact result of the model. This led us to apply our new NMF-LSC approach to the calculation of diffusion coefficients, which can be related to the time integral of the real part of the VVCF.

4.2   Theory

4.2.1   Force-Force Time Correlation Function

VER rate constants can be related to the Fourier transform (FT) of the FFCF (cf. Chapters 1, 2, and 3). The full LSC approximation to the quantum mechanical FFCF for position dependent force derived by Shi and Geva [134]:

$$
\begin{aligned}
C_F(t) \;\approx\; & \int d\mathbf{Q}_0 \frac{\langle \mathbf{Q}_0 |\, \mathrm{e}^{-\beta \widehat{H}_b}\, |\mathbf{Q}_0\rangle}{Z_b} \int d\mathbf{P}_{n,0} \prod_{j=1}^{f} \left(\frac{1}{\alpha^{(j)}\pi\hbar^2} \right)^{1/2} \times \\
& \exp\left[-\frac{(P_{n,0}^{(j)})^2}{\hbar^2 \alpha^{(j)}} \right] [\delta F(\mathbf{Q}_0) + D(\mathbf{Q}_0, \mathbf{P}_{n,0})]\delta F(\mathbf{Q}_t^{(Cl)})
\end{aligned}
\tag{4.9}
$$

where $\mathbf{P}_{n,0}$ is the the initial mass weighted normal mode transformed momentum and

$$
\alpha^{(j)} = \frac{\Omega^{(j)}}{\hbar} \coth[\beta\hbar\Omega^{(j)}/2]
\tag{4.10}
$$

The delocalized force term $D(\mathbf{Q}_0, \mathbf{P}_{n,0})$ is purely quantum mechanical and is given by

$$
D(\mathbf{Q}_0, \mathbf{P}_0) = -i \sum_{i=1}^{f} \frac{\tilde{F}_i' P_{n,0}^{(i)}}{\hbar\alpha^{(i)}} + \sum_{i=1}^{f} \frac{\tilde{F}_{i,i}''}{4\alpha^{(i)}} - \sum_{i,j=1}^{f} \frac{\tilde{F}_{i,j}'' P_{n,0}^{(i)} P_{n,0}^{(j)}}{2\hbar^2 \alpha^{(i)}\alpha^{(j)}}
\tag{4.11}
$$

where F, $F_i' = \left.\frac{\partial F}{\partial Q^{(i)}}\right|_{\mathbf{Q}=\mathbf{Q}_0}$, $F_{i,j}'' = \left.\frac{\partial^2 F}{\partial Q^{(i)}\partial Q^{(j)}}\right|_{\mathbf{Q}=\mathbf{Q}_0}$ is the force of the bath on the relaxing molecule and its first and second derivatives, respectively, and

$$
\tilde{F}_i' = \sum_{j=1}^{f} (M^{(j)})^{-1/2} T_{j,i} F_j'; \; \tilde{F}_{ij}'' = \sum_{k=1}^{f}\sum_{l=1}^{f} (M^{(k)} M^{(l)})^{-1/2} T_{k,j} T_{l,i} F_{kl}''
\tag{4.12}
$$

are the mass weighted normal mode transformed force derivatives.

To avoid calculating the normal mode eigenvalues, the $\coth[\beta\hbar\Omega^{(j)}/2]$ term in Eq. (4.10) can be expanded to first order in $\hbar$. This is the key step in the NMF-LSC approximation and eliminates the need to diagonalize the mass weighted Hessian matrix. The eigenvalue dependence is removed, yielding the following result:

$$\alpha \approx \alpha_0 \equiv \frac{2}{\beta\hbar^2} \tag{4.13}$$

This approximated alpha term can then be substituted into Eq. (4.9) and Eq. (4.11), which leads to the NMF-LSC approximation of the FFCF:

$$
\begin{aligned}
C_F(t) \quad \approx \quad & \int d\mathbf{Q}_0 \frac{\langle\mathbf{Q}_0|\,\mathrm{e}^{-\beta\widehat{H}_b}\,|\mathbf{Q}_0\rangle}{Z_b} \int d\mathbf{P}_0 \prod_{j=1}^{f}\left(\frac{\beta}{2\pi M^{(j)}}\right)^{1/2} \times \\
& \exp\left[\frac{-\beta(P_0^{(j)})^2}{2M^{(j)}}\right][\delta F(\mathbf{Q}_0) + D(\mathbf{Q}_0,\mathbf{P}_0)]\cdot\delta F(\mathbf{Q}_t^{(Cl)})
\end{aligned} \tag{4.14}
$$

where

$$D_0(\mathbf{Q}_0,\mathbf{P}_0) \approx \frac{-i\beta\hbar}{2}\sum_{i=1}^{f}\frac{F_i''P_0^{(i)}}{M^{(i)}} + \frac{\beta\hbar^2}{8}\sum_{i=1}^{f}\frac{F_{i,i}''}{M^{(i)}} - \frac{\beta^2\hbar^2}{8}\sum_{i,j=1}^{f}\frac{F_{i,j}''P_0^{(i)}P_0^{(j)}}{M^{(i)}M^{(j)}}. \tag{4.15}$$

It is important to note that the NMF-LSC approximation still includes the purely quantum mechanical delocalized force and samples the initial positions quantum mechanically, but the initial momentum is now sampled purely classically. The need to calculate and diagonalize the Hessian matrix has also been removed from the expression, eliminating the LHA computational bottleneck.

4.2.2 Diffusion

The Hamiltonian of a bath of N identical diffusing molecules with f degrees of freedom is

$$\widehat{H}_b = \sum_{i=1}^{f}\frac{(\hat{P}^{(i)})^2}{2M} + \hat{V}(\hat{\mathbf{Q}}) \tag{4.16}$$

consisting of the intermolecular and intramolecular degrees of freedom for the system $[\hat{\mathbf{Q}} = (\hat{Q}^{(i)}, \ldots, \hat{Q}^{(f)})$, $\hat{\mathbf{P}} = (\hat{P}^{(i)}, \ldots, \hat{P}^{(f)})$, $\hat{V}(\hat{\mathbf{Q}}) = V(\hat{Q}^{(i)}, \ldots, \hat{Q}^{(f)})$, M are the corresponding coordinates, momenta, potential energy, and mass of a molecule, respectively].

The quantum mechanical velocity -velocity time correlation function (VVCF) of such a system is expressed in the following way:

$$C_v(t) = \frac{1}{N} \langle \hat{\mathbf{v}}(0) \cdot \hat{\mathbf{v}}(t) \rangle_0 \tag{4.17}$$

where $\left\langle \hat{A} \right\rangle_0 = \mathrm{Tr}[\mathrm{e}^{-\beta \widehat{H}_b} \hat{A}]/Z_b$, $\beta = \frac{1}{k_B T}$, $Z_b = \mathrm{Tr}[\mathrm{e}^{-\beta \widehat{H}_b}]$, $\hat{\mathbf{v}}(t) = \mathrm{e}^{i \widehat{H}_b t/\hbar} \hat{\mathbf{v}} \, \mathrm{e}^{-i \widehat{H}_b t/\hbar}$, $\hat{\mathbf{v}} = (\hat{v}^{(1)}, \ldots, \hat{v}^{(f)}) = \hat{\mathbf{P}}/M$ are the velocities of the bath. This VVCF can also be written as a momentum time autocorrelation function

$$C_v(t) = \frac{1}{N} \frac{1}{M^2} \langle \hat{\mathbf{P}}(0) \cdot \hat{\mathbf{P}}(t) \rangle_0 \tag{4.18}$$

with $\hat{\mathbf{P}}$ being the momentum and M the molecular mass. The diffusion coefficient for the system molecules is calculated from the VVCF according to the following Green-Kubo relationship[68]:

$$D = \frac{1}{3} \int_0^\infty dt \, \mathrm{Re}[\langle \hat{\mathbf{v}}(0) \cdot \hat{\mathbf{v}}(t) \rangle_0] \tag{4.19}$$

According to the LSC approximation, the VVCF for a system of N identical molecules takes the following semiclassical form:

$$C_v(t) = \frac{1}{N} \sum_{i=1}^{f} \frac{1}{Z_b} \frac{1}{M^2 \times (2\pi\hbar)^f} \int d\mathbf{Q}_0 \int d\mathbf{P}_0 [\hat{P}^{(i)} \, \mathrm{e}^{-\beta \widehat{H}}]_W(\mathbf{Q}_0, \mathbf{P}_0) \hat{P}_W^{(i)}(\mathbf{Q}_t^{(Cl)}, \mathbf{P}_t^{(Cl)}) \tag{4.20}$$

Here

$$P_W^{(i)}(\mathbf{Q}_t^{(Cl)}, \mathbf{P}_t^{(Cl)}) = P_t^{(i),(Cl)} \tag{4.21}$$

and

$$[\hat{P}^{(i)} \, \mathrm{e}^{-\beta \widehat{H}}]_W(\mathbf{Q}_0, \mathbf{P}_0) = \int d\boldsymbol{\Delta} \, \mathrm{e}^{-i\mathbf{P}_0 \boldsymbol{\Delta}/\hbar} \langle \mathbf{Q}_0 + \boldsymbol{\Delta}/\mathbf{2} | \hat{P}^{(i)} \, \mathrm{e}^{-\beta \widehat{H}} | \mathbf{Q}_0 - \boldsymbol{\Delta}/\mathbf{2} \rangle \quad (4.22)$$

The multidimensional Wigner phase space integral in Eq. (4.22) can be preformed analytically by employing the LHA to the bath Hamiltonian in Eq. (4.4). The Wigner integral in Eq. (4.22) is rewritten in the following way:

$$[\hat{P}^{(i)} \, \mathrm{e}^{-\beta \widehat{H}_b}]_W(\mathbf{Q}_0, \mathbf{P}_0) = \langle \mathbf{Q}_0 | \, \mathrm{e}^{-\beta \widehat{H}_b} | \mathbf{Q}_0 \rangle \int d\boldsymbol{\Delta} e^{-i\mathbf{P}_0 \boldsymbol{\Delta}/\hbar} \frac{\langle \mathbf{Q}_0 + \boldsymbol{\Delta}/\mathbf{2} | \hat{P}^{(i)} \, \mathrm{e}^{-\beta \widehat{H}_b} | \mathbf{Q}_0 - \boldsymbol{\Delta}/\mathbf{2} \rangle}{\langle \mathbf{Q}_0 | \, \mathrm{e}^{-\beta \widehat{H}_b} | \mathbf{Q}_0 \rangle},$$
$$(4.23)$$

however, the LHA is not applied to the $\langle \mathbf{Q}_0 | e^{-\beta \widehat{H}} | \mathbf{Q}_0 \rangle$ term preceding the integral. Instead the LHA is applied to the $\frac{\langle \mathbf{Q}_0 + \boldsymbol{\Delta}/\mathbf{2} | \hat{P}^{(i)} \, \mathrm{e}^{-\beta \widehat{H}_b} | \mathbf{Q}_0 - \boldsymbol{\Delta}/\mathbf{2} \rangle}{\langle \mathbf{Q}_0 | \mathrm{e}^{-\beta \widehat{H}_b} | \mathbf{Q}_0 \rangle}$ ratio. This will allow the Wigner integral to be solved analytically in terms of $\boldsymbol{\Delta}$ and avoid the sign problem associated with highly oscillatory integrals [79]. The momentum, $\hat{P}^{(i)}$, of a diffusing molecule in Eq. (4.22) is expressed in terms of the mass weighted normal mode momenta

$$\hat{P}^{(i)} = M^{1/2} \sum_{j=1}^{f} T_{ij} \hat{P}_n^{(j)}, \quad (4.24)$$

the Hamiltonian $\hat{H}_b$ is replaced by its LHA, and the following identities are used to explicitly solve the $\frac{\langle \mathbf{Q} + \boldsymbol{\Delta}/\mathbf{2} | \hat{P}^{(i)} e^{-\beta \widehat{H}_b} | \mathbf{Q} - \boldsymbol{\Delta}/\mathbf{2} \rangle}{\langle \mathbf{Q}_0 | e^{-\beta \widehat{H}_b} | \mathbf{Q}_0 \rangle}$ (the proportionality constants C_0 and C_1 are independent of Q_1 and Q_2) :

$$\langle Q_1 | \, \mathrm{e}^{-\beta [\hat{P}^2/2 + \Omega^2 \hat{Q}/2]} | Q_2 \rangle = C_0 \exp \left\{ -\frac{\Omega}{2\hbar} \frac{1}{\sinh(\beta\hbar\Omega)} \times [\cosh(\beta\hbar\Omega)(Q_1^2 + Q_2^2) - 2Q_1 Q_2] \right\}$$
$$(4.25)$$

$$\langle Q_1 | \hat{P} \, \mathrm{e}^{-\beta [\hat{P}^2/2 + \Omega^2 \hat{Q}/2]} | Q_2 \rangle =$$

$$iC_1\Omega \coth(\beta\hbar\Omega) \left(Q_1 - \frac{Q_2}{\cosh(\beta\hbar\Omega)} \right) \times$$

$$\exp \left\{ \begin{array}{c} -\frac{\Omega}{2\hbar} \frac{1}{\sinh(\beta\hbar\Omega)} \times \\ [\cosh(\beta\hbar\Omega)(Q_1^2 + Q_2^2) - 2Q_1 Q_2] \end{array} \right\} (4.26)$$

The Gaussian integrals over $\{\Delta^{(k)}\}$ are then performed analytically. This leads to the following result:

$$[\hat{P}^{(i)} e^{-\beta\hat{H}_b}]_W(\mathbf{Q}_0, \mathbf{P}_0) = \langle\mathbf{Q}_0| e^{-\beta\hat{H}_b} |\mathbf{Q}_0\rangle \prod_{j=1}^{f} \left(\frac{4\pi}{M\alpha^{(j)}}\right)^{1/2} \exp\left[\frac{-(P_{n,0}^{(j)})^2}{\hbar^2\alpha^{(j)}}\right] \times \{\mathbf{P}_0 + D(\mathbf{Q}_0)\}$$

(4.27)

where

$$D(\mathbf{Q}_0) = \frac{i}{\hbar}M^{1/2}\sum_{k=1}^{f} T_{ik}\frac{G_n^{(k)}(Q_0)}{\alpha^{(k)}}$$

(4.28)

and α is the same as in Eq (4.10) and $G_n^{(k)}(Q_0)$ is the same as in Eq. (??).

We can employ the same NMF approximation that was used in calculating the NMF-LSC FFCF by replacing α with α_0 in Eq. (4.27) and Eq. (4.28), transforming the expression back to the primitive coordinate space, and substituting the expression into Eq. (4.20). This resulting NMF-LSC approximation to the VVCF is

$$C_v(t) \approx \frac{1}{N}\sum_{i=1}^{f}\frac{1}{M^2}\int d\mathbf{Q}_0\frac{\langle\mathbf{Q}_0| e^{-\beta\hat{H}_b} |\mathbf{Q}_0\rangle}{Z_b}\int d\mathbf{P}_0 \prod_{j=1}^{f}\left(\frac{\beta}{2\pi M}\right)^{1/2}$$

(4.29)

$$\times \exp\left[\frac{-\beta(P_0^{(j)})^2}{2M}\right][P_0^{(i)} + D_0(\mathbf{Q}_0)]\cdot P_t^{(i),(Cl)}$$

(4.30)

where

$$D_0(\mathbf{Q}_0) = \frac{i\beta\hbar}{2}\sum_{i=1}^{f}\left.\frac{\partial V(\mathbf{Q})}{\partial Q^{(i)}}\right|_{\mathbf{Q}=\mathbf{Q}_0}.$$

(4.31)

As in Eq. (4.14), $D_0(\mathbf{Q}_0)$, is a purely quantum mechanical term, which will be referred to as the *delocalized momentum.* The initial position sampling and delocalized force terms are fully quantum mechanical, but the initial momentum sampling is fully classical.

4.3   Applications

4.3.1   Exponential Coupling to a Harmonic Bath

To test the NMF-LSC approximation to the FFCF, it was applied to a bath of uncoupled harmonic oscillators at different frequencies,

$$\hat{H}_b = \sum_{j=1}^{f} \left(\frac{(\hat{P}^{(j)})^2}{2M^{(j)}} + \frac{1}{2}M^{(j)}(\omega^{(j)})^2(\hat{Q}^{(j)})^2 \right) \tag{4.32}$$

and a force that is exponential in the bath coordinates

$$\hat{F}(\hat{\mathbf{Q}}) = e^{R(\hat{\mathbf{Q}})} \tag{4.33}$$

where

$$R(\hat{\mathbf{Q}}) = \sum_{j} c^{(j)} \sqrt{\frac{2M^{(j)}\omega^{(j)}}{\hbar}} \hat{Q}^{(j)} \ . \tag{4.34}$$

The exact quantum mechanical FFCF for this model can be obtained analytically[99] and has been established as a convenient benchmark[120, 28]. The exact quantum mechanical FFCF is

$$C(t) = e^{B(0)}(e^{B(t)} - 1) \ , \tag{4.35}$$

where

$$B(t) = \langle \hat{R}_0(t)\hat{R}(0) \rangle_0 = \int_0^\infty d\omega \Gamma(\omega)\{[n(\omega) + 1]e^{-i\omega t} + n(\omega)e^{i\omega t}\} \ , \tag{4.36}$$

$$\Gamma(\omega) = \sum_k \left(c^{(k)}\right)^2 \delta(\omega - \omega^{(k)}) \tag{4.37}$$

and $n(\omega) = [\exp(\beta\hbar\omega) - 1]^{-1}$. It is important to note that the expression in Eq. (4.1) is exact when the bath is harmonic. The differences from the exact solution come from the use of the quadratic approximation of $\delta F(\mathbf{Q_0} + \mathbf{\Delta}/2)$. Although the LHA is exact for a harmonic potential, the NMF-LSC approximation involves an approximation to the α term that is a result of the LHA. By applying the NMF-LSC

approximation to the FFCF of this system, we can compare to both the exact solution and the full LSC-LHA solution to understand the accuracy of our new method.

The full LSC approximation to the FFCF of harmonic bath with exponential force coupling is has been derived by Shi and Geva[134] and is given by

$$C(t) \approx e^{B_R(0)} \left[\left(e^{B_R(t)} - 1 \right) + i e^{B_R(t)} B_I(t) - \frac{1}{2} e^{B_R(t)} B_I^2(t) \right], \qquad (4.38)$$

where $B_R(t)$ and $B_I(t)$ are the real and imaginary parts of $B(t)$, respectively. The NMF-LSC approximation to the FFCF is given by

$$
\begin{aligned}
C(t) \quad \approx \quad & e^{\sum_{k=1}^f \frac{(c^{(k)})^2}{2} \coth(\frac{\beta\hbar\omega^{(k)}}{2}) \cos^2(\omega^{(k)}t)} \times \\
& e^{\sum_{k=1}^f \frac{(c^{(k)})^2}{\beta\hbar\omega^{(k)}} \sin^2(\omega^{(k)}t)} \times \\
& e^{\frac{1}{2}B_R(0)} \left[\left(e^{B_R(t)} - 1 \right) + i e^{B_R(t)} B_I(t) - \frac{1}{2} e^{B_R(t)} B_I^2(t) \right].
\end{aligned}
\qquad (4.39)
$$

It is interesting to note that $\frac{(c^{(k)})^2}{\beta\hbar\omega^{(k)}}$ is the first order approximation of $\frac{(c^{(k)})^2}{2} \coth(\frac{\beta\hbar\omega^{(k)}}{2})$ in orders of $\hbar$. If $\frac{(c^{(k)})^2}{\beta\hbar\omega^{(k)}}$ were replaced by $\frac{(c^{(k)})^2}{2} \coth(\frac{\beta\hbar\omega^{(k)}}{2})$ in Eq. (4.39), the result would be the full LSC approximation.

The real and imaginary parts of the exact [Eq. (4.35)] and approximate [Eq. (4.38)] FFCF for this model are shown in Fig 4.1a and 4.1b, respectively, along with the exact, full LSC, and classical expressions. The calculations were performed with the following spectral density,

$$\Gamma(\omega) = 2\lambda \frac{\omega^\alpha}{\omega_c^{\alpha+1}} \exp\left(-\frac{\omega^2}{\omega_c^2}\right), \qquad (4.40)$$

with the parameters: $\lambda = 0.20$, $\alpha = 3$ and $\beta\hbar\omega_c = 4.0$. Fig. 4.1a shows that although the real part of the NMF-LSC approximation is in good agreement with the full LSC and exact expressions at $t = 0$, there is some deviation near the minimum. This deviation becomes more pronounced when looking at the imaginary part in Fig.

4.1b. The stronger deviation from the exact expression is due to the increase in classical character introduced by approximating the α term to first order in $\hbar$.
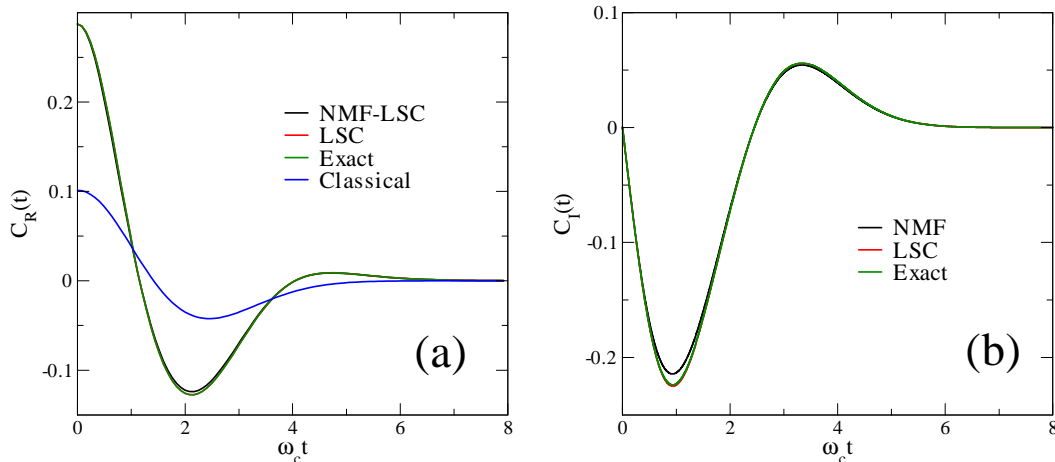

Figure 4.1: A comparision of the real (a), and imagionary (b) parts of the FFCF for the NMF-LSC, LSC-LHA, exact, and classical solutions to the FFCF of a system of uncoupled harmonic oscillaotrs with exponential coupling to the force.

The FT of the NMF-LSC [Eq. (4.39)], full-LSC [Eq. (4.38)], exact [Eq. (4.35)] and classical FFCFs are shown in Fig 4.2 on a semilog plot. The approximate FT of the FFCF is given as obtained from the full, real part and imaginary part of the respective FFCFs, [for the exact FFCF, $\tilde{C}(\omega) = 4 \int_0^\infty dt \cos(\omega t) C_R(t)/(1 + e^{-\beta\hbar\omega}) = -4 \int_0^\infty dt \sin(\omega t) C_I(t)/(1 - e^{-\beta\hbar\omega})$]. At $\omega = 0$, the NMF-LSC FFCF coincides with the classical FFCF and not the exact quantum mechanical expression. This behavior is not seen at higher frequencies though, showing that the NMF-LSC still contains some of the quantum character. The LSC-LHA approximation agrees well with the exact expression as previously reported by Shi and Geva[134]; however, at high frequencies the NMF-LSC results deviate greatly from the exact expressions. Although the NMF-LSC seems to fail at high frequencies, its success with capturing the quantum effects in the real time part of the FFCF was our motivation for applying the method to diffusion.
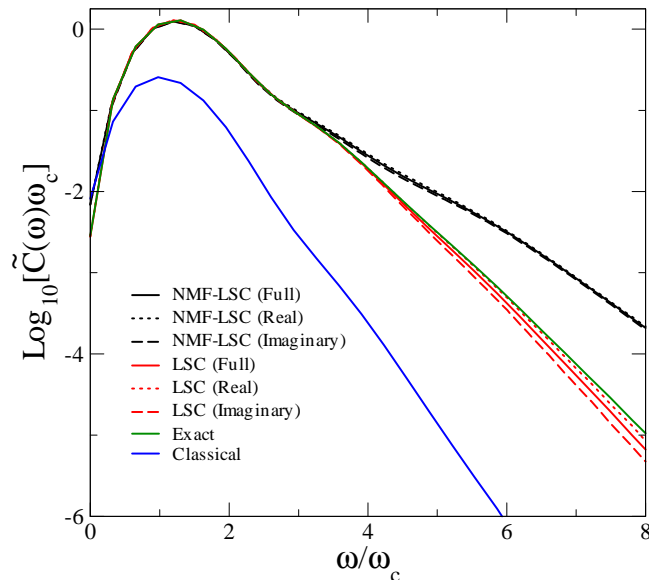
Figure 4.2: A comparision of the full, real, and imagionary contributions to the FT of the FFCF for the NMF-LSC, LSC-LHA, and exact solutions to the FFCF of a system of uncoupled harmonic oscillaotrs with exponential coupling to the force.

4.3.2 Liquid *para*-Hydrogen and Liquid *ortho*-Deuterium

In order to calculate the VVCF for liquid *para*-hydrogen or liquid *ortho*-deuterium using the NMF-LSC approximation, the interactions between molecules were described using the Silvera-Goldman potential[137, 138]. This potential has been widely used to calculate the VVCF in liquid *para*-hydrogen and *ortho*-deuterium and has been shown to agree very well with experimental results when used in MC and molecular dynamics (MD) simulations[9, 130]. The Silvera-Goldman potential treats the molecules as though they were spherical particles and depends only on the distance between them.

The Silvera-Goldman potential is given by:

$$V(r) = \exp(\alpha - \delta r - \gamma r^2) - \left(\frac{C_6}{r^6} + \frac{C_8}{r^8} + \frac{C_{10}}{r^{10}} \right) f_c(r) + \frac{C_9}{r^9} f_c(r) \qquad (4.41)$$

where

$$
f_c(r) = \begin{cases} e^{-(r_c/r-1)^2} & (r \leqslant r_c) \\ 1 & (r > r_c) \end{cases} \tag{4.42}
$$

and $\alpha = 1.713$, $\delta = 1.5671$, $\gamma = 0.00993$, $C_6 = 12.14$, $C_8 = 215.2$, $C_{10} = 4813.9$, $C_9 = 143.1$, $r_c = 8.321$, in atomic units.

The NMF-LSC approximation to the VVCF in Eq. (4.29) is calculated according to the following procedure. The initial equilibrium positions are sampled according to the quantum mechanical probability $\int d\mathbf{Q}_0 \frac{\langle \mathbf{Q}_0 | e^{-\beta \hat{H}_b} | \mathbf{Q}_0 \rangle}{Z_b}$ using either path integral molecular dynamics (PIMD) or path integral Monte Carlo (PIMC) methods. The initial momenta are sampled classically using the Gaussian distribution $\int d\mathbf{P}_0 \prod_{j=1}^{f} \left(\frac{\beta}{2\pi M}\right)^{1/2} \exp\left[\frac{-\beta(P_0^{(j)})^2}{2M}\right]$. The delocalized momentum, D_0 (eq. 4.31), is evaluated at the initial quantum mechanical configuration, $\mathbf{Q}_0$. The system is then propagated classically using molecular dynamics (MD), after which, the VVCF average over the total number of molecules is evaluated. This process is then repeated over many different trajectories in order to calculate the ensemble average VVCF.

Using the methods described above, we evaluated the VVCF and diffusion coefficient for liquid *para*-hydrogen at 14 K, $\rho = 0.0235$ Å^{-3} and 25 K, $\rho = 0.0190$ Å^{-3} and liquid *ortho*-deuterium at 20.7 K, $\rho = 0.0254$ Å^{-3}, each with a periodically replicated simulation cell size of 256 molecules. Each system was equilibrated using the PIMD VV3 algorithm with 4 Nosé-Hoover chains[59] and $P = 52$, $P = 32$, for liquid *para*-hydrogen at 25 K and 14 K, respectively, and $P = 32$ for liquid *ortho*-deuterium. Each trajectory was propagated for 4 ps using the velocity Verlet algorithm. The VVCF was averaged over 20 000 trajectories for all systems.

The real part of the NMF-LSC VVCF function for *para*-H$_2$ at 14 K, 25 K, and *ortho*-D$_2$ is shown Fig. 4.3a. Because of the purely classical initial momentum
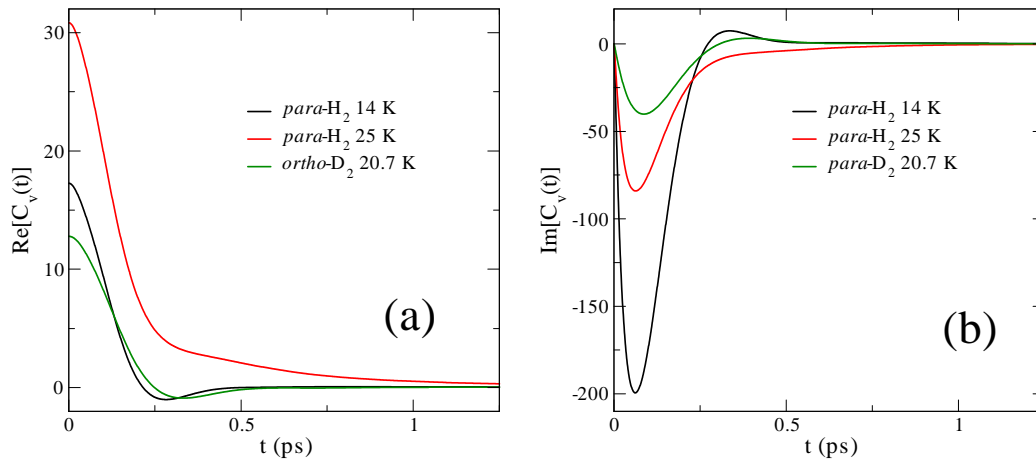
Figure 4.3: Real (a) and imaginary (b) parts of the VVCF calculated for liquid *para*-hydrogen at 14 K, 25 K, and liquid *ortho*-hydrogen at 20.7 K

sampling, the VVCF at $t = 0$ is dependent on the temperature of the system. The VVCFs shown in Fig. 4.3 also shows negative amplitudes resulting from direction reversing collisions between molecules for the lower temperature14 K *para*-H_2 and 20.7 K *ortho*-D_2 systems, but not for the 25 K system. The imaginary part of the VVCF is shown in Fig. 4.3b. It should be noted that the imaginary part of the VVCF, which is purely quantum mechanical, is very large compared to the real part. This suggests, as was seen in Fig. 4.2, that the NMF-LSC method seems to overestimate quantum effects. This is a curious result because the NMF-LSC actually samples the initial momentum classically. One would expect to see reduced quantum character.

The diffusion coefficients calculated from the real part of the VVCF are shown in Table 4.1. The table also compares the NMF-LSC calculated diffusion coefficient to experimental values and values calculated using various quantum dynamics methods. What is found is that most of these methods, including the NMF-LSC , agree reasonably well with the experimental value. We believe this is not due to the reliability or
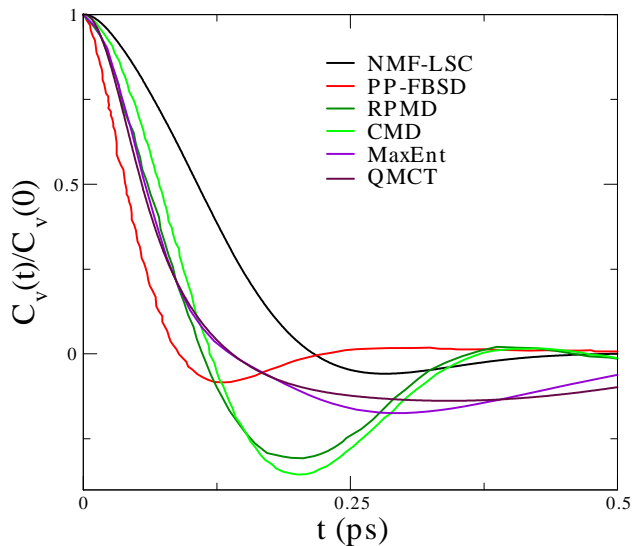
Figure 4.4: A comparison of the normalized real part of the VVCF for *para*-hydrogen at 14 K calculated using the NMF-LSC method, pair propagator-foward backward semiclassical dynamics (PP-FBSD)[96], ring polymer molecular dynamics (RPMD) [84], centroid molecular dynamics (CMD) [55], maximum entropy analytic continuation (MaxEnt) [121], and quantum mode coupling theory (QMCT)[123]

robustness of these methods at capturing quantum effects, but is instead due to the poor choice of diffusion as a benchmark. Because diffusion can be calculated from the real part of the VVCF, many of the quantum effects can be poorly estimated and still have no effect on the diffusion coefficient. This was seen in Fig. 4.3b, where, the over estimated imaginary part had no effect on the final diffusion coefficient. Part of the problem lies with the fact that there is no exact solution to the VVCF in liquid hydrogen. As can be seen in Fig. 4.4, the normalized real part of the NMF-LSC VVCF for *para*-H_2 at 14 K compared with other methods. The NMF-LSC VVCF does not agree well with the other the methods presented; however, there is not good agreement among all of the methods presented. Instead, what is seen is that the methods that are most theoretically similar show agreement with each other.

	Diffusion Coefficient ($\text{Å}^2/\text{ps}$)		
	H_2 (14 K)	H_2 (25 K)	D_2 (20l7 K)
NMF-LSC	0.600±0.004	1.958±0.008	0.505±0.003
PP-FBSD	0.75±0.07	1.68±0.05	$\cdots$
CMD	0.35±0.05	1.52±0.08	0.40±0.06
RPMD	1.59±0.01	0.33 ±0.01	$\cdots$
QMCT	0.30	1.69	0.49
MaxEnt	0.28	1.47	$\cdots$
Experiment	0.4	1.6	0.36

Table 4.1: A comparison of the diffusion coefficient for *para*-hydrogen at 14 K 25 K, and *ortho*-deuterium at 20.7 K calculated using the NMF-LSC method, pair propagator-foward backward semiclassical dynamics (PP-FBSD)[96], ring polymer molecular dynamics (RPMD) [84], centroid molecular dynamics (CMD) [55], maximum entropy analytic continuation (MaxEnt) [121], and quantum mode coupling theory (QMCT)[123]

4.4   Conclusion

We have introduced an NMF approximation to the original LHA-LSC approximation developed by Shi and Geva. This new NMF-LSC removes the computational bottleneck involved in performing a normal mode analysis for each set of sampled coordinates. This new approximation to quantum mechanical TCFs samples the initial positions quantum mechanically, but samples the momentum classically and still retains a modified purely quantum mechanical delocalization term. The NMF-LSC approximation was applied to two systems: the calculation of the FFCF of a bath of uncoupled harmonic oscillators coupled to an exponential force and the diffusion coefficient and VVCF of liquid H_2 at two different state points and liquid D_2 at a single state point. We found that the although the NMF-LSC FFCF coincided well with the exact solution in the real part of the time domain, at high frequencies it deviated greatly. We also found that although calculated diffusion coefficients agree well with experimental measurements, the NMF-LSC seems to overestimate the purely

quantum mechanical imaginary part of the VVCF. We see this as a evidence that diffusion is a poor benchmark for testing quantum dynamics methods, as the final result can poorly estimate quantum effect and yet still agree well with experimental results. Part of this problem lies in the fact that there is no way to calculate an exact solution to the quantum mechanical VVCF in a liquid with many degrees of freedom.

CHAPTER V

Isomerization of Hexatriene in Methanol and Cyclohexane

5.1 Introduction

The influence of solvent dynamics on solute is extremely important to understanding chemical processes in solutions. Solvent-solute interactions can play a strong role on chemical reactivity and energy transfer between the solute and solvent. Studies by Harris et. al.[46] on the isomerization rate constant of 1,3,5-*cis*-hexatriene (Z-HT) from the cZt-HT to tzt-HT conformers (where c and t designate cis and trans conformations about the single bonds) have shown that the isomerization process is highly dependent on solvent choice. This isomerization is shown schematically in Fig. 5.1 on the gas phase general AMBER force-field (GAFF)[19, 157] potential surface as where the charges were assigned using the AM1-BCC model[57, 58]. In their study, Harris and coworkers measured the temperature dependence of the cZt-HT $\rightarrow$ tzt-HT hexatriene isomerization and attempted to understand the conformational relaxation in terms of viscosity in the context of Kramers theory. In this context, the rate constant can be written as

$$k = k_{TST} \; \kappa \tag{5.1}$$

75

where k, is the relaxation rate constant, k_{TST} is the transition state theory (TST) approximated rate constant, and κ is the transmission coefficient that corrects the k_{TST} rate constant for solvent effects. In the limit of high friction, the transmission coefficient can be written as

$$\kappa = \frac{\omega_a}{\eta^\gamma} \tag{5.2}$$

where γ is a parameter such that $0 \leq \gamma \leq 1$, ω_a is the imaginary curvature of the energy barrier, and η is the shear viscosity. The transmission coefficient is able to correct for solvent effects by taking into account the effect of the free energy barrier in either aiding or hindering the ability of the reaction to overcome the barrier and the effect of the solvent's viscosity in either increasing or reducing recrossing over the barrier. In comparing the effects of polar and nonpolar solvents on the isomerization, it was found that for isomerization in cyclohexane (at 298 K, $\eta = 0.894$ mPa s), hexadecane (at 298 K, $\eta = 3.032$ mPa s), methanol (at 298 K, $\eta = 0.544$ mPa s), and propanol (at 298 K, $\eta = 1.945$ mPa s), the rates in the alkanes were faster than the alcohols. It was also found that the rates between the individual alkanes and the alcohols did not follow the η^{-1} dependence predicted by Kramers theory.

Although a Kramers theory description of rate constants can be a powerful predictive tool for understanding how solvent affects chemical reactions, it cannot always give a microscopic description of the process occurring. As was seen in the experiments Harris and coworkers, Kramers theory may also prove to be an inadequate explanation. In this case computer simulation can be used to calculate the isomerization rate constant using a linear response approach[11, 12, 13, 122, 124, 159]. Using a molecular dynamics (MD) simulation of hexatriene in various solvents, we have been able to directly monitor the reaction coordinate, ϕ, which corresponds to the isomerization dihedral angle, and calculate the rate constant using from the

linear response formalism. We can also calculate the free energy surface, calculate the amount of barrier recrossing, and calculate the entropy change to go from the product state to the transition state. From this data we have created a model of how the solvent interacts with the solute and influences the isomerization reaction, thus going beyond Kramers theory to directly explain the experimentally measured results.

5.2 Theory

The isomerization rate constant can be calculated within a computer simulation using linear response theory (cf. Chapter 1). Within this formalism the isomerization rate constant can be written in terms of the reactive-flux (RF) correlation function:

$$k^{RF} = \frac{\left\langle \dot{\phi}(0)\delta(\phi - \phi^*)h\left[\phi(t) - \phi^*\right]\right\rangle_0}{\langle h\left[\phi - \phi^*\right]\rangle \langle 1 - h\left[\phi - \phi^*\right]\rangle_0} \tag{5.3}$$

where ϕ is the isomerization dihedral angle, $\dot{\phi}$ is the velocity of the dihedral angle, ϕ^* is the dihedral angle at the transition state. $\delta(\phi - \phi^*)$ is the Dirac delta function, and is the Heaviside function such that

$$h(\phi - \phi^*) = \begin{cases} 1 \ , \ \phi > \phi^* \\ 0 \ , \ \phi < \phi^* \end{cases} \tag{5.4}$$

In a molecular dynamics simulation, the rate constant is measured by first equilibrating the molecule restrained at the transition state, ϕ^* (resulting from the delta function $\delta(\phi - \phi^*)$), and then correlating the velocity of the dihedral angle at $t = 0$ to the Heaviside function, $h\left[\phi(t) - \phi^*\right]$. It should be noted that the reactive flux correlation function is able to take into account barrier recrossing due to its time dependence. Whenever the reaction coordinate crosses from the product state to the

reactant state the Heaviside function will be equal to zero and the overall rate will be lowered. In practice, the RF-TCF reaches a plateau in short time scales accessible by computer simulation (ps) and the rate constant is measured from the plateau. Also, because the average in Eq. (5.3) involves preparing the system restrained at the transition state, the reactive flux must be multiplied by the probability of being at the transition state, namely:

$$\Pr(\phi^*) = \frac{e^{-\beta G(\phi^*)}}{\int d\phi e^{-\beta G(\phi)}} \tag{5.5}$$

where $\beta = \frac{1}{k_B T}$, k_B is the Boltzmann constant, T is the absolute temperature, and $G(\phi)$ is the Gibbs energy as a function of the dihedral angle. This probability corresponds to the thermal average of the delta function, $\langle \delta(\phi - \phi^*) \rangle_0$

If we assume there is no barrier recrossing, namely that at time $t = 0$, if the reaction coordinate is is going in certain direction it will always end up in that the well it was moving towards, then the reactive flux can approximated using transition state theory. The resulting TST constant, k^{TST}, is given by

$$k^{RF} = \frac{\left\langle \dot{\phi}(0)\delta(\phi - \phi^*)h\left[\dot{\phi}(0)\right] \right\rangle_0}{\langle h[\phi - \phi^*] \rangle \langle 1 - h[\phi - \phi^*] \rangle_0} \tag{5.6}$$

In contrast to Eq. (5.3), the TST rate constant cannot take into account barrier recrossing and is only dependent on equilibrium effects. As a result, k^{TST} can be thought of as the upper limit of the rate constant and will always be larger than k^{RF}.

Once the Gibbs free energy is known, the entropy can be directly calculated using the Maxwell relation[24]

$$S = -\left(\frac{\partial G}{\partial T}\right)_P \tag{5.7}$$

where P means the entropy is measured at constant pressure. The Maxwell relation can then be calculated using a three point difference formula.

5.3 Applications

In order to microscopically understand the effect of solvent on the isomerization of hexatriene, we used the AMBER molecular dynamics software package[19] to simulate the isomerization of hexatriene in methanol and cyclohexane. We have run these simulations in propanol, butanol, hexadecane, n-hexane, cycloheptane, and n-heptane; however, these results are still in preparation and will not be discussed here except to explain our future directions. We will instead focus on our studies in methanol and cyclohexane. All simulations were preformed using the GAFF and charges were assigned using the AM1-BCC semiempirical method and were done at $T =$280 K, 300 K, and 320 K.

Hexatriene molecules were prepared in the tzt-HT state and solvent molecules were then added to a truncated octahedral simulation box (378 methanol and 238 cyclohexane molecules, respectively). The systems were then energy minimized for 25,000 steps. After this, the simulations were equilibrated at constant volume and temperature for 500 ps with a time step of 1 fs. Next, the simulations were equilibrated at constant pressure and temperature between 1000-2000 ps until the density relaxed to a value near the experimental density. The Gibbs energy profile was then calculated using umbrella sampling simulations that were preformed at constant pressure and constant temperature for 1000 ps for each angles step, $\Delta\phi = 4°$, with measurements recorded every 50 steps. The results were then analyzed using the weighted histogram analysis method (WHAM)[38]. Once the transition state

was found, the k^{TST} calculations were preformed by restraining the dihedral angle
at the transition state and running10 restrained equilibrium simulations at constant
temperature and pressure for 200 ps, recording the fluctuations of the reaction coor-
dinate velocity every 100 steps and correlating the Heaviside function to the reaction
coordinate velocity and averaging the results. The k^{RF} calculations were calculated
by equilibrating the system with the dihedral angle restrained at the transition state
at constant temperature and pressure and then removing the temperature and angle
restraints. The unrestrained simulations were than run at constant pressure for 1
ps and the fluctuations of the reaction coordinate were recorded and the Heaviside
function was correlated to the velocity of the reaction coordinate at $t = 0$. These
simulations were averaged over 50,000 trajectories.

The Gibbs free energy profile for methanol and cyclohexane are shown in Figs.
5.2a and 5.2b, respectively. From these calculations the transition state was found to
$\phi^* = 90°$. It can also be seen that as the temperature is increased, barrier height to
go from the reactant to transition state, $\Delta G_{R \to TS}$ increases. Comparing the barrier
heights between methanol and cyclohexane, the barrier heights are consistently lower
in cyclohexane than in methanol. This is shown in Table 5.1. The reasons for this
will be further explored below.

	$\Delta G_{R \to TS}$ (kcal/mol)	
T (K)	Methanol	Cyclohexane
280	5.21	4.61
300	5.34	4.78
320	5.49	5.17

Table 5.1: Reactant to transition state barrier height, $\Delta G_{R \to TS}$, for methanol and
cyclohexane at 280 K, 300 K, and 320 K.

The RF-TCFs for methanol and cyclohexane are shown in Figs. 5.3a and 5.3b,

respectively. As can be seen in the figure, at short times the rates exhibit transient behavior seen before they plateau to the k^{RF} value. Also, as the temperature is increased the rates consistently become higher as is expected. The figure also shows that the rates for hexatriene isomerization in methanol are lower than in cyclohexane. This becomes further apparent in Fig. 5.4, which shows the temperature dependence of k^{RF} (a) and k^{TST} (b). As expected, the TST rates are faster than the RF rates. Also, our simulations are able to qualitatively capture the increased rate in cyclohexane regardless of whether the rate is calculated using RF or TST methods.

Because both RF and TST calculation show that the rates are faster in cyclohexane than in methanol, we are unable to tell if the increased rate is due dynamic effects, such as barrier recrossing or equilibrium effects such as barrier height. In order to understand what is the reason for the faster isomerization rate in cyclohexane, we calculated how much recrossing was seen in either solvent at 300 K. Fig. 5.5 shows a histogram of the number of recrossings seen each trajectory. The isomerization in cyclohexane actually shows more recrossing than in methanol. This is surprising because more recrossing should lead to a slower rate. Because of this, the faster rate must be due to equilibrium effects. From the table, we know that the barrier is lower in cyclohexane than in methanol. To understand why this is, we calculated the entropy change to go from the reactant state to the transition state, $\Delta S_{R \to TS}$. Comparing the entropy changes in both solvents at 300 K, we that in methanol $\Delta S_{R \to TS} = -10.4$ cal/mol K and in cyclohexane $\Delta S_{R \to TS} = 25.1$ cal/mol K. The isomerization is more entropically favorable in cyclohexane than in methanol. We believe the reason for this has to do with the way the solvent arranges itself around. Fig. 5.6 compares the radial distribution functions, $g(r)$, between the

terminal carbon in hexatriene and the center of mass in methanol or cyclohexane at 300 K. The figure shows that cyclohexane forms an extra solvation shell around hexatriene. Because methanol can form hydrogen bonds, the solvent can form a more open structure around hexatriene and interact less with the solute. Cyclohexane, on the other hand, does not hydrogen bond, and as a result, can interact more directly with the solute and fit into the space that opens when hexatriene is in its transition state. As a result, cyclohexane is a able to sample more configurations, leading to an increase in entropy and a lowering of the barrier. This may also be the reason for the increased recrossing seen in cyclohexane. Cyclohexane can pack closer to hexatriene and can collide with the isomerizing bond.

5.4   Conclusion

Using the RF-TCF and TST, we have been able to microscopically analyze the isomerization of hexatriene in methanol and cyclohexane. We found that our calculations were able to qualitatively capture the faster isomerization rate in cyclohexane versus methanol, however, further analysis was required to determine whether the increased rate was due to dynamic or equilibrium effects. By calculating the amount of recrossing, we were able to find even though the rate was slower in methanol than in cyclohexane, methanol had fewer barrier recrossings. Further analysis showed, that the faster rate is due to an entropic lowering of the barrier, a result the fact that cyclohexane is able to interact more with the solute because of its less open structure compared to methanol . This is an extremely interesting result because, in this case, cyclohexane is actually acting as catalyst. Cyclohexane's interactions

with the solute lower the free energy barrier and increase the rate constant. Importantly, using the linear response formalism allowed us to create a microscopic model of the interactions of the solvent with the solute that would not have been possible using Kramers theory. We have been able to measure microscopic phenomena that is beyond the scope of macroscopic theories and yet still allows us to explain the experimentally observed results.
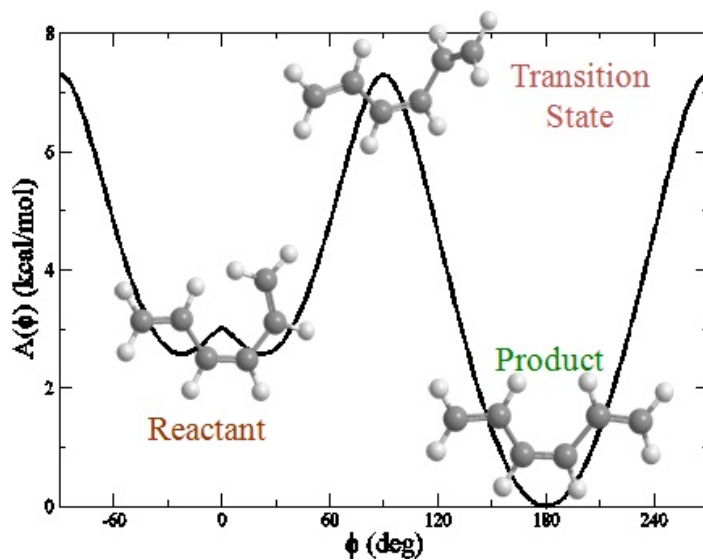
Figure 5.1: Potential surface of isomerization around single bond of hexatriene from cZt-tZt state as a function of dihedral angle.
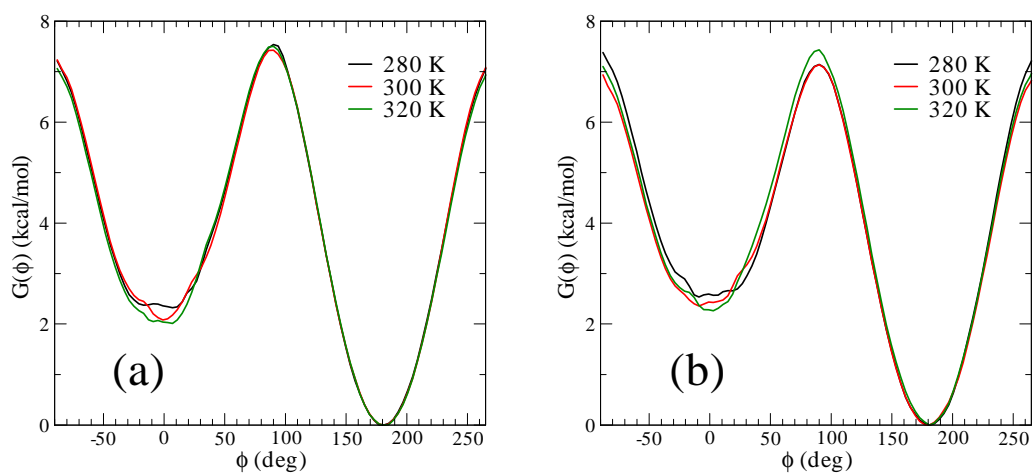

Figure 5.2: Gibbs free energy profile of the isomerization of hexatriene in methanol (a) and cyclohexane (b) at 280 K, 300 K, 320 K.
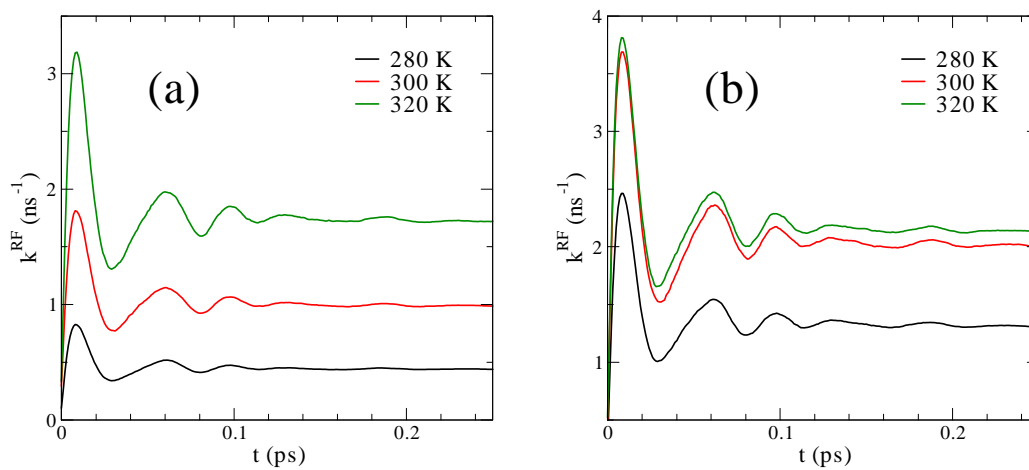
Figure 5.3: RF-TCF for isomerization of hexatriene in methanol (a) and cyclohexane (b) at 280 K, 300 K, 320 K.

Figure 5.4: Arrhenius temperature dependence plot of the hexatriene isomerization rate constant calculated using the RF (a) and TST (b) methods.

Figure 5.5: Histogram of the number of barrier recrossings seen in each trajectory for the isomerization of hexatriene in methanol and cyclohexane

Figure 5.6: Solute-solvent radial distribution function of hexatriene in methanol and cyclohexane.

CHAPTER VI

Conclusions and Future Directions
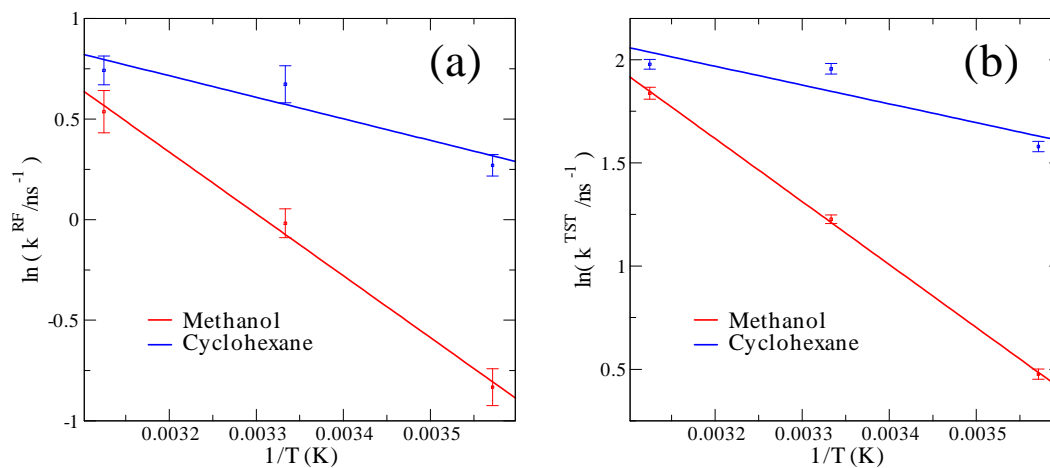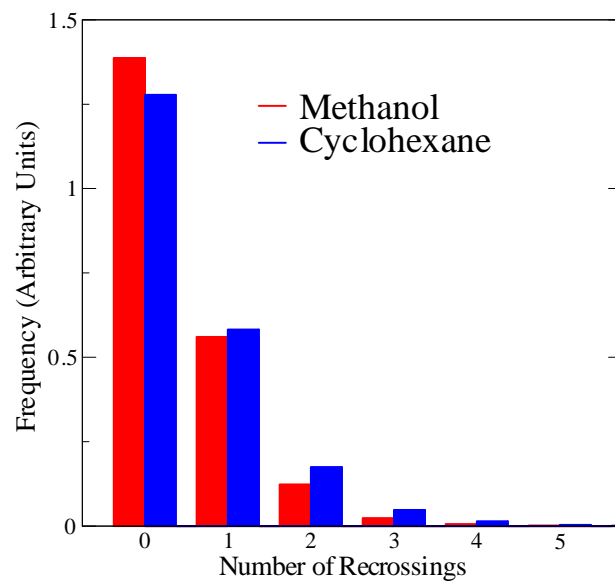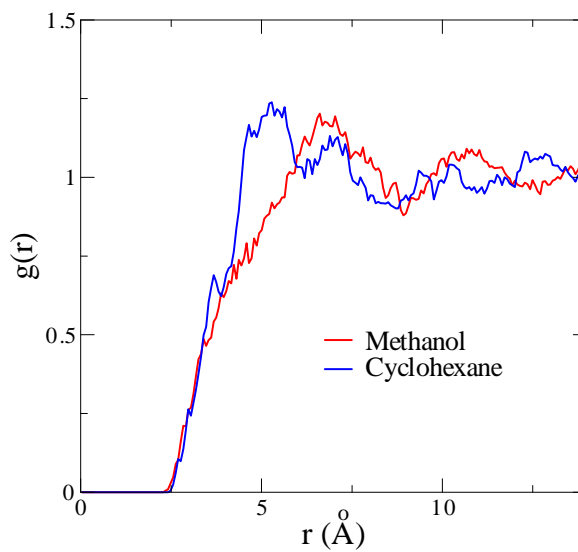
The calculation of time correlation functions (TCF) in liquids is of central importance to chemical phenomena because of the microscopic insight it can provide. Through the use of computer simulation, a molecular level picture of the fundamental processes at work in a liquid can be gained. Linear response theory can be used to calculate chemical reaction rates via the reactive-flux time correlation function (RF-TCF), after which the computer simulation can then be further analyzed in order to explain results that may be difficult or impossible to explain with experiments alone. Vibrational energy relaxation (VER) rates can be calculated via a force-force correlation function (FFCF) and can lead to an understanding of the importance quantum effects in the system. Diffusion coefficients can be calculated can be calculated from the velocity-velocity correlation (VVCF) and can be used gain some insight into the motions of the solvent.

In this work, we presented a new method for calculating quantum mechanical VER rate constants that was both easier to implement and more accurate then the method previously derived in our group. because of its relative ease in implementation, our force derivative free linearized semiclassical local harmonic approximation

(FDF-LSC-LHA) method was applied to the study of VER in polar solvents. This was the first ever use of a linearized semiclassical (LSC) method to a polar solvent and was able to give us a new insight into the importance of taking into account quantum effects. We found that in the case of low frequency molecules, the classical and quantum mechanical FFCFs coincided well with each other, and the FFCF was able to take this into account. We also found that, for VER in liquid hydrogen chloride, the classical picture predicted an electrostriction mechanism, whereas the electrostatic forces served mainly to position the solvent closer to the relaxing molecule and had little contribution to the FFCF, Conversely, the quantum mechanical calculations showed that the electrostatic forces did provide a significant contribution to the FFCF. This study is an example of the danger in making mechanism predictions based off of classical calculations in cases were quantum mechanical effects cannot be ignored and may actually change the mechanism. Future studies can continue to explore when electrostriction will play a significant role and when quantum mechanical effects may cause a difference to the mechanism. Specifically, a comparison of the more classical I_2^+ in a polar solvent such as water to the more quantum mechanical CN^- also solvated in water. It would be very interesting to see if this study would yield similar results to those seen in our study.

Another future study would be to directly tune the solvent polarity. Experimentally there is no way to tune partial charges in the solvent, but instead a mixture of polar and non polar solvent molecules can prepared. The VER rate constant can then be measured as a function mole fraction to see whether increasing the nonpolar character of the solvent mixture eventually decreases the rate enhancement seen in polar solvents.

We also presented a new approximation to the LSC-LHA in which we eliminated

the computationally expensive normal mode analysis and sampled the initial momentum quantum mechanically. This new NMF-LSC method was found to overestimate the quantum mechanical effects in the system, but was able to accurately calculate diffusion coefficients in liquid hydrogen. Our conclusion from this study was that diffusion, which is a common benchmark for quantum dynamics methods, is in fact a poor benchmark because it avoids dealing with the purely quantum mechanical imaginary part of the VVCF. Future work in this study could involve trying to include more quantum character into the derivation. This may involve using the different TCF flavors as a starting point to a similar derivation, where the increase in accuracy may compensate for the fact that the initial momentum sampling is done classically.

Lastly, we used the linear response formalism to calculate isomerization rate constant in hexatriene via the RF-TCF and TST. In these studies, we found that we were able to gain a microscopic picture of the effect of solvent on the rate constant that is not possible using macroscopic explanations such as Kramers theory. We found that the faster rate in cyclohexane versus methanol was due to the way the solvent can arrange itself around the solute molecule, something that would be very difficult to measure directly experimentally. We are currently in the process of studying the effects of many different solvents in order to understand the effects of chain length in the alcohol solvents and the effects of linear versus cyclic alkanes. Future work may also involve studying similar isomerization processes in more complicated molecules. One possible case is stilbene, where isomerization occurs around a higher energy double bond. Another possible system is to apply this same methodology to work done by Anna and coworkers[2] in which they study the isomerization of dicobalt octacarbonyl. This study could be especially interesting because it would involve the forming and breaking of bridging carbonyls across the cobalt metal cen-

ters. They have also seen differences between solvating the molecule in cyclic and linear alkanes. Studying this system similarly to the work we did on hexatriene may yield a microscopic insight into the effect of the various solvents on the chemical process seen in their experiments.

The calculation of TCFs in liquids can be difficult, especially when quantum mechanical effects play an important role; however, it can also be extremely fruitful endeavor. The TCF formalism allows computer simulations to model dynamic processes that would normally not be possible on the time scales accessible by computer simulation. From these calculation, we can gain a microscopic insight into the effects of solvent on the solute, which is extremely important to chemistry since much chemistry of interest occurs in solution. We can also gain a chemical insight that may not possible to gain from experiment. It is not possible to experimentally to separate the classical and quantum effects in a system, but in a computer simulation we can easily do this and understand how the quantum part effects the overall process. Even in system where quantum effects play little to no role, we can gain a microscopic insight into the system that may not possible experimentally due to that large size of system. Because of this, computer simulation of TCF can be a powerful compliment to experimental work in order to gain a deeper understanding of the chemical processes involved.

BIBLIOGRAPHY

BIBLIOGRAPHY

[1] S. C. An, C. J. Montrose, and T. A. Litovitz. Low frequency structure in depolarized spectrum of Argon. *J. Chem. Phys.*, 64:3717, 1976.

[2] M. R.; Kubarych K. J. Anna, J. M.; Ross. Dissecting enthalpic and entropic barriers to ultrafast equilibrium isomerization of a flexible molecule using 2dir chemical exchange spectroscopy. *J. Chem. Phys. A. Lett.*, 113:6544, 2009.

[3] J. S. Bader and B. J. Berne. Quantum and classical relaxation rates from classical simulations. *J. Chem. Phys.*, 100:8359, 1994.

[4] P. H. Berens, S. R. White, and K. R. Wilson. Molecular dynamics and spectra. *J. Chem. Phys.*, 75:515, 1981.

[5] B. J. Berne, J. Jortner, and R. Gordon. Vibrational relaxation of diatomic molecules in gases and liquids. *J. Chem. Phys.*, 47:1600, 1967.

[6] B. J. Berne and D. Thirumalai. On the simulation of quantum systems: Path integrals methods. *Annu. Rev. Phys. Chem.*, 37:401, 1986.

[7] S. R. J. Brueck and R. M. Osgood. Vibrational energy relaxation in liquid N_2-CO mixtures. *Chem. Phys. Lett.*, 39:568, 1976.

[8] W. F. Calaway and G. E. Ewing. Vibrational relaxation of small molecules in liquid phase: Liquid Nitrogen doped with O_2, CO, and CH_4. *J. Chem. Phys.*, 63:2842, 1975.

[9] G. J. Cao, J.; Martyna. Adiabatic path integral molecular dynamics methods ii. algorithms. *J. Chem. Phys.*, 104:2028, 1996.

[10] D. M. Ceperley. Path integrals in the theory of condensed helium. *Rev. Mod. Phys.*, 67:279, 1995.

[11] D Chandler. Statistical mechanics of isomerizartion in liquids and the transition state theory. *J. Chem. Phys.*, 68:2959, 1978.

[12] D Chandler. *Introduction to Modern Statistical Mechanics*. Oxford University Press, 1987.

[13] D; Kuharski Chandler. Two simulation studies of chemical dynamics in liquids. *Faraday Discuss. Chem. Soc.*, 85:320, 1988.

[14] M. Chateau, C. Delalande, R. Frey, G. M. Gale, and F. Pradère. Vibrational population relaxation of compressed $^nH_2$ fluid in the 15-110 K range. *J. Chem. Phys.*, 71:4799, 1979.

[15] J. Chesnoy and G. M. Gale. Vibrational energy relaxation in liquids. *Ann. Phys. Fr.*, 9:893, 1984.

[16] J. Chesnoy and G. M. Gale. Vibrational relaxation in condensed phases. *Adv. Chem. Phys.*, 70 (part 2):297, 1988.

[17] J. Chesnoy and J. J. Weis. Density dependence of the dephasing and energy relaxation times by computer simulations. *J. Chem. Phys.*, 84:5378, 1986.

[18] D. Chesnoy J.; Ricard. *Chem. Phys.*, 67:347, 1982.

[19] T.E. Cheatham III C.L. Simmerling J. Wang R.E. Duke R. Luo M. Crowley R.C.Walker W. Zhang K.M. Merz B.Wang S. Hayik A. Roitberg G. Seabra I. Kolossváry K.F.Wong F. Paesani J. Vanicek X.Wu S.R. Brozell T. Steinbrecher H. Gohlke L. Yang C. Tan J. Mongan V. Hornak G. Cui D.H. Mathews M.G. Seetin C. Sagui V. Babin D.A. Case, T.A. Darden and P.A. Kollman. Amber. *(2008)*, University of California, San Francisco, AMBER 10.

[20] C. Delalande and G. M. Gale. A semiclassical model for vibrational energy relaxation in simple liquids and compressed fluids. *J. Chem. Phys.*, 71:4804, 1979.

[21] C. Delalande and G. M. Gale. Vibrational energy relaxation in fluid mixtures : Hydrogen in Argon. *J. Chem. Phys.*, 73:1918, 1980.

[22] Y. Deng and R. M. Stratt. High-frequency vibrational energy relaxation in liquids: The foundation of the instantaneous-pair theory and some generalizations. *J. Chem. Phys.*, 117:10752, 2002.

[23] Y. Deng and R. M. Stratt. Vibrational energy relaxation of polyatomic molecules in liquids: The solvent's perspective. *J. Chem. Phys.*, 117:1735, 2002.

[24] H. Devoe. *Thermodynamics and Chemistry.* Prentice Hall, 2001.

[25] P. A. Egelstaff. Neutron scattering studies of liquid diffusion. *Adv. Phys.*, 11:203, 1962.

[26] S. A. Egorov, K. F. Everitt, and J. L. Skinner. Quantum dynamics and vibrational relaxation. *J. Phys. Chem. A*, 103:9494, 1999.

[27] S. A. Egorov and J. L. Skinner. A theory of vibrational energy relaxation in liquids. *J. Chem. Phys.*, 105(16):7047, 1996.

[28] S. A. Egorov and J. L. Skinner. Semiclassical approximations to quantum correlation functions. *Chem. Phys. Lett.*, 293:439, 1998.

[29] S. A. Egorov and J. L. Skinner. Vibrational energy relaxation of polyatomic solutes in simple liquids. *J. Chem. Phys.*, 112:275, 2000.

[30] T. Elsaesser and W. Kaiser. Vibrational and vibronic relaxation of large polyatomic molecules in liquids. *Annu. Rev. Phys. Chem.*, 42:83, 1991.

[31] K. F. Everitt, S. A. Egorov, and J. L. Skinner. Vibrational energy relaxation in liquid Oxygen. *Chem. Phys.*, 235:115, 1998.

[32] K. F. Everitt and J. L. Skinner. Vibrational energy relaxation of Oxygen in liquid mixtures with Argon. *J. Chem. Phys.*, 110:4467, 1999.

[33] K. F. Everitt, J. L. Skinner, and B. M. Ladanyi. Vibrational energy relaxation in liquid oxygen (revisited) and in liquid nitrogen. *J. Chem. Phys.*, 116:179, 2002.

[34] B. Faltermeier, R. Protz, and M. Maier. Concentration and temperature dependence of electronic and vibrational relaxation of O_2 in liquid mixtures. *Chem. Phys.*, 62:377, 1981.

[35] B. Faltermeier, R. Protz, M. Maier, and E. Werner. Vibrational energy relaxation of O_2 in liquid mixtures with Ar and N_2. *Chem. Phys. Lett.*, 74:425, 1980.

[36] L. Frommhold. *Collision-induced absorption in gases*, volume 2 of *Cambridge Monographs on Atomic, Molecular, and Chemical Physics*. Cambridge University Press, England, 1st edition, 1993.

[37] S. Garashchuk and D. Tannor. Wave packet correlation function approach to $H_2(v) + H \rightarrow H + H_2(v')$: Semiclassical implementation. *Chem. Phys. Lett.*, 262:477, 1996.

[38] A. Grossfield. Wham: the weighted histogram analysis method, 2010.

[39] M. C. Gutzwiller. Phase integral approximation in momentum space and bound states of an atom. *J. Math. Phys.*, 8:1979, 1967.

[40] M. C. Gutzwiller. Periodic orbits and classical quantization conditions. *J. Math. Phys.*, 12:343, 1971.

[41] M. C. Gutzwiller. *Chaos in Classical and Quantum Mechanics*. Springer-Verlag, Berlin, 1990.

[42] P. Hamm, M. Lim, and R. M. Hochstrasser. Vibrational energy relaxation of the cyanide ion in water. *J. Chem. Phys.*, 107(24):1523, 1997.

[43] J. C. Hammes-Schiffer, S.; Tully. Mecl parameters. *J. Chem. Phys.*, 101:4657, 1994.

[44] A. L. Harris, J. K. Brown, and C. B. Harris. The nature of simple photodissociation reactions in liquids on ultrafast time scales. *Annu. Rev. Phys. Chem*, 39:341, 1988.

[45] C. B. Harris, D. E. Smith, and D. J. Russell. Vibrational relaxation of diatomic molecules in liquids. *Chem. Rev.*, 90:481, 1990.

[46] R. J. Harris, D. A.; Orozco M. B.; Sension. Solvent dependent conformational relaxation of cis-1,3,5-hexatriene. *J. Phys. Chem. A*, 110:9333, 2006.

[47] J. Hautman and M. L. Klein. Effects of particle size fluctuations in a breathing Lennard-Jones liquid. *Mol. Phys.*, 80:647, 1993.

[48] E. J. Heilweil, M. P. Casassa, R. R. Cavanagh, and J. C. Stephenson. Temperature dependence of the vibrational population lifetime of $OH(\text{v} = 1)$ in fused silica. *Chem. Phys. Lett.*, 117:185, 1985.

[49] E. J. Heilweil, M. P. Casassa, R. R. Cavanagh, and J. C. Stephenson. Population lifetimes of $OH(\text{v} = 1)$ and $OD(\text{v} = 1)$ stretching vibrations of alcohols and silanols in dilute solution. *J. Chem. Phys.*, 85:5004, 1986.

[50] E. J. Heilweil, F. E. Doany, R. Moore, and R. M. Hochstrasser. Vibrational energy relaxation of the Cyanide ion in aqueous solution. *J. Chem. Phys.*, 76:5632, 1982.

[51] E. J. Heller. Cellular dynamics : A new semiclassical approach to time dependent quantum mechanics. *J. Chem. Phys.*, 94:2723, 1981.

[52] E. J. Heller. Reply to comment on: Semiclassical time evolution without root searches: Comments and perspective. *J. Chem. Phys.*, 95:9431, 1991.

[53] M. F. Herman and E. Kluk. A semiclassical justification for the use of non-spreading wave packets in dynamics calculations. *Chem. Phys.*, 91:27, 1984.

[54] M. Hillery, R. F. O'Connell, M. O. Scully, and E. P. Wigner. Distribution functions in physics: Fundamentals. *Phys. Rep.*, 106(3):121, 1984.

[55] G. A. Hone, T. D. ; Voth. A centroid molecular dynamics study of liquid para-hydrogen. *J. Chem. Phys.*, 121:6412, 2004.

[56] R. T. Jacobsen, R. B. Stewart, and M. Jahangiri. *J. Phys. Chem. Ref. Data*, 15:735, 1986.

[57] B.L.; Jack D.B.; Bayly C.I. Jakalian, A.; Bush. Fast, efficient generation of high-quality atomic charges. am1-bcc model: I. method. *J. Comput. Chem.*, 21:132, 2000.

[58] D.B.; Bayly C.I. Jakalian, A.; Jack. Fast, efficient generation of high-quality atomic charges. am1-bcc model: Ii. parameterization and validation. *J. Comput. Chem*, 23:123, 2002.

[59] S. Jang and G. A. Voth. Simple reversible molecular dynamics algorithms for nosé-hoover chain dynamics. *J. Chem. Phys.*, 107:9514, 1997.

[60] B. J. Ka and E. Geva. Vibrational energy relaxation of polyatomic molecules in liquid solution via the linearized semiclassical method. *J. Phys. Chem. A*, 110:9555, 2006.

[61] B. J. Ka, Q. Shi, and E. Geva. Vibrational energy relaxation rates via the linearized semiclassical approximations: Applications to neat diatomic liquids and atomic-diatomic liquid mixtures. *J. Phys. Chem. A*, 109:5527, 2005.

[62] K. G. Kay. Integral expressions for the semi-classical time-dependent propagator. *J. Chem. Phys.*, 100:4377, 1994.

[63] K. G. Kay. Semiclassical propagation for multidimensional systems by an initial value method. *J. Chem. Phys.*, 101:2250, 1994.

[64] S. Keshavamurthy and W. H. Miller. Semi-classical correction for quantum-mechanical scattering. *Chem. Phys. Lett.*, 218:183, 1994.

[65] D. A. V. Kliner, J. C. Alfano, and P. F. Barbara. Photodissociation and vibrational relaxation of I_2^- in Ethanol. *J. Chem. Phys.*, 98:5375, 1993.

[66] E. Kluk, M. F. Herman, and H. L. Davis. Comparison of the propagation of semiclassical frozen gaussian wave functions with quantum propagation for a highly excited anharmonic oscillator. *J. Chem. Phys.*, 84:326, 1986.

[67] G R Kneller. Inelastic neutron scattering from classical systems: Stationary phase approximation of the scattering law. *Mol. Phys.*, 83:63, 1994.

[68] M.; Hashitsume N. Kubo, R.; Toda. *Statistical Physics*. Springer-Verlag, Heidelberg, 2nd ed. edition, 1991.

[69] O. Kühn and N. Makri. Forward-backward semiclassical calculation of spectral line shapes: I_2 in a rare gas cluster. *J. Phys. Chem. A*, 103:9487, 1999.

[70] B. M. Ladanyi and R. M. Stratt. On the role of dielectric friction in vibrational energy relaxation. *J. Chem. Phys.*, 111:2008, 1999.

[71] R. Laenen, C. Rauscher, and A. Laubereau. Dynamics of local substructures in water observed by ultrafast infrared hole burning. *Phys. Rev. Lett.*, 80:2622, 1998.

[72] L. Landau and E. Z. Teller. Theory of sound dispersion. *Z. Sowjetunion*, 34:10, 1936.

[73] A. Laubereau and W. Kaiser. Vibrational dynamics of liquids and solids investigated by picosecond light pulses. *Rev. Mod. Phys.*, 50:607, 1978.

[74] C. P. Lawrence and J. L. Skinner. Vibrational spectroscopy of HOD in liquid D_2O. I. vibrational energy relaxation. *J. Chem. Phys.*, 117:5827, 2002.

[75] S. Levit, K. Mohring, U. Smilansky, and T. Dreyfus. Focal points and phase of semiclassical propagator. *Ann. Phys. (N.Y)*, 114:223, 1978.

[76] S. Levit and U. Smilansky. Hamiltonian path integrals and uniform semiclassical approximations for propagator. *Ann. Phys. (N.Y)*, 108:165, 1977.

[77] S. Li and W. H. Thompson. Simulation of the vibrational relaxation of I_2 in Xe. *J. Chem. Phys.*, 107:8696, 2003.

[78] R. G. Littlejohn. The Van Vleck formula, Maslov theory, and phase space geometry. *J. Stat. Phys.*, 68:7, 1992.

[79] N. Makri. Time-dependent quantum methods for large systems. *Annu. Rev. Phys. Chem.*, 50:167, 1999.

[80] N. Makri and W. H. Miller. Coherent state semiclassical initial value representation for the Boltzmann operator in thermal correlation functions. *J. Chem. Phys.*, 116:9207, 2002.

[81] N. Makri and K. Thompson. Semiclassical influence functionals for quantum systems in anharmonic environments. *Chem. Phys. Lett.*, 291:101, 1998.

[82] V. P. Maslov and M. V. Fedoriouk. *Semi-classical approximation in quantum mechanics*. Reidel, Boston, 1981.

[83] D. A. McQuarrie. *Statistical Mechanics*. University Science Books, 2000.

[84] D. E. Miller, T. F.; Manolopoulos. Quantum diffusion in liquid para-hydrogen from ring polymer molecular dynamics. *J. Chem. Phys.*, 122:184503, 2005.

[85] D. E.; Madden P. A.; Konieczny M.; Oberhofer H. Miller, T. F.; Manolopoulos. Comment on "a centroid molecular dynamics study of liquid para hydrogen and ortho deuterium" [j. chem. phys. [bold 121], 6412 (2004)]. *J. Chem. Phys.*, 122(5):057101, 2005.

[86] D. W. Miller and S. A. Adelman. Vibrational energy transfer in fluids. *Int. Rev. Phys. Chem.*, 13:359, 1994.

[87] W. H. Miller. Classical S-matrix : Numerical application to inelastic collisions. *J. Chem. Phys.*, 53:3578, 1970.

[88] W. H. Miller. Classical-limit quantum mechanics and the theory of molecular collisions. *Adv. Chem. Phys.*, 25:69, 1974.

[89] W. H. Miller. Comment on: Semiclassical time evolution without root searches. *J. Chem. Phys.*, 95:9428, 1991.

[90] W. H. Miller. Quantum and semiclassical theory of chemical reaction rates. *Faraday, Discuss.*, 110:1, 1998.

[91] W. H. Miller. The semiclassical initial value representation: A potentially practical way for adding quantum effects to classical molecular dynamics simulations. *J. Phys. Chem. A*, 105:2942, 2001.

[92] A. Moustakas and E. Weitz. Vibrational relaxation of HCl as a function of Xenon density: The role of HCl-Xe complexes. *J. Chem. Phys.*, 98:6947, 1993.

[93] S. Mukamel. *Principles of Nonlinear Optical Spectroscopy.* Oxford, New York, 1995.

[94] D. J. Myers, S. Chen, M. Shigeiwa, B. J. Cherayil, and M. D. Fayer. Temperature dependent vibrational lifetimes in supercritical fluids near the critical point. *J. Chem. Phys.*, 109:5971, 1998.

[95] D. J. Myers, R. S. Urdahl, B. J. Cherayil, and M. D. Fayer. Temperature dependence of vibrational lifetimes at the critical density in supercritical mixtures. *J. Chem. Phys.*, 107:9741, 1997.

[96] N. Nakayama, A.; Makri. Foward-backward semiclassical dynamics for quantum fluids using pair propagators: Application to liquid para-hydrogen. *J. Chem. Phys.*, 119:8592, 2003.

[97] E. Navrotskaya, I.; Geva. Vibrational energy relaxation rates of h2 and d2 in liquid argon via the linearized semiclassical method. *J. Phys. Chem. A*, 2007.

[98] A. Nitzan, S. Mukamel, and J. Jortner. Some features of vibrational relaxation of a diatomic molecule in a dense medium. *J. Chem. Phys.*, 60:3929, 1974.

[99] A. Nitzan, S. Mukamel, and J. Jortner. Energy gap law for vibrational relaxation of a molecule in a dense medium. *J. Chem. Phys.*, 63:200, 1975.

[100] M. Ovchinnikov and V. A. Apkarian. Condensed phase spectroscopy from mixed-order semiclassical molecular dynamics: Absorption, emission, and resonant Raman spectra of I_2 isolated in solid Kr. *J. Chem. Phys.*, 105:10312, 1996.

[101] M. Ovchinnikov and V. A. Apkarian. Mixed-order semiclassical dynamics in coherent state representation: The connection between phonon sidebands and guest–host dynamics. *J. Chem. Phys.*, 108:2277, 1998.

[102] M. Ovchinnikov, V. A. Apkarian, and G. A. Voth. Semiclassical molecular dynamics computation of spontaneous light emission in the condensed phase: Resonance Raman spectra. *J. Chem. Phys.*, 184:7130, 2001.

[103] J. C. Owrutsky, Y. R. Kim, M. Li, M. J. Sarisky, and R. M. Hochstrasser. Determination of the vibrational energy relaxation time of the azide ion in protic solvents by 2-color transient infrared spectroscopy. *Chem. Phys. Lett.*, 184:368, 1991.

[104] J. C. Owrutsky, M. Li, B. Locke, and R. M. Hochstrasser. Vibrational relaxation of the CO stretch vibration in hemoglobin-CO, myoglobin-CO, and protoheme-CO. *J. Phys. Chem.*, 99:4842, 1995.

[105] J. C. Owrutsky, D. Raftery, and R. M. Hochstrasser. Vibrational relaxation dynamics in solutions. *Annu. Rev. Phys. Chem.*, 45:519, 1994.

[106] D. W. Oxtoby. Vibrational population relaxation in liquids. *Adv. Chem. Phys.*, 47 (Part 2):487, 1981.

[107] D. W. Oxtoby. Vibrational relaxation in liquids. *Annu. Rev. Phys. Chem.*, 32:77, 1981.

[108] D. W. Oxtoby. Vibrational relaxation in liquids: Quantum states in a classical bath. *J. Phys. Chem.*, 87:3028, 1983.

[109] M. E. Paige and C. B. Harris. Ultrafast studies of chemical reactions in liquids: Validity of gas phase vibrational relaxation models and density dependence of bound electronic state lifetimes. *Chem. Phys.*, 149:37, 1990.

[110] M. E. Paige, D. J. Russell, and C. B. Harris. Studies of chemical reactivity in the condensed phase. II. Vibrational relaxation of Iodine in liquid Xenon following geminate recombination. *J. Chem. Phys.*, 85:3699, 1986.

[111] P. Pechukas. Time-dependent semiclassical scattering theory. II. Atomic collisions. *Phys. Rev.*, 181:174, 1969.

[112] E. Pollak and J. Liao. A new quantum transition state theory. *J. Chem. Phys.*, 108:2733, 1998.

[113] G.; Rossky P. J. Poulsen, J. A.; Nyman. Quantum diffusion in liquid para-hydrogen: An application of the feynaman-kleinert linearized path integral approximation. *J. Phys. Chem. B*, 108:19799, 2004.

[114] D. Provost and P. Brumer. Uniform semiclassical wave-packet propagation and eigenstate extraction in smooth chaotic systems. *Phys. Rev. Lett.*, 74:250, 1995.

[115] N. Pugliano, A. Z. Szarka, S. Gnanakaran, and R. M. Hochstrasser. Vibrational population dynamics of the HgI photofragment in Ethanol solution. *J. Chem. Phys.*, 103:6498, 1995.

[116] D. R. Rabani, E.; Reichman. Collective and single-particle dynamics in liquid ortho-deuterium: A quantum mode-coupling approach. *Europhys. Lett.*, 60(5):656, 2002.

[117] D. R. Rabani, E.; Reichman. Molecular hydrodynamic approach to dynamical correlations in quantum liquids. *Phys. Rev. E*, 65:036111–1, 2002.

[118] D. R. Rabani, E.; Reichman. A self-consistent mode-coupling theory for dynamical correlation in quantum liquids: Rigorous formulation. *J. Chem. Phys.*, 116:6271, 2002.

[119] D. R. Rabani, E.; Reichman. A fully self-consistent treatment of collective fluctuations in quantum liquids. *J. Chem. Phys.*, 120:1458, 2004.

[120] E. Rabani and D. R. Reichman. A short-time quantum mechanical expansion approach to vibrational relaxation. *J. Phys. Chem. B*, 105:6550, 2001.

[121] G.; Berne B. J. Rabani, E.; Reichman; D. R. Krilov. The calculation of transport properties in quantum liquids using the maximum entropy analytic continuation method: Application to liquid para-hydrogen. *PNAS*, 99:1129, 2002.

[122] B. J.; Chandler D. Rebertus, D. W.; Berne. A molecular dynamics and monte carlo study of solvent effects on the conformational equilibrium of n-butane in ccl[sub 4]a),b). *J. Chem. Phys.*, 70(7):3395, 1979.

[123] E. Reichman, D. R.; Rabani. Self-consistent mode-coupling theory for self0diffusion in quantum liquids. *Phys. Rev. Let.*, 87:265702, 2001.

[124] B. J.; Chandler D. Rosenberg, R. O.; Berne. Isomerization dynamics in liquids by molecular dynamics. *Chem Phys. Lett.*, 75(1):162, 1980.

[125] D. Rostkier-Edelstein, P. Graf, and A. Nitzan. Computing vibrational energy relaxation for high frequency modes in condensed environments. *J. Chem. Phys.*, 107:10470, 1997.

[126] D. Rostkier-Edelstein, P. Graf, and A. Nitzan. Erratum: Computing vibrational energy relaxation for high frequency modes in condensed environments (J. Chem. Phys. **107**, 10470 (1997)). *J. Chem. Phys.*, 108:9598, 1998.

[127] P. Roussignol, C. Delalande, and G. M. Gale. Vibrational relaxation of Deuterium in Argon fluid. *Chem. Phys.*, 70:319, 1982.

[128] D. E. Sagnella, J. E. Straub, T. A. Jackson, M. Lim, and P. A. Anfinrud. Vibrational population relaxation of carbon monoxide in the heme pocket of photolyzed carbonmonoxy myoglobin: Comparison of time-resolved mid-IR absorbance experiments and molecular dynamics simulations. *Proc. Natl. Acad. Sci. USA*, 96:14324, 1999.

[129] A. Salloum and H. Dubost. Vibrational energy transfer from CO to O_2 in rare gas matrices. I. Vibrational excitation and relaxation of O_2 (X, v=4-20). *Chem. Phys.*, 189:179, 1994.

[130] J. G.; Klein M. L. Scharf, D.; Martyna. Structure and energetics of fluid para-hydrogen. *Low Temp. Phys.*, 19:364, 1993.

[131] P. Schofield. Space-time correlation function formalism for slow neutron scattering. *Phys. Rev. Lett.*, 4:239, 1960.

[132] J. S. Shao and N. Makri. Forward-backward semiclassical dynamics without prefactors. *J. Phys. Chem. A*, 103:7753, 1999.

[133] Q. Shi and E. Geva. A relationship between semiclassical and centroid correlation functions. *J. Chem. Phys.*, 118:8173, 2003.

[134] Q. Shi and E. Geva. A semiclassical theory of vibrational energy relaxation in the condensed phase. *J. Phys. Chem. A*, 107:9059, 2003.

[135] Q. Shi and E. Geva. Vibrational energy relaxation in liquid oxygen from a semiclassical molecular dynamics simulation. *J. Phys. Chem. A*, 107:9070, 2003.

[136] E. L. Sibert III and R. Rey. Vibrational relaxation in liquid chloroform following ultrafast excitation of the CH stretch fundamental. *J. Chem. Phys.*, 116:237, 2002.

[137] V. V. SIlevera, I. F.; Goldman. The isotropic intermolecular potential for h2 and d2 in the solid and gas phases. *J. Chem. Phys.*, 69:4209, 1978.

[138] I. F. Silvera. The solid molecular hydrogens in the condensed phase: Fundamentals and static properties. *Rev. Mod. Phys.*, 52:393, 1980.

[139] J. L. Skinner. Semiclassical approximations to golden rule rate constants. *J. Chem. Phys.*, 107:8717, 1997.

[140] J. L. Skinner and K. Park. Calculating vibrational energy relaxation rates from classical molecular dynamics simulations: Quantum correction factors for processes involving vibration-vibration energy transfer. *J. Phys. Chem. B*, 105:6716, 2001.

[141] B. W. Spath and W. H. Miller. Semiclassical calculation of cumulative reaction probabilities. *J. Chem. Phys.*, 104:95, 1996.

[142] R. M. Stratt and M. Maroncelli. Nonreactive dynamics in solution: The emerging molecular view of solvation dynamics and vibrational relaxation. *J. Phys. Chem.*, 100:12981, 1996.

[143] X. Sun and W. H. Miller. Mixed semiclassical-classical approaches to the dynamics of complex molecular systems. *J. Chem. Phys.*, 106:916, 1997.

[144] X. Sun and W. H. Miller. Forward-backward initial value representation for semiclassical time correlation functions. *J. Chem. Phys.*, 110:6635, 1999.

[145] X. Sun, H. Wang, and W. H. Miller. On the semiclassical description of quantum coherence in thermal rate constants. *J. Chem. Phys.*, 109:4190, 1998.

[146] X. Sun, H. Wang, and W. H. Miller. Semiclassical theory of electronically nonadiabatic dynamics: Results of a linearized approximation to the initial value representation. *J. Chem. Phys.*, 109:7064, 1998.

[147] V. V. Sychev, A. A. Vasserman, A. D. Kozlov, G. A. Spiridonov, and V. A. Tsymarny. *Thermodynamic Properties of Oxygen.* Number 5 in National Standard Reference Data Service of the USSR: A Series of Property Tables. Hemisphere, Moscow, English edition, 1987.

[148] K. Thompson and N. Makri. Rigorous forward-backward semiclassical formulation of many-body dynamics. *Phys. Rev. E*, 59:R4729, 1999.

[149] A. Tokmakoff and M. D. Fayer. Homogeneous vibrational dynamics and inhomogeneous broadening in glass forming liquids: Infrared photon-echo experiments from room temperature to 10K. *J. Chem. Phys.*, 103:2810, 1995.

[150] A. Tokmakoff, B. Sauter, and M. D. Fayer. Temperature-dependent vibrational relaxation in polyatomic liquids: Picosecond infrared pump-probe experiments. *J. Chem. Phys.*, 100:9035, 1994.

[151] R. S. Urdahl, D. J. Myers, K. D. Rector, P. H. Davis, B. J. Cherayil, and M. D. Fayer. Vibrational lifetimes and vibrational line positions in polyatomic supercritical fluids near the critical point. *J. Chem. Phys.*, 107:3747, 1997.

[152] I.; Geva E.; J. Vazquez, F. X.; Navrotskaya. Ver rates via lsc without fd. *J. Phys. Chem. A*, 114:5682, 2010.

[153] J. H. Van Vleck. The correspondence principle in the statistical interpretation of quantum mechanics. *Proc. Nat. Acad. Sci.*, 14:178, 1928.

[154] H. Wang, X. Song, D. Chandler, and W. H. Miller. Semiclassical study of electronically nonadiabatic dynamics in the condensed phase: Spin-boson problem with debye spectral density. *J. Chem. Phys.*, 110:4828, 1999.

[155] H. Wang, X. Sun, and W. H. Miller. Semiclassical approximations for the calculation of thermal rate constants for chemical reactions in complex molecular systems. *J. Chem. Phys.*, 108:9726, 1998.

[156] H. Wang, M. Thoss, and W. H. Miller. Forward-backward initial value representation for the calculation of thermal rate constants for reactions in complex molecular systems. *J. Chem. Phys.*, 112:47, 2000.

[157] P.; Kollman P.A Wang, J.; Cieplak. *J. Comput. Chem.*, 21:1049, 2000.

[158] R.M.; Caldwell J.W.; Kollamn P.A.; Case D.A. Wang, J.; Wolf. *J. Comput. Chem.*, 25:1157, 2004.

[159] D. Wilson, M. A.; Chandler. Molecular-dynamics study of cyclohexane inter-conversion. *Chemical Physics*, 149:11, 1990.

[160] S. Woutersen, U. Emmerichs, H. Nienhuys, and H. J. Bakker. Anomalous temperature dependence of vibrational lifetimes in water and ice. *Phys. Rev. Lett.*, 81:1106, 1998.

[161] D. Zimdars, A. Tokmakoff, S. Chen, S. R. Greenfield, and M. D. Fayer. Picosecond infrared vibrational photon echoes in a liquid and glass using a free electron laser. *Phys. Rev. Lett.*, 70:2718, 1993.

[162] R. Zwanzig. Theory of vibrational relaxation in liquids. *J. Chem. Phys.*, 34:1931, 1961.

[163] R. Zwanzig. *Nonequilbrium Statistical Mechanics.* Oxford University Press, 2001.